Hysteretic Friction in the Transient Rolling Contact Problem of Linear Viscoelasticity

by

Daniel Chertok

Eng. Math., Leningrad Polytechnic Institute, USSR, 1990

A THESIS SUBMITTED IN PARTIAL FULFILLMENT
OF THE REQUIREMENTS FOR THE DEGREE OF
DOCTOR OF PHILOSOPHY
in the Department
of
Mathematics and Statistics

SIMON FRASER UNIVERSITY
April 1998

APPROVAL

Name: Daniel Chertok

Degree: Doctor of Philosophy

Title of thesis: Hysteretic Friction in the Transient Rolling Contact Problem of Linear Viscoelasticity

Examining Committee: Dr. R. Lockhart
Chair

Dr. G.A.C. Graham
Senior Supervisor

Dr. K. Promislow

Dr. M. Singh

Dr. A. Das

Dr. A. Peirce, External Examiner
Institute of Applied Mathematics
University of British Columbia

Date Approved: April 8, 1998

Dedication

To those who believed in me

Abstract

The problem of a smooth rigid cylindrical indentor rolling across a viscoelastic half-space in one direction with variable speed is considered. The boundary of the half-space is assumed to be free of Coulomb friction and the standard linear model is adopted to describe viscoelastic material response. The indentor is assumed to be in contact with the half-space over a time-dependent interval $C(t)$, which is to be determined. The normal pressure on the surface of the half-space must be continuous and vanish outside the contact interval $C(t)$.

A governing integral equation for a "pressure-like" function $v(x,t)$, $x \in C(t)\,\forall t > 0$ is derived and an adaptive numerical algorithm is constructed for its solution subject to appropriate subsidiary conditions. The results obtained with the help of this algorithm are compared and found consistent with those for the available steady-state analytic solution. It is observed that more pronounced viscoelastic properties of the material of the half-space lead to longer contact intervals, higher hysteretic friction and more asymmetric pressure distribution. The shapes of the graphs of transient and steady-state hysteretic friction for variable *speed* are substantially different. After a period of acceleration, the transient value of the hysteretic friction exceeds the corresponding steady-state value.

The stress tensor components σ_{11}, σ_{12} and σ_{22} are computed and analyzed. Results for the case of a time-dependent load are also obtained.

Keywords: *viscoelasticity, hysteretic friction, transient*

Acknowledgements

I would like to thank my supervisor, Professor G.A.C. Graham, for his invaluable support and guidance. I am also deeply indebted to Dr. J.M. Golden for fruitful discussions during the course of this work and insights into the nature of the problem.

I am pleased to use this opportunity to thank the members of my Examining Committee, Dr. A. Das, Dr. A. Peirce, Dr. K. Promislow and Dr. M. Singh for many a helpful suggestion on improving this thesis. I am especially grateful to Dr. Promislow for his encouragement during the final stage of preparation of this work.

Words cannot express my gratitude to my family and friends for their indispensable moral support. And last but not least, I would like to thank the people of Canada for granting me the opportunity to carry out this research.

Contents

List of Figures

Chapter 1

Introduction

The rolling contact problem has been of substantial interest to engineers and scientists since time immemorial. The physical models of the phenomena taking place as a rigid indentor moves across a viscoelastic half-space have numerous applications in engineering and mechanics. The frictional losses occurring during the motion of an automobile tire on an asphalt pavement, of a locomotive wheel on a rail, of a calender on pulp mix or of a bushing in a roller bearing can be described by the same model of linear viscoelasticity.

The surface (Coulomb) friction, however, does not constitute the major part of frictional losses in the material engaged in rolling contact. Experiments show that most of the energy dissipation in the rolling contact problem is due to the internal losses in the material termed *hysteretic friction.* To investigate this specific type of problem, it is convenient to neglect the Coulomb friction altogether in order to simplify the mathematics. Then the formidable general problem reduces to an idealization amenable to analytical and numerical treatment. The frictionless assumption allows one to focus on the essence of the viscoelastic material response and provides an adequate theoretical framework for describing the behaviour of many materials, including steels, rubbers and elastomers.

The object of this thesis is *to investigate the behaviour of the hysteretic friction in the transient non-inertial frictionless rolling contact problem of a single rigid cylindrical indentor moving across a viscoelastic half-space modelled by the standard*

linear solid.

After a case study in Chapter 2, the mathematical formulation of the problem is given and the simplifying assumptions are stated. The nature of the hysteretic friction is discussed following the model in Bowden and Tabor [11].

In Chapter 3 a mathematical formalism describing the original physical problem is presented. The complex potential theory is used to derive the viscoelastic Kolosov-Muskhelishvili equations. An internal energy loss argument is employed to evaluate the hysteretic friction.

In Chapter 4 the main integral equation is derived using the decomposition of hereditary integrals and the solution of an elastic problem. The subsidiary conditions for determining the boundaries $a(t)$ and $b(t)$ of $C(t)$ at each moment of time t are formulated. The general integral equation is reduced to the case of a cylindrical indentor and standard linear model in the frictionless approximation. An approach to handling the singularities in the main integral equation is also proposed and a steady-state solution for a constantly moving indentor is computed.

In Chapter 5 modern numerical methods for solving the main integral equation are surveyed. A general computational algorithm is proposed and its implementation is discussed, including a numerical treatment of integral singularities.

In Chapter 6 the numerical results are presented for several patterns of indentor speed and loading variation. The discussion is focussed on the cases of constant acceleration, acceleration followed by deceleration, periodic acceleration and periodic loading. The characteristic parameters of motion chosen for the comparison of the results are the contact interval width, indentor tip shift (a measure of asymmetry of the contact interval) and the coefficient of hysteretic friction. It is observed that the shape of the graph of the hysteretic friction mimics the shape of the graph of the indentor tip shift. It is deduced empirically that the hysteretic friction has a peak following a period of acceleration. In most cases, the transient hysteretic friction follows the steady-state hysteretic friction with a time delay. This effect is especially evident for the case of a variable load. Stress distributions are presented for all stress tensor components for all types of speed and loading variation patterns.

In the conclusion the results are summarized and possible directions of further

research are proposed. The latter include the contact problem for more than one indentor and for a single indentor moving to and fro.

Chapter 2

Viscoelastic Contact Problem

2.1 Historical Remarks

The viscoelastic rolling contact problem has been of substantial interest to engineers and scientists since the time of Leonardo da Vinci. However, it was not until the late XVIII century that the first acceptable formalization of the friction phenomenon was proposed by Coulomb [21]. The investigations of this outstanding French scientist lead to what we now know as Coulomb's Law of Friction. As part of his research, he experimented with the rolling of wooden cylinders and observed the relationship between the coefficient of friction, the radius of the cylinder and the load acting upon it. Nevertheless, it was a young French engineer Dupuit [27], who first related the frictional resistance of rolling bodies to their inelasticity, but his work was largely forgotten.

Further developments lead to several simple models being proposed to describe the behaviour of materials with memory. The first to appear was the Maxwell model [89] which treats such materials as a combination of a spring and dashpot as shown in Figure 2.1: In this model the elastic properties of the spring are offset by the damping properties of the dashpot. Among later models we should mention the Voigt model, the standard linear solid and the power law model (see, e.g., [19, 121]).

A substantial theoretical breakthrough in the formal side of the viscoelasticity theory can be attributed to Boltzmann [9], who introduced the concept of hereditary

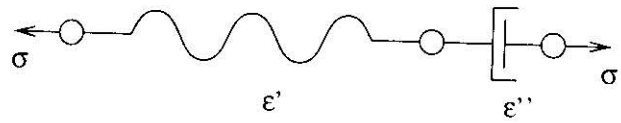

Figure 2.1: The Maxwell model: σ - stress, ϵ' - spring element, ϵ'' - dashpot element

integrals and derived a constitutive equation for such material:

$$\sigma(x,t) = \beta\epsilon(x,t) + \int_{-\infty}^{t} m(t-\tau)(\epsilon(x,t) - \epsilon(x,\tau))d\tau, \tag{2.1.1}$$

where $\sigma(x,t)$ and $\epsilon(x,t)$ are stress and strain tensors respectively, $\beta > 0$ is a constant, $m(t)$ is a positive, monotonously decreasing function.

An experimental substantiation of this mathematical formalism was provided by Reynolds [107], who proposed the first theory of viscoelastic rolling friction which established parallels between sliding and rolling friction. His classic experiments involving the rolling of metal cylinders over a flat rubber surface illustrated graphically the concept of hysteretic losses in the material and exposed the variable nature of the contact patch between the indented material and the moving indentor.

A major contribution to the theory of contact problems was made by Hertz [62], who considered the steady-state static contact between a rigid cylinder and an elastic half-space as shown in Figure 2.2. Hertzian analysis applies only to small displacements, i.e. for $d_0 \ll R$. It can also be used as an approximate solution for larger displacements. A physical reason for restricting d_0 is that we can neglect the deformations inside the roller due to the reaction forces induced by the deformation of the rubber-like material under it [92]. The Hertzian analysis provides a means of calculating the extent of the contact interval and the pressure p at the point x inside it:

$$a_0 = \sqrt{\frac{WR(1-\nu^2)}{\pi E}} \tag{2.1.2}$$

$$p = \frac{2W}{\pi a_0^2}(a_0^2 - x^2), \tag{2.1.3}$$

where W is the normal load per unit length of the cylinder, R is the cylinder radius, E and ν are the Young's modulus and the Poisson's ratio respectively.

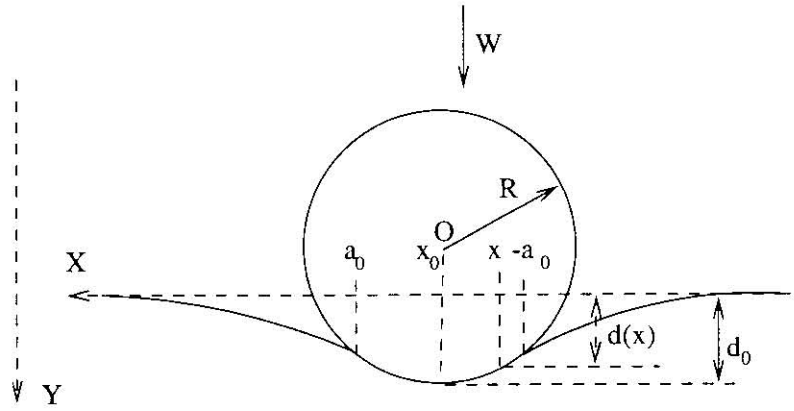

Figure 2.2: Hertzian contact: $[-a_0, a_0]$ - contact interval, O - centre of the cylinder, R - radius of the cylinder, x_0 - point of deepest indentation of the half-space, x - current point coordinate, $d(x)$ - vertical displacement at x, d_0 - maximum vertical displacement, W - normal load

In the beginning of this century significant progress has been made in the application of the complex potential theory to the elastic contact problem by Kolosov [77]. Subsequent expansion of the theory by Muskhelishvili summarized later in his classical monograph [98] resulted in the derivation of the Kolosov-Muskhelishvili equations relating stresses to complex potentials for the indentation problem. At approximately the same time as Kolosov, Volterra [124] formulated what has later become known as the Classical Correspondence Principle [83, 84, 105]. A common modern interpretation of this principle (see, e.g., [19, 45, 121] postulates that *a viscoelastic solution can be obtained from the known elastic solution to the corresponding boundary value problem, provided the boundary regions do not change with time.* To construct a viscoelastic solution, one must take an integral transform (Laplace or Fourier, as appropriate) of the viscoelastic field equations and boundary conditions. The resulting transformed relationships will have the form of an elastic boundary value problem, to which the solution is known. An inverse transform of this solution (in transformed quantities) will then deliver the viscoelastic solution of the original problem.

As one can see from the definition, the requirement that the boundaries be stationary renders the Classical Correspondence Principle inapplicable to moving load problems [106]. However, a generalization of this principle including some classes of mixed boundary value problems with time-dependent regions is possible (see [52, 53, 55]).

The appearance of modern computational tools sparked rapid development of the viscoelastic theory of rolling friction in the 1950s and 60s. The widely cited work of Tabor [115] and Greenwood and Tabor [58] provided an explanation for the phenomenon of hysteretic, or internal, friction; Lee and Radok [85], Morland [93], [94], [95] and Hunter [64], [65] subsequently contributed to the solution of the viscoelastic contact problem. Of particular interest to us is Hunter's paper [65], where a solution is provided for the rolling contact of a rigid cylinder with a viscoelastic half-space. It represents the first solution of this type of problem, albeit in the steady-state case, and traditionally serves as a yardstick for validating the new results [45]. The non-inertial approximation and the standard linear model used by Hunter are also the basic assumptions employed throughout this thesis. Morland investigated the same problem in his paper [93], while his later work was largely devoted to the rolling of viscoelastic cylinders. The results of [93] are similar to those of [65]; the latter were obtained using a different method. Oden and Lin [102] discussed the contact problem in application to a viscoelastic cylinder, while Panek and Kalker [103] considered a three-dimensional contact of a rigid indentor with a viscoelastic half-space. The sliding of a rigid indentor across a viscoelastic material drew the attention of Nachman and Walton [99]. Walton *et al.* [126] and Walton [125] incorporated frictional effects into the aforementioned model.

Subsequent ramifications of the original viscoelastic contact problem lead Alblas and Kuipers [3] to consider steady-state motion of a rigid cylinder over a thin viscoelastic layer in the absence of friction. They proposed an analytic solution obtained through an approximation procedure and provided a numerical illustration. Aboudi [1] developed an iterative algorithm for obtaining a numerical solution for the dynamic rolling contact problem of a rigid sphere on a viscoelastic half-space described by a power-law model. Akopyan [2] solved the periodic contact of two viscoelastic strips pressed against a system of rotating viscoelastic disks by reducing the problem to a

system of Volterra equations amenable to analytic treatment. In late 1980s Dobordzhginidze [24] incorporated the effects of slipping and traction into the contact of two viscoelastic bodies. His analytical solution utilized Mellin integral transforms and gave an approximate estimate of the length of slipping and traction intervals. Also worth mentioning here is an investigation into the contact of an ageing growing body with a rigid base by Arutyunyan and Manzhirov [4]. This paper provides numerical examples that describe stress distribution as a function of growth speed. Physically the process is quite similar to the motion of an indentor of very large radius over a viscoelastic body of finite dimensions. A discussion of a one-dimensional dynamic contact problem can be found in [76].

The question of existence and uniqueness of solution for different types of contact problems has been addressed, among others, by Fichera [32], Duvait and Lions [28], Kresin and Mazya [79], Ciobanu [20], Badalov and Usmanov [6], Khludnev [73], Jarušek [67, 69] and Jarušek and Eck [68]. Results for generalized types of the viscoelastic contact problem have been obtained, for example, by Carini and de Donato [14] and Telega [116], while Singh [111] investigated some aspects of the contact problem within the framework of microelastisity theory. . Solution methods based on modifications of the Bubnov-Galerkin technique have been presented by Badalov and Anzhiev [7], Badalov and Khuzhayarov [8] and Figueiredo and Trabucho [33, 34]. An interesting technique involving the separation of the original contact problem into a pure boundary value problem and a dynamic problem has been developed by Mark and Meister [88].

A comprehensive discussion of the contact problem can be found, for example, in monographs by Galin [38], Hills *et al.* [63], Johnson [70] and Shames and Cozzarelli [109]. Among the most recent treatises on the subject, we can mention those by Drozdov and Kolmanovskii [25] and Drozdov [26]. We should also mention an seminal paper by Gurtin and Sternberg [59] in this connection.

Of most interest to us is the decomposition of hereditary integrals, a technique developed by Golden and Graham, which can naturally be applied to a wide class of moving load problems. The first mentions of this technique can be found in [50, 51] and [119, 120]. Golden [40] discussed an arbitrary shaped indentor sliding with a

constant speed on a viscoelastic half-space without friction. He used the frictionless and non-inertial (quasi-static) assumptions to investigate the response of a material with general relaxation and creep functions and showed that the problem reduces to solving an integral equation with a non-singular kernel. The author then eliminated the time dependency from this equation by carrying out a variable transformation and derived an integral equation equivalent to the original problem. This equation was treated analytically for both discrete and continuous spectra and an approximate solution was provided for the case of equal decay constants. A later paper by the same author [41] dealt with the frictional moving contact problem. He provided a viscoelastic analog of the Boussinesq–Cerruti formula [87] and constructed a solution in the small viscoelasticity approximation. Graham [54] considered a general contact problem with adhesion and friction and provided some insights on how this problem can be solved, while Golden [42] later treated the frictional contact problem. A three-dimensional generalization of the steady-state indentation problem can be found in Golden and Graham [45].

In continuation of their previous research, Golden and Graham [43] outlined an approach for solving the general transient moving load problem under the quasistatic and frictionless assumptions. A detailed analytic solution in the small viscoelasticity approximation has been developed in the above mentioned papers, whose main conclusions were later summarized in [45] and [47]. Further developments in the same area included [44, 46] concerning the three-dimensional steady-state normal indentation problem for a general viscoelastic material, [31], which dealt with the steady state indentation of a half-space by several moving indentors and [48], where inertial effects were incorporated into the model developed in [41].

From our standpoint, the approach described in [43], [45] and [47] suits the needs of our research best. The mathematical model used throughout the works cited above for describing the physical processes occurring in the transient moving load problem of a rigid indentor traversing a viscoelastic half-space is sufficiently adequate for qualitative analysis, mathematically transparent and amenable to numerical treatment. In the rest of this chapter we shall discuss the basic assumptions underlying the model

in question and the restrictions placed upon its use by these assumptions. The physical idealizations adopted with the Golden–Graham approach do not compromise the qualitative validity of the results, at the same time reducing substantially the amount of analytical and numerical work needed to be done and making the solution of the original problem possible.

The results of this thesis were presented at the 1997 Annual Meeting of the Canadian Applied Mathematics Society (CAMS) in Toronto [16] and the Ninth Meeting of the Working Group of the Scientific Council on the World Ocean Problems of the Russian Academy of Science in Moscow [17]. A summary of this work can also be found in [18].

2.2 Formulation of the Problem

We shall consider the problem of a single rigid indentor moving across a viscoelastic isotropic half-space $y > 0$. We shall assume that the indentor is moving in the negative direction of the x-axis with a known speed $-V(t)$ ($V(t) > 0$) as illustrated in Figure 2.1. In view of the above, the coordinate of the point of deepest indentation for any time t is given by:

$$x_0(t) = -\int_0^t V(\tau)d\tau \tag{2.2.1}$$

For the *plane strain* conditions to be satisfied, we must consider an indentor of infinite length in the z direction. We shall restrict ourselves to the case of a uniform load along the length of the indentor.

We shall assume that the motion has started at time $t_0 = 0$, before which instance the indentor had been resting for an infinitely long period of time, i.e., since "time immemorial" $t = -\infty$. The origin of the coordinate frame associated with the problem is placed at the point of the deepest indentation under the resting indentor.

The latter is being acted upon by a load $W(t)$, whose value is prescribed for any time. Being pressed into the viscoelastic half-space, the indentor forces the surface underneath it to conform to the indentor's profile. The interval where such compliance is perfect, i.e., where the indentor is in full contact with the half-space, we shall

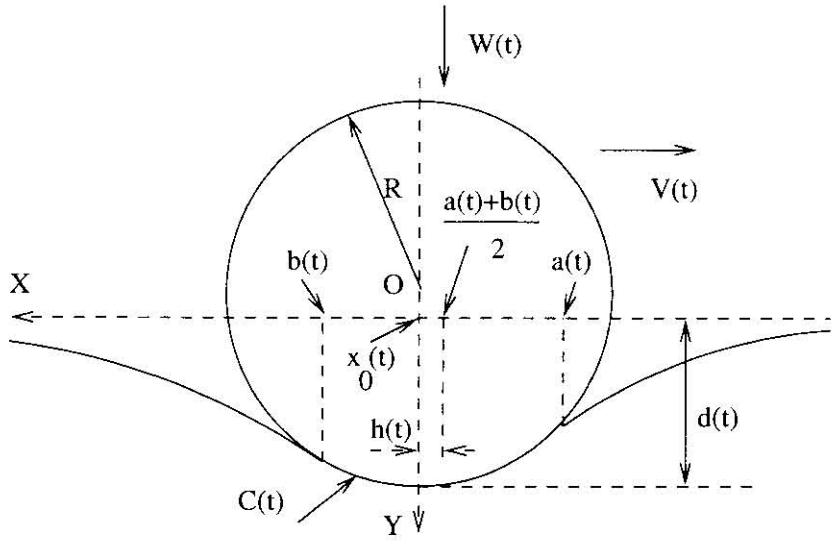

Figure 2.1: Schematic representation of the problem: $C(t) = [a(t), b(t)]$ – contact interval, $x_0(t)$ – point of deepest indentation of the half-plane, x – current point coordinate, $u(x,t)$ – vertical displacement at x, $d(t)$ – maximum displacement, $V(t)$ – indentor speed, $W(t)$ – distributed load

hereinafter term *the contact interval* denoting it as $C(t) = [a(t), b(t)]$. Here $a(t)$ and $b(t)$ are the abscissae of the endpoints. The extent of $C(t)$ is known *a priori* only at times $t \leq 0$, when it can be found using the technique described in later chapters. The radius of the indentor R is chosen to be much larger than the length of the contact interval. This assumption is necessary to remain within the framework of Hertzian analysis and, essentially, the linear theory.

For the derivation of an expression for the displacement in the contact interval let us turn our attention to Figure 2.2.

$$|OA| = \sqrt{R^2 - |AC|^2}, \tag{2.2.2}$$

where $|AC| = x - x_0(t)$. Also,

$$|AB| = R - |OA| = R - \sqrt{R^2 - |AC|^2}. \tag{2.2.3}$$

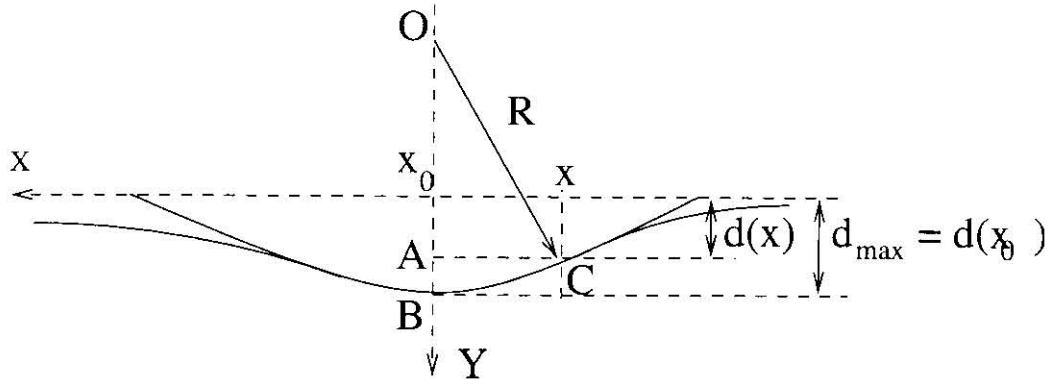

Figure 2.2: Approximate calculation of the derivative of the indentor profile for a cylindrical indentor of large radius: $x_0(t)$ - point of deepest indentation, d_{max} - maximum displacement (occurring at the tip of the indentor with coordinate $x_0(t)$), $d(x)$ - displacement at x.

Hence,

$$d(x) = d(x_0(t)) - |AB| = d(x_0(t)) - R + \sqrt{R^2 - (x - x_0(t))^2} \tag{2.2.4}$$

Of particular interest to us will be the derivative of the displacement $d(x)$. From 2.2.4,

$$d'(x) = -\frac{x - x_0(t)}{\sqrt{R^2 - (x - x_0(t))^2}} = -\frac{x - x_0(t)}{R\sqrt{1 - \left(\frac{x - x_0(t)}{R}\right)^2}}. \tag{2.2.5}$$

Recalling that by assumption, $\frac{x - x_0(t)}{R} \ll 1$, we can approximate (2.2.5) as

$$d'(x) \approx -\frac{x - x_0(t)}{R} \tag{2.2.6}$$

to the first order of accuracy. We shall use (2.2.6) later in this thesis without stressing its approximate nature. Also, because $x_0 = x_0(t)$ for the moving indentor is a function of the current instance of time t, we shall further use a widely accepted notation $u(x,t)$ instead of $d(x)$ for the vertical displacement at point x inside and outside the contact patch to emphasize the time dependency. The derivative of $d(x)$ in (2.2.5) and (2.2.6) will become a partial derivative with respect to x for $u(x,t)$.

As the indentor starts moving, the shape and extent of the contact interval change. To simplify the mathematics, we shall henceforth adopt a *non-inertial approximation.* In our view, this idealization does not seem overly restrictive, since for gradually varying speeds the resistance of the material of the half-space to the motion of the indentor is far more substantial then the effect of inertial forces upon the latter. To avoid the temperature dependence in the constitutive equations, we shall adhere to the isothermality hypothesis.

By and large, in the rest of the analysis we assume that the shape of the indentor is circular. We also use the standard linear model as described in [45]. The model in question is qualitatively adequate for theoretical purposes, being at the same time quite simple in the mathematical sense. It allows one to evaluate the integrals involving convolutions of the complex viscoelastic moduli in the closed form.

We shall also use *frictionless approximation.* It allows one to investigate the phenomenon of internal energy losses in the material within the theoretical framework of linear viscoelasticity. Since the value of ordinary Coulomb friction in the case of the rolling contact problem is relatively small (see, e.g., [11] and [36]), we can, for theoretical purposes, neglect it in favour of focussing on purely hysteretic effects. The impact of this assumption on the boundary conditions for the problem under consideration will be spelled out in Chapter 3.

It is worth mentioning here, that the frictionless assumption may be replaced with the so-called *proportionality assumption* when constructing a solution of the initial-boundary value problem. The proportionality assumption states that the shear and bulk (viscoelastic) moduli are proportional, from which fact it naturally follows that the (viscoelastic) *Lamè constants* $\lambda(t)$ and $\mu(t)$ are proportional. This leads to a constant Poisson's ratio for the material and essentially allows one to describe the creep behaviour of the viscoelastic material in terms of relaxation or vice versa. The proportionality assumption is valid for all incompressible viscoelastic materials and for small deformations of rubbers and elastomers.

Changes in the shape and extent of the contact interval lead to the redistribution of pressure inside it. Having found the pressure distribution at every moment in time, we shall be able to calculate the resisting force exerted inside the material by the

moving indentor and relate it to the applied load. The resulting ratio, a dimensionless quantity, is termed *the coefficient of hysteretic friction.* The determination of this quantity, along with the length of the contact interval $C(t)$ and the measure of its asymmetry $h(t)$ (see Figure 2.1) presents the object of this thesis. A relationship between the abovementioned parameters will be established and an explanation for their behaviour will be provided for the case of transient motion.

2.3 The Nature of Hysteretic Friction

We shall now provide a brief explanation of the phenomenon of hysteretic friction based largely upon [11], [36] and [92].

In any dynamic contact of two bodies there exists a frictional force opposing the direction of motion. This force is due to molecular adhesion between the surfaces of the two bodies and deformation of the bodies themselves (see [92]). First, consider the adhesion component of friction. The experiments of Reynolds [107] with the rolling of a metal cylinder on red bung rubber showed that the surface of the indented material was stretched inside the contact interval by a visually detectable amount. Reynolds's explanation of this phenomenon attributed the stretching to an interfacial slip between the cylinder and the surface of rubber. However, as pointed out in [92], the contribution of this microslip effect, and hence of the whole adhesion term, to the total value of rolling friction is fairly small. It has been confirmed experimentally (see [11]) that lubrication of the contact surfaces does not substantially reduce the total value of rolling friction. We must therefore conclude that a major part of the latter has to be attributed to the deformation of the viscoelastic half-space.

For a perfectly elastic material, the application of an instantaneous stress leads to an instantaneous development of strain. As soon as the pressure is removed, the material immediately recovers and the strain vanishes. Therefore, as the rolling cylinder advances along the surface of an underlying *elastic* material, the contact interval remains symmetric, as shown in Figure 2.3

In fact, as the indentor inches forward, the pressure is being applied to the segment $[a(t); a(t-\Delta t)]$ of the new contact interval $C(t)$ for the first time in the history of

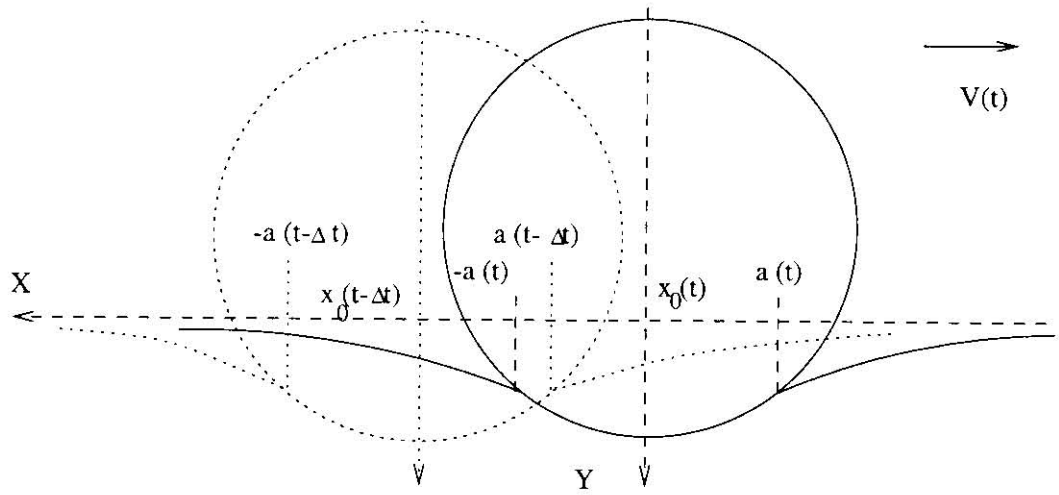

Figure 2.3: Rolling of a cylindrical indentor over elastic half-space. The contact interval is symmetric at all times: $C(t-\Delta t) = [-a(t-\Delta t); a(t-\Delta t)]; C(t) = [-a(t); a(t)]$.

motion. At the same time, the pressure is lifted from the segment $[-a(t); -a(t-\Delta t)]$ and the material instantaneously regains its pre-stressed shape. The increase in pressure in the front of $C(t)$ is fully compensated by its decrease in the rear and no redistribution of pressure occurs. In other words, since the energy stored in the material in the process of deformation is fully released during the process of recovery, no energy losses take place.

The picture is qualitatively different for a viscoelastic material. In this case instantly applied stress does not result in an instantaneous response any more. To illustrate this behaviour, we refer to the so-called *standard linear solid.* This relatively simple and quite transparent idealization allows us to describe qualitatively the observed experimental data pertaining to such model. However, this model does not seem to be adequate for quantitative analysis. The standard linear model is represented in Figure 2.4.

Suppose that a fixed stress σ is suddenly applied at time t_0 to the model described by the system depicted in Figure 2.4. The spring E_1 is instantaneously deformed and transmits the stress to a combination of spring E_2 and dashpot η in parallel. Here

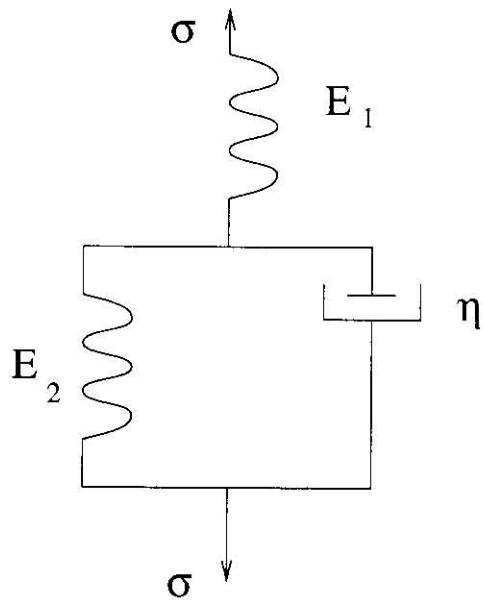

Figure 2.4: Standard linear model. E_1, E_2 – spring elements, η – dashpot element

the deformation is gradual and depends on the relationship between the values of the Hooke's modulus of the spring material and the viscosity of the fluid in the dashpot. Since we are only interested in *visco*elastic solids, we assume that the dashpot is characterized by a non-vanishing viscosity (the fact that we are considering a *solid* requires that $E_2 \neq 0$). This implies a finite value of strain ϵ resulting from a finite applied stress σ. We can write:

$$\epsilon(t) = J(t - t_0)\sigma, \tag{2.3.1}$$

where $J(t)$ is the *creep function.* In the case of a standard linear solid

$$J(t) = J_0 + J_1(1 - e^{-\frac{t}{\tau'}}), \tag{2.3.2}$$

where t is the time, J_0 and J_1 are positive constants, τ' is a positive decay constant. A sketch of the behaviour of $J(t)$ is represented in Figure 2.5. Note that for other types of viscoelastic solids $J(t)$ may diverge as $t^\alpha, \alpha < 1$. Observe also that a standard linear solid eventually recovers after the applied stress has been removed. However, this happens after a time delay that is caused by internal losses in the material.

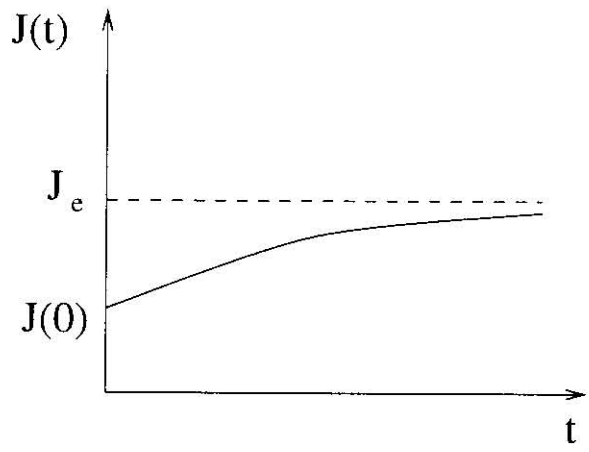

Figure 2.5: Creep function of a standard linear solid. $J_e = J(\infty) = \lim_{t\to\infty} J(t)$ - elastic limit.

Suppose now that we suddenly apply fixed strain ϵ to the model described by Figure 2.4. The value of stress induced in the system will then gradually relax , absorbed by the viscous element represented by the dashpot. We can write:

$$\sigma(t) = G(t - t_0)\epsilon, \tag{2.3.3}$$

where $G(t)$ is the *relaxation function.* In the case of a standard linear solid

$$G(t) = G_0 + G_1 e^{-\frac{t}{\tau}}, \tag{2.3.4}$$

where t is the time, G_0 and G_1 are positive constants, τ is the positive decay constant related to τ' through

$$\tau = \tau' \frac{J_0}{J_0 + J_1} \tag{2.3.5}$$

or

$$\tau' = \tau \frac{G_0 + G_1}{G_0}. \tag{2.3.6}$$

The qualitative behaviour of $G(t)$ is depicted in Figure 2.6. While internal molecular forces in the body resist the deformation caused by the imposition of initial strain, they eventually relax to their limiting value. This is reflected in the fact that $G(t)$ asymptotically tends to G_e as time progresses.

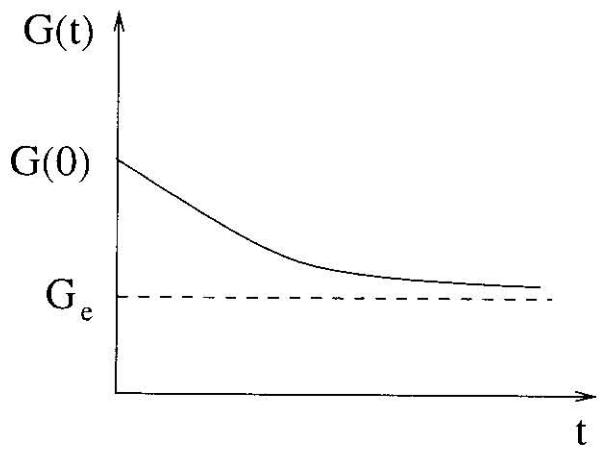

Figure 2.6: Relaxation function of a standard linear solid.

The creep and relaxation phenomena help us explain the physical processes taking place during the contact interaction of a rigid indentor with a viscoelastic half-space. First, let us use a simplified model of a viscoelastic medium introduced in the analysis of Bueche and Flom [35] and shown in Figure 2.7. Here the medium is treated as a set of independent viscoelastic columns. As the indentor rolls over the surface, the columns in the front of it are being depressed, while those in the rear are being freed from normal pressure. A typical strain history of a column being subjected to a suddenly imposed stress and then after a while released from pressure is shown in Figure 2.8 As stress is applied to the column, i.e. the indentor rolls over it for the first time (point A on the graph), the material responds elastically which results in an instantaneous development of strain $\epsilon(A)$. Throughout the period (AB) when the stress is maintained, i.e. the column remains under the indentor, the material creeps to a new value of strain $\epsilon(B)$. At this point stress is removed, i.e. the column is left behind the indentor (point C on the graph), and the material recovers elastically with the value of strain changing from $\epsilon(B)$ to $\epsilon(C)$. Subsequent recovery is in the form of creep which accompanies the decrease in the strain value from $\epsilon(C)$ to $\epsilon(D)$. The last part of strain history (CD) ends when the solid regains its pre-stressed state. This simplified model has been used in an analysis by May *at al.* [90], who

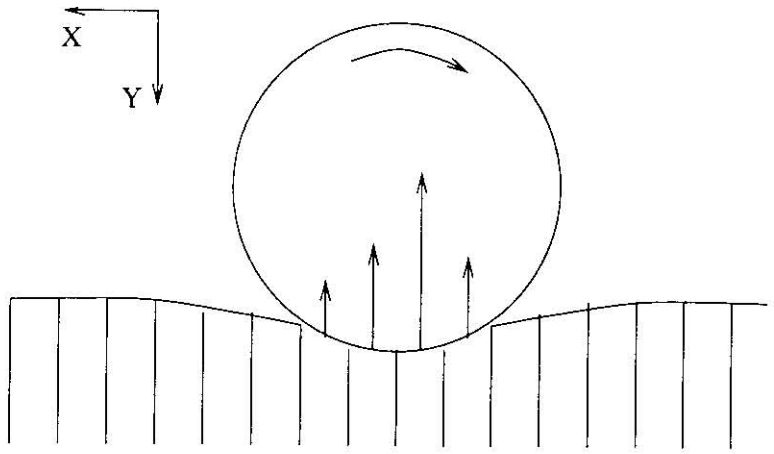

Figure 2.7: Bueche and Flom model: An indentor moving across a viscoelastic half-space represented as a set of independent viscoelastic columns.

were the first to point out the existence of a global maximum of hysteretic friction as a function of speed for a certain finite (intermediate) value of the indentor speed.

If the speed of the indentor is low, the segments of strain history pertinent to viscoelastic behaviour (AB and CD) are shorter than the time required for the indentor to move from one elementary column to another. Therefore we can assume that only elastic recovery takes place and the picture is the same as in the case of an elastic material. However, if the speed of the indentor is higher (*intermediate speed*), an elementary column behind the indentor does not have enough time to recover completely at the same time as the new column enters the contact interval and is being depressed. Obviously, this situation can arise not only when the indentor itself is moving at intermediate speeds, but also when the characteristic creep time for the medium is large. It is well confirmed by experiment that the part of the contact interval between the front point of contact and the point of deepest indentation is larger than its rear part. In other words, the centre of the contact interval is shifted in the direction of motion (see Norman [100]).

As the contact interval becomes deformed, the pressure inside it is redistributed.

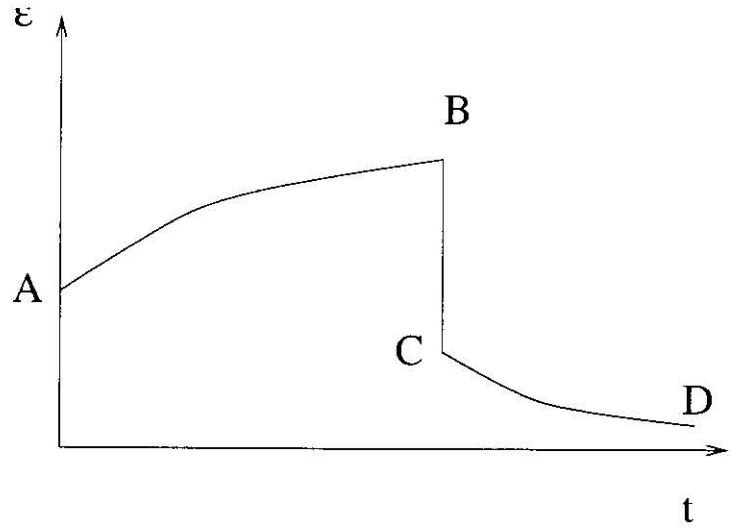

Figure 2.8: Typical history of strain. A– stress is suddenly applied, B– stress is instantaneously removed, C– material recovered elastically, D– material continues to recover viscoelastically (complete recovery asymptotically achieved at large times

The total normal load $W(t)$ acting upon the indentor remains unchanged:

$$W(t) = \int_{a(t)}^{b(t)} p(x,t)dx, \tag{2.3.7}$$

where $p(x,t)$ is the normal pressure at the point x inside the contact interval.Notice here, that the line of application of the resulting force $\vec{W}(t)$ passes through the centre of the indentor. However, the resultant of the normal reaction $\vec{N}(t)$ of the viscoelastic half-space under the indentor does not pass through the line of deepest indentation any more, but rather is shifted in the direction of motion as shown in Figure 2.10. This shift begets a moment about the centre of the cylinder. The value of the above mentioned moment can be found as

$$M(t) = \int_{a(t)}^{b(t)} (x - x_0(t))p(x,t)dx. \tag{2.3.8}$$

In order for the indentor to remain in a state of equilibrium as required by the non-inertial hypothesis adopted earlier, an equal moment acting in the opposite direction must exist. It is natural to assume that this moment is due to a force acting upon

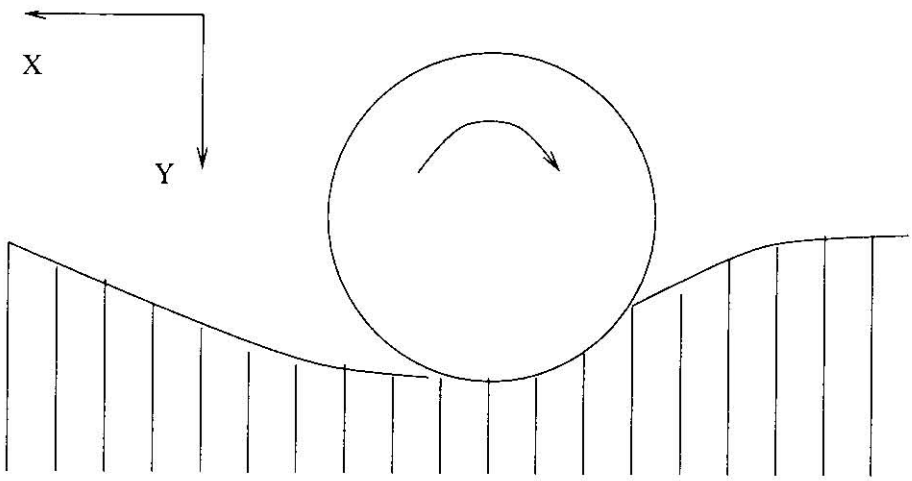

Figure 2.9: Asymmetric contact interval.

the indentor inside the contact interval and opposing the direction of motion. Since we have adopted the frictionless hypothesis earlier, we must conclude that the nature of this force lies outside the phenomenon of regular Coulomb friction. Such a force can be computed by equating its moment to the resulting moment of pressure forces and dividing it by the indentor radius R:

$$F_h(t) = \frac{1}{R}M(t) = \frac{1}{R}\int_{a(t)}^{b(t)}(x - x_0(t))p(x,t)dx. \tag{2.3.9}$$

For speeds much higher than intermediate, (*high speeds*), the impact of the indentor on a given viscoelastic column becomes almost instantaneous, and the material response is elastic (AB). The contact interval again becomes symmetric, although its length differs from the *low speed* case.

The Bueche and Flom analysis allows us to make important qualitative conclusions about the existence of F_h. The model considered up to this point, however, does not account for the shear stress between the elementary columns, which is responsible for a substantial part of the force resisting the rolling of the cylinder. To remedy the situation, the model can be improved to include interaction between the columns, as is done, for example, in the Winkler medium [19]. We shall nevertheless return to the general standard linear continuum model from now on.

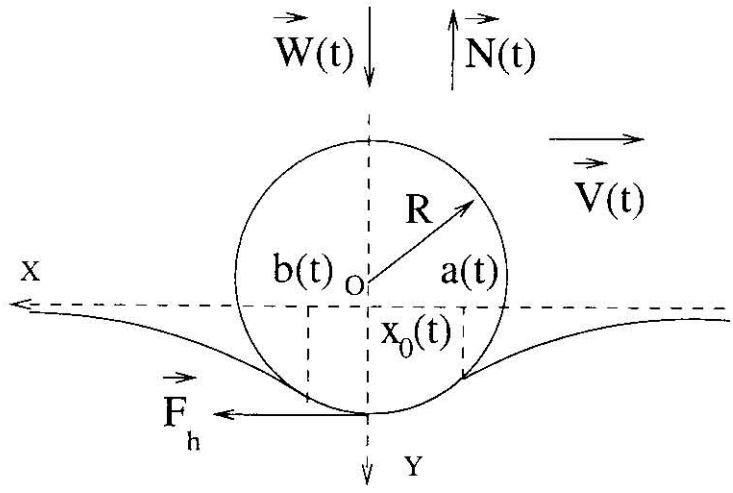

Figure 2.10: Dynamic equilibrium of the indentor on the half-space. $\vec{F}_h$– hysteretic friction, $\vec{N}(t)$– resultant of the normal reaction of the viscoelastic solid under the indentor.

To comment on the physical nature of F_h, let us recall a well-known relationship between stress and strain in materials with memory. A graphic representation of this relationship is presented in Figure 2.11 and is called a *hysteresis loop*. The shaded area inside the hysteresis loop represents the energy dissipated during the loading-unloading cycle reflected by the loop. Internal losses in the material are due to energy irreversibly consumed during the rearrangement of molecules inside the material and dissipated into heat. These losses do not occur in an elastic material where all the energy required to deform the body is released in the process of its recovery. In a viscoelastic material, however, such energy losses may be quite high. The parallels between the way F_h and the ordinary Coulomb friction affect the rolling of the indentor prompt one to term F_h *hysteretic friction*. As pointed out by Bowden and Tabor in [11], even in metals hysteretic losses, or hysteretic friction, can reach quite sizeable proportions. Hysteretic friction plays an important role in the analysis of processes occurring in roller bearings, during the motion of a locomotive wheel on the rail whenever it can be treated in the viscoelastic range (i.e., when no plastic deformation is accounted for), in analyzing geological flows etc. When ordinary

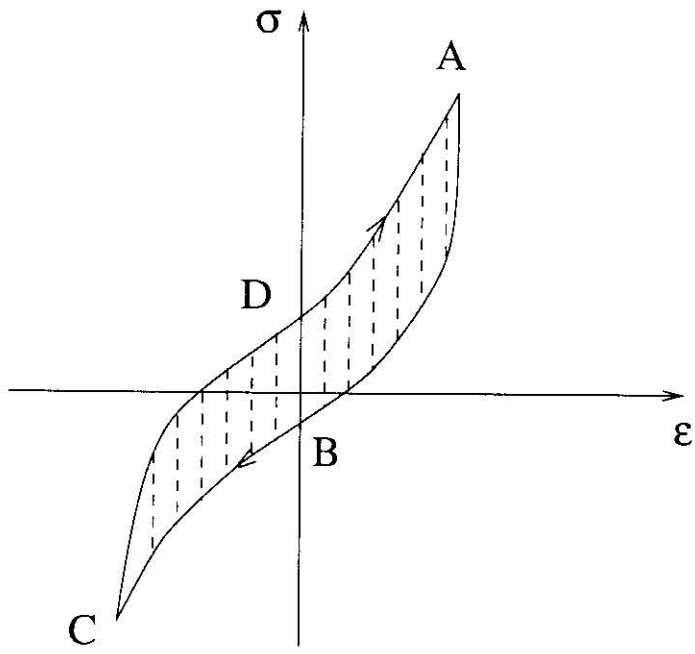

Figure 2.11: Hysteresis loop for materials with memory.

Coulomb friction is left out of consideration, the theory of hysteretic friction offers a theoretical framework that allows one to investigate this specifically viscoelastic phenomenon in great detail.

A mathematical expression for hysteretic friction is derived in Section 3.3 on the basis of energy considerations.

Chapter 3

Mathematical Formalism

3.1 Constitutive Equations and Boundary Conditions

To derive a set of integral equations governing the behaviour of a viscoelastic material under the previously stated conditions, we recall the elastic stress-strain relationship ([113])

$$\sigma_{ij}(\vec{r},t) = 2\mu\epsilon_{ij}(\vec{r},t) + \delta_{ij}\lambda\epsilon_{kk}(\vec{r},t) \tag{3.1.1}$$

where σ_{ij} and ϵ_{ij} are the stress and strain tensors respectively, $\delta_{ij} = \begin{cases} 0, & i \neq j \\ 1, & i = j \end{cases}$ is the Kroneker delta symbol, λ and μ are Lamé constants. Here the stress at time t is determined by the strain at time t and vice versa.

For an isotropic viscoelastic material, we must account for the previous history of stress and strain in order to be able to determine their current values. This can be achieved by incorporating the time dependency into all members of (3.1.1) and replacing products with convolutions:

$$\sigma_{ij}(\vec{r},t) = 2\int_{-\infty}^{t} dt'\,\mu(t-t')\epsilon_{ij}(\vec{r},t') + \delta_{ij}\int_{-\infty}^{t} dt'\,\lambda(t-t')\epsilon_{kk}(\vec{r},t'), \tag{3.1.2}$$

where $\vec{r}$ is the position vector of the given point (x,y).

In (3.1.2) λ and μ are viscoelastic response functions (see, e.g., [45]), $\delta(t) =$

$\begin{cases} 0, & t \neq 0 \\ \infty, & t = 0 \end{cases}$, $\int_{-\infty}^{\infty} \delta(t)dt = 1$ is the Dirac delta function, $H(t) = \begin{cases} 0, & t \leq 0 \\ 1, & t \geq 0 \end{cases}$ is the Heaviside step function.

The above approach relating the elastic and viscoelastic constitutive equations allows for the application of the Classical Correspondence Principle [37], which provides for the derivation of a viscoelastic solution from its elastic counterpart. This principle can also be extended to include a wider class of problems as shown in [45].

The boundary conditions for the problem under consideration are as follows. Inside the contact interval $C(t)$ the surface of the viscoelastic half-space conforms to the shape of the indentor as shown on Fig. 3.1 Therefore, the vertical displacement at

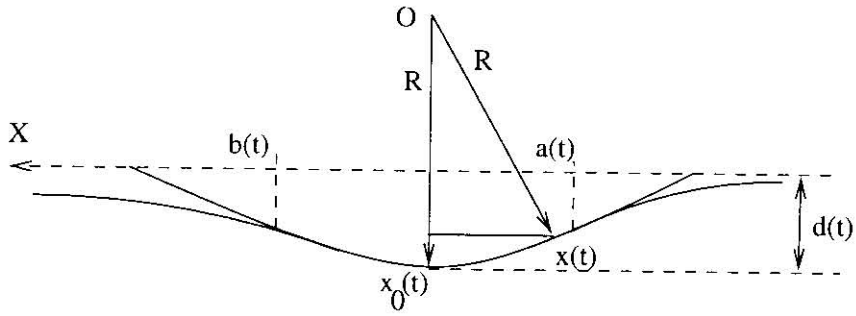

Figure 3.1: Contact interval boundary: $C(t) = [a(t), b(t)]$ – contact interval, $x_0(t)$ – point of deepest indentation of the half-space, $d(t)$ – maximum displacement, R – indentor radius, $x(t)$ – current point coordinate.

the point with coordinate x can be found from geometric considerations. Outside the contact interval $C(t)$ the displacement is unprescribed because the material relaxes to its steady state only gradually. Hence the boundary conditions yield, in view of (2.2.6):

$$u_y(x,t) = \begin{cases} d(t) - \frac{(x-x_0(t))^2}{2R}, & x \in C(t) \\ unknown, & x \notin C(t) \end{cases} \tag{3.1.3}$$

Since we shall henceforth be mostly interested in the vertical displacement, we shall hitherto drop the y-subindex of u.

The pressure, contrary to vertical displacement, is zero outside $C(t)$. Inside $C(t)$

the distribution of pressure, unlike in the elastic case, becomes asymmetric as the indentor moves along and thus cannot be determined without the knowledge of all previous history:

$$p(x,t) = \begin{cases} (\ nonnegative\ )unknown, & x \in C(t) \\ 0, & x \notin C(t) \end{cases} \tag{3.1.4}$$

Coulomb friction is neglected and hence does not contribute to the boundary conditions.

As follows from the discussion in Chapter 2, the extent of the contact interval depends on the whole history of strain and stress up to the present moment t. This constant change of the contact interval boundaries with time renders the aforementioned correspondence principles generally inapplicable. In view of this, we must directly compute the solution from the governing field equations. The technique aimed at attacking this problem is described further.

3.2 Complex Variable Solution

In this section we shall alternately use the proportionality assumption and frictionless approximation mentioned in Section 2.2. The proportionality assumption allows one to extend the results of subsequent derivation beyond the frictionless case, however, it restricts the problem under consideration to almost incompressible materials. The frictionless approximation, which is perfectly relevant in our case, lifts the latter restriction, but on the other hand leaves out the possibility of extending the derivation procedure to the frictional case. No matter how the resulting equations are derived, their validity is determined by the physical parameters of the problem and one is, therefore, at liberty to take any of the too routes in the derivation process, as long as the underlying physical assumptions hold.

An analytic solution of the transient rolling contact problem for an isotropic viscoelastic half-space is given by the (viscoelastic) Kolosov-Muskhelishvili equations [45]:

$$\sigma_{11}(\vec{r},t) + \sigma_{22}(\vec{r},t) = 2[\phi(z,t) + \bar{\phi}(\bar{z},t)] = 4\Re[\phi(z,t)] \tag{3.2.1}$$

$$\Sigma(\vec{r},t) = \sigma_{22}(\vec{r},t) - i\sigma_{12}(\vec{r},t) = \phi(z,t) + \bar{\phi}(\bar{z},t) + z\bar{\phi}'(\bar{z},t) + \bar{\psi}(\bar{z},t) \qquad (3.2.2)$$

$$2\int_{-\infty}^{t} dt'\mu(t-t')D'(\vec{r},t') = \int_{-\infty}^{t} dt'k(t-t')\phi(z,t') - \bar{\phi}(\bar{z},t) - z\bar{\phi}'(\bar{z},t) - \bar{\psi}(\bar{z},t), \qquad (3.2.3)$$

where ϕ and ψ are harmonic complex potentials defined for $y > 0$, i.e. inside the viscoelastic half-space, $\Sigma(\vec{r},t)$ is the complex stress on the boundary $C(t)$, σ_{ij} are stress tensor components, $D'(\vec{r},t) = \frac{\partial}{\partial x}u(\vec{r},t)$ is the derivative of the (complex) displacement.

The function $k(t)$ is a so-called *causal* function whose Fourier transform for the case of plane strain relates to that of the Poisson's ratio as

$$\hat{k}(\omega) = 3 - 4\hat{\nu}(\omega) \qquad (3.2.4)$$

Recall here that the Fourier transform of a function $f(t)$ is given by:

$$\hat{f}(\omega) = \int_{-\infty}^{+\infty} dt f(t)e^{-i\omega t} \qquad (3.2.5)$$

A relationship between $\hat{\lambda}(\omega)$, $\hat{\mu}(\omega)$ and $\hat{\nu}(\omega)$ follows immediately from (3.2.4):

$$\hat{\nu}(\omega) = \frac{\hat{\lambda}(\omega)}{2(\hat{\lambda}(\omega) + \hat{\mu}(\omega))} \qquad (3.2.6)$$

The proportionality assumption immediately leads to $\hat{\nu}(\omega) = \nu_0$ being a constant, which, in turn, results in the following simple relationship between $\nu(t)$ and ν_0: $\nu(t) = \nu_0\delta(t)$. Consequently, in view of (3.2.4) we can easily conclude that

$$k(t) = k_0\delta(t), \qquad (3.2.7)$$

where k_0 is a constant. Observe here, that under the proportionality assumption

$$\int_{-\infty}^{t} dt'k(t-t') = k_0 \qquad (3.2.8)$$

Now let us extend the region of analyticity of $\phi(z,t)$ into the lower half-plane as follows [98]:

$$\phi(z,t) = -\bar{\phi}(z,t) - z\bar{\phi}'(z,t) - \bar{\psi}(z,t), \quad \Im z < 0\ . \qquad (3.2.9)$$

Since $\Im\bar{z} < 0$, taking the complex conjugate of (3.2.9) yields:

$$\bar{\psi}(\bar{z},t) = -\phi(\bar{z},t) - \bar{\phi}(\bar{z},t) - \bar{z}\bar{\phi}'(\bar{z},t), \quad \Im z < 0 \ . \tag{3.2.10}$$

This can be substituted into (3.2.1) – (3.2.3) to obtain:

$$\Sigma(\vec{r},t) = \sigma_{22}(\vec{r},t) - i\sigma_{12}(\vec{r},t) = \phi(z,t) + \phi(\bar{z},t) + (z-\bar{z})\bar{\phi}'(\bar{z},t) \tag{3.2.11}$$

$$2\int_{-\infty}^{t} dt'\mu(t-t')D'(\vec{r},t') = \int_{-\infty}^{t} dt'k(t-t')\phi(z,t') + \phi(\bar{z},t) + (\bar{z}-z)\bar{\phi}'(\bar{z},t) \tag{3.2.12}$$

Equation (3.2.12) with the aid of (3.2.8) can immediately be reduced to:

$$2\int_{-\infty}^{t} dt'\mu(t-t')D'(\vec{r},t') = k_0\phi(z,t) + \phi(\bar{z},t) + (\bar{z}-z)\bar{\phi}'(\bar{z},t) \tag{3.2.13}$$

For the purpose of simplifying (3.2.13) further, let us for a moment consider a frictional generalization of the contact problem. Let us introduce the coefficient of Coulomb friction f. Then:

$$\sigma_{12}(x,t) = -f\sigma_{22}(x,t) \tag{3.2.14}$$

Thus

$$\Sigma(x,t) = \sigma_{22}(x,t) - i\sigma_{12}(x,t) = (1+if)\sigma_{22}(x,t) = -(1+if)p(x,t) \tag{3.2.15}$$

Denoting:

$$\lim_{\Im z \to 0+} \phi(z,t) = \phi^+(x,t) \tag{3.2.16}$$

$$\lim_{\Im z \to 0+} \phi(\bar{z},t) = \phi^-(x,t), \tag{3.2.17}$$

and taking the limit of (3.2.34) as z approaches the x axis from above yields with the help of (3.2.15):

$$\phi^+(x,t) - \phi^-(x,t) = -(1+if)p(x,t) \tag{3.2.18}$$

Also, for the complex conjugates:

$$\bar{\phi}^+(x,t) - \bar{\phi}^-(x,t) = -(1-if)p(x,t) \tag{3.2.19}$$

Defining κ as:

$$\kappa = \frac{1-if}{1+if}, \tag{3.2.20}$$

we obtain:

$$\bar{\phi}^+(x,t) - \kappa\phi^+(x,t) = \bar{\phi}^-(x,t) - \kappa\phi^-(x,t) \tag{3.2.21}$$

That is, the function $\bar{\phi} - \kappa\phi$ has a zero jump across the real axis. Assuming that the boundary stresses along the x axis fall off as $\frac{1}{x^2}$ as $x \to \pm\infty$, which is a physically reasonable assumption, we conclude, following Green and Zerna [57], that $\phi(z,t)$ behaves as $\frac{1}{|z|}$ for $|z| \to \infty$. This clearly implies that both $\phi(z,t)$ and $\bar{\phi}(z,t)$ approach zero as $|z| \to \infty$. Therefore, we must conclude from Liouville's theorem [82] that $\bar{\phi}(z,t) - \kappa\phi(z,t) = 0$ everywhere in the complex plane, or:

$$\bar{\phi}(z,t) = \kappa\phi(z,t). \tag{3.2.22}$$

Taking the complex conjugate of (3.2.13) and utilizing (3.2.22), we arrive at:

$$2\int_{-\infty}^{t} dt'\mu(t-t')\bar{D}'(z,t) = k_0\kappa\phi(\bar{z},t) + \kappa\phi(z,t) + (z-\bar{z})\phi'(z,t) \tag{3.2.23}$$

We note in passing that the indented material lies in the upper half-space $y > 0$, which is consistent with the chosen direction of the coordinate axes. By virtue of this, we can justify subtracting (3.2.23) from (3.2.13) and taking the limit of the resulting equation as z approaches the real axis from above to obtain the following relationship on the boundary of the half-plane:

$$2\int_{-\infty}^{t} dt'\mu(t-t')u'(x,t) = \frac{1}{2i}\left\{(k_0-\kappa)\phi^+(x,t) + (1-k_0\kappa)\phi^-(x,t)\right\} \tag{3.2.24}$$

In the frictionless limit $\kappa = -1$ and the above relationship holds. However, in view of (3.2.22), we can take the imaginary part of (3.2.3) and rewrite it as:

$$2\int_{-\infty}^{t} dt'\mu(t-t')u'(x,t) = \frac{1}{2i}\int_{-\infty}^{t} dt'\left[\delta(t-t') + k(t-t')\right]\left[\phi^+(x,t') + \phi^-(x,t')\right] \tag{3.2.25}$$

Equation (3.2.25) may be recast into a simpler form:

$$i\int_{-\infty}^{t} dt' l(t-t')u'(x,t') = \phi^+(x,t) + \phi^-(x,t), \tag{3.2.26}$$

where

$$\hat{l}(\omega) = \frac{4\hat{\mu}(\omega)}{1+\hat{k}(\omega)} = \frac{\hat{\mu}(\omega)}{1-\hat{\nu}(\omega)}, \tag{3.2.27}$$

which did not require the proportionality assumption in its derivation. This means that in the frictionless case there is no need to assume proportionality between the shear and bulk moduli.

We can now proceed to establish the boundary conditions on $\phi(z,t)$ both inside and outside $C(t)$. Outside the contact interval there are no stresses on the boundary of the viscoelastic half-space and (3.2.18) yields:

$$\phi^+(x,t) - \phi^-(x,t) = 0, x \notin C(t) \tag{3.2.28}$$

Furthermore, under the proportionality assumption

$$l(t) = \frac{4\mu(t)}{k_0 - \kappa} \tag{3.2.29}$$

$$\eta = -\frac{1-\kappa k_0}{k_0 - \kappa} = \frac{f+ih}{f-ih} \tag{3.2.30}$$

$$h = \frac{k_0+1}{k_0-1} = \frac{2(1-\nu)}{1-2\nu}, \tag{3.2.31}$$

where both η and h are complex quantities. This allows us to rewrite (3.2.24) as

$$\phi^+(x,t) - \eta\phi^-(x,t) = iv(x,t), \tag{3.2.32}$$

where $v(x,t)$ is defined as

$$v(x,t) = \int_{-\infty}^{t} dt' l(t-t')u'(x,t'). \tag{3.2.33}$$

Observing that $\eta\bar{\eta} = 1$ and so $|\eta| = 1$, we can set $\eta = e^{i2\pi\theta}, \theta \in [0, \frac{1}{2}]$. Therefore,

$$tan(2\pi\theta) = \frac{\Im\eta}{\Re\eta} = \frac{2fh}{f^2-h^2} = 2\frac{\frac{h}{f}}{1-\frac{h}{f}^2}, \tag{3.2.34}$$

which is equivalent to $tan(\pi\theta) = \frac{h}{f}$ or

$$\theta = \frac{1}{\pi} arctan\frac{h}{f}. \tag{3.2.35}$$

Assuming for a moment that $v(x,t)$ is known, which is ordinarily not the case, we can treat (3.2.28) and (3.2.32) as a Hilbert problem in $\phi(z,t)$. The solution to this problem is known [82] and has the form:

$$\phi(z,t) = \frac{X(z,t)}{2\pi}\int_{C(t)} dx' \frac{v(x',t)}{(x'-z)X^+(x',t)} + P(z,t)X(z,t), \tag{3.2.36}$$

where for a single contact interval

$$X(z,t) = (z - a(t))^{1-\theta}(z - b(t))^{\theta}, \tag{3.2.37}$$

where $P(z,t)$ is a polynomial chosen so that $|\phi(z,t)|\underset{|z|\to\infty}{\longrightarrow} 0$. In the case of a smooth indentor, $P(z,t) \equiv 0$. For the solution of (3.2.36) to exist, a *solvability condition* in the form of

$$\int_{C(t)} dx \frac{v(x,t)}{X^{+}(x,t)} = 0, \tag{3.2.38}$$

where $X^{+}(x',t) = \lim_{\Im z \to 0+} X(x',t)$ must also hold [82].

Now we would like to derive a relationship between $v(x,t)$ inside and outside the contact interval. For that purpose, we can continue $v(x,t)$ analytically onto the outside of $C(t)$. Equation (3.2.32) combined with (3.2.28) yields

$$\phi(x,t)(1-\eta) = iv(x,t), x \notin C(t) \tag{3.2.39}$$

In view of analyticity, $\phi^{+}(x,t) = \phi^{-}(x,t) = \phi(x,t)$. Recalling the definition of θ, we can rewrite (3.2.39) as

$$v(x,t) = -2\sin(\pi\theta)e^{i\pi\theta}\phi(x,t), x \notin C(t). \tag{3.2.40}$$

Substituting (3.2.40) into (3.2.36), we obtain:

$$v(x,t) = -\frac{\sin\pi\theta e^{i\pi\theta}X(x,t)}{\pi}\int_{C(t)} dx' \frac{v(x',t)}{(x'-x)X^{+}(x',t)}, \quad x \notin C(t). \; . \tag{3.2.41}$$

We shall now derive the equation for pressure inside the contact interval. Because the extent of $C(t)$ is not known in advance, even though the total normal load can be safely assumed to be known, the pressure distribution has to be determined at each time t separately. With the help of (3.2.18) and (3.2.32) we can write:

$$-(1+if)p(x,t) = \phi^{+}(x,t)(1-\frac{1}{\eta}) + \frac{i}{\eta}v(x,t) \tag{3.2.42}$$

We now recall [82] that if at any regular point ζ on a smooth arc C $f(\zeta)$ obeys the Hölder condition with $0 < \mu \leq 1$, i.e.

$$|f(z) - f(\zeta)| \leq A|z-\zeta|^{\mu}, \tag{3.2.43}$$

where A is some constant, then the Cauchy-type integral

$$F(z) = \frac{1}{2\pi i}\int_C \frac{f(u)du}{u-z} \tag{3.2.44}$$

has limiting values $F^+(\zeta)$ and $F^-(\zeta)$ on both sides of the arc C such that for any $\zeta \in C$

$$\begin{cases} F^+(\zeta) &= F(\zeta) + \frac{1}{2}f(\zeta) \\ F^-(\zeta) &= F(\zeta) - \frac{1}{2}f(\zeta) \end{cases} \tag{3.2.45}$$

Since $\frac{\phi(z,t)}{X(z,t)}$ and $\frac{iv(x,t)}{X^+(x,t)}$ can be substituted into (3.2.44) - (3.2.45) for F and f respectively, one can therefore obtain:

$$p(x,t) = -\frac{1}{1+if}\left[(1-\frac{1}{\eta})\frac{X^+(x,t)}{2\pi}\int_{C(t)} dx' \frac{v(x',t)}{(x'-x)X^+(x',t)} + \frac{i}{2}(1+\frac{1}{\eta})v(x,t)\right] \tag{3.2.46}$$

Recalling that $\eta = e^{i2\pi\theta}$, we can replace $\frac{1}{2}(1+\frac{1}{\eta})$ by $\cos(\pi\theta)e^{-i\pi\theta}$ and $\frac{1}{2}(1-\frac{1}{\eta})$ by $-i\sin(\pi\theta)e^{-i\pi\theta}$. Thereby

$$p(x,t) = \frac{ie^{-i\pi\theta}}{1+if}\left[\frac{\sin(\pi\theta)X^+(x,t)}{\pi}\int_{C(t)} dx' \frac{v(x',t)}{(x'-x)X^+(x',t)} - \cos(\pi\theta)v(x,t)\right] \tag{3.2.47}$$

For the frictionless limit ($\theta = \frac{1}{2}, f = 0$) we have for a single load:

$$X^+(x,t) = (x-a(t))^{\frac{1}{2}}(x-b(t))^{\frac{1}{2}}, \tag{3.2.48}$$

or, since $X^+(x,t)$ is a real number for any $x \notin C(t)$

$$X^+(x,t) = \begin{cases} -\sqrt{(a(t)-x)(b(t)-x)}, & x < a(t) \\ \sqrt{(x-a(t))(x-b(t))}, & x > b(t) \end{cases} \tag{3.2.49}$$

Hence (3.2.41) reduces to

$$v(x,t) = \mp\frac{n(x,t)}{\pi}\int_{C(t)} dx' \frac{v(x',t)}{(x'-x)m(x',t)}, \tag{3.2.50}$$

where "-" corresponds to $x < a(t)$ and "+" to $x > b(t)$,

$$\begin{cases} n(x,t) &= |x-a(t)|^{\frac{1}{2}}|x-b(t)|^{\frac{1}{2}}, & x \notin C(t), \\ m(x,t) &= \sqrt{(b(t)-x)(x-a(t))}, & x \in C(t) \end{cases} \tag{3.2.51}$$

and (3.2.47) becomes

$$p(x,t) = -\frac{m(x,t)}{\pi}\int_{C(t)} dx' \frac{v(x',t)}{(x'-x)m(x',t)}. \tag{3.2.52}$$

Integrating (3.2.52) along $C(t)$ with respect to x and changing the order of integration, we obtain an expression for the normal load $W(t)$:

$$W(t) = -\int_{C(t)} dx \frac{xv(x,t)}{m(x,t)} \tag{3.2.53}$$

since

$$\frac{1}{\pi}\int_{C(t)} dx \frac{m(x,t)}{x'-x} = \frac{b+a}{2} - x, x \in C(t), \tag{3.2.54}$$

$$W(t) = \int_{C(t)} dx p(x,t), \tag{3.2.55}$$

bearing in mind that, with the help of (3.2.49), (3.2.38) becomes:

$$\int_{C(t)} dx \frac{v(x,t)}{m(x,t)} = 0. \tag{3.2.56}$$

The *loading condition* (3.2.53) coupled with the *solvability condition* (3.2.38) completes the system for determining the solution of the main equation (3.2.56) in terms of the three unknown functions: $v(x,t), a(t)$ and $b(t)$. An equivalent of (3.2.53) in the frictional case has a more complicated structure, but can also be derived if necessary [45].

3.3 Calculation of Hysteretic Friction

Inside the contact interval $C(t)$ the pressure on the boundary of the viscoelastic half-space balances off the $y-y$ component of the stress tensor:

$$p(\vec{r},t) = -\sigma_{22}(\vec{r},t) \tag{3.3.1}$$

In the presence of Coulomb friction the shear stress on the boundary is

$$s(\vec{r},t) = -V(t)fp(\vec{r},t) \tag{3.3.2}$$

where $V(t)$ is the speed of the moving indentor, f is the coefficient of friction. This is the ordinary rolling friction that can be observed in both elastic and viscoelastic materials. However, as has been pointed out earlier (Section 2.3), the very molecular structure of a viscoelastic material provides for energy losses that cannot be attributed to the surface interaction between two surfaces. Therefore, we must analyze the total energy balance during the process of motion of the indentor across the impacted half-space to arrive at the appropriate mathematical model of hysteretic friction.

The rate of work $\dot{E}$ done by external and body forces on a viscoelastic medium is given in the most general case by:

$$\dot{E}(t) = \int_V dv b_i(\vec{r},t)\dot{u}_i(\vec{r},t) + \int_B ds s_i(\vec{r},t)\dot{u}_i(\vec{r},t), \tag{3.3.3}$$

where b_i are the components of body forces acting upon the half-space, u_i are the displacements, s_i surface tractions, V is the volume of the medium, B the surface of the boundary of $C(t)$ and " . " denotes the time derivative. The zero body force assumption implies that $b_i = 0$. Inside the contact interval we have for the (vertical) displacements:

$$u = d(t) - h(x - x_0(t)), \tag{3.3.4}$$

where $d(t)$ is the point of deepest indentation, x is the current coordinate of the point, $x_0(t)$ is the coordinate of the tip of the indentor, $h(\xi)$ is the shape of the indentor profile. On an undeformed boundary, $ds = dx, S_x(\vec{r},t) = 0, S_y(\vec{r},t) = p(x,t)$. Thus from (3.3.3) we can deduce:

$$\dot{E} = \int_{C(t)} dx p(x,t)\dot{u}(x,t) \tag{3.3.5}$$

Hence, employing (3.3.4),

$$\dot{E}(t) = \dot{d}(t)\int_{C(t)} dx p(x,t) + \int_{C(t)} dx p(x,t)h'(x - x_0(t))\dot{x}_0(t), \tag{3.3.6}$$

where the prime indicates the derivative of h with respect to its argument. Recalling

$$W(t) = \int_{C(t)} dx p(x,t), \tag{3.3.7}$$

where $\dot{x}_0(t) = V(t)$ is the indentor velocity, we arrive at

$$\dot{E}(t) = \dot{d}(t)W(t) + \int_{C(t)} dx p(x,t)h'(x - x_0(t))V(t) \tag{3.3.8}$$

for an indentor moving in the negative direction of the $x-$axis. Observe here that the first term in (3.3.8) is the power of the normal load on the maximum displacement while the second comprises of two factors. One of them is the speed $V(t)$, the other has the same dimension as the normal load. It is therefore natural to normalize the said second term by $W(t)$:

$$f_H = \frac{1}{W(t)} \int_{C(t)} dxp(x,t)h'(x - x_0(t)). \tag{3.3.9}$$

Then the second term in (3.3.8) will take the "frictional" form cf. (3.3.2):

$$\dot{E}(t) = \dot{d}(t)W(t) + V(t)f_H W(t). \tag{3.3.10}$$

As follows from the boundary conditions (3.1.3), (2.2.6), (3.3.9) can be rewritten as:

$$f_H = \frac{1}{W(t)} \int_{C(t)} dxp(x,t) \left(-\frac{x - x_0(t)}{R} \right) \tag{3.3.11}$$

This expression for the coefficient of hysteretic friction is valid in the transient case. Mathematically f_H is a ratio between the force required to keep the indentor in motion and the normal load acting upon the indentor. The analogy between the Coulomb friction coefficient f in (3.3.2) and f_H in (3.3.11) is quite transparent.

Chapter 4

The Main Integral Equation

4.1 Decomposition of Hereditary Integrals

Equation (3.2.33) provides a simple means of calculating $v(x,t)$ once the displacement derivative $u'(x,t)$ is known. However, boundary conditions (3.1.3) do not allow for the determination of $u'(x,t)$ unless $x \in C(t)$. Therefore, we shall decompose the time interval $(-\infty, t]$ onto segments so that the given point x is either inside or outside $C(t)$ for each given subinterval.

For a single indentor, this means that for each point x we can introduce a *transition time* $t_1(x)$. This instance marks the moment when the indentor first comes into contact with the boundary of the viscoelastic half-space with coordinate x. For all $t < t_1(x)$ we can observe that $x \notin C(t)$, so the *displacement derivative* $\frac{du}{dx}$ on the boundary is unprescribed, while stresses on the boundary are zero, as follows from the boundary. For all $t \geq t_1(x)$ such that $x \in C(t)$ the displacement derivative $\frac{du}{dx}$ is known (because for all such x the surface of the half-space complies with the surface of the indentor), while stresses (at each x such that $x \in C(t)$) are yet unprescribed as follows from the boundary conditions (3.1.3) and (3.1.4).

In view of the above, (3.2.33) takes the form:

$$v(x,t) = \int_{t_1(x)}^{t} dt'\, l(t-t')u'(x,t') + \int_{-\infty}^{t_1(x)} dt'\, l(t-t')u'(x,t') \qquad (4.1.1)$$

The first integral in (4.1.1) involves only known quantities. The second integral can be

rewritten in terms of $v(x,t)$ since the relationship (3.2.33) can be inverted as follows from (3.2.27) (recall also that $l(t) = k(t) = 0 \forall t < 0$):

$$u'(x,t) = \int_{-\infty}^{t} dt' k(t-t') v(x,t'), \tag{4.1.2}$$

where $k(t)$ is a convolution inverse of $l(t)$, i.e.:

$$\int_{0}^{t} dt' l(t-t') k(t') = \delta(t) \tag{4.1.3}$$

Recalling the definition of $t_1(x)$, we can write with the help of (4.1.2):

$$v(x,t) = \int_{-\infty}^{t_1(x)} dt' l(t-t') \int_{-\infty}^{t'} dt'' k(t'-t'') v(x,t'') + \int_{t_1(x)}^{t} dt' l(t-t') u'(x,t'), x \in C(t) \tag{4.1.4}$$

Interchanging the order of integration in the first term of (4.1.4), we obtain:

$$v(x,t) = \int_{-\infty}^{t_1(x)} dt' T_1(t,t') v(x,t') + \int_{t_1(x)}^{t} dt' l(t-t') u'(x,t'),\ x \in C(t), \tag{4.1.5}$$

where:

$$T_1(t,t') = \int_{t'}^{t_1(x)} dt'' l(t-t'') k(t''-t') \tag{4.1.6}$$

In the case of an indentor moving to and fro, the point x may have left the contact interval $C(t)$ and subsequently re-entered it several times throughout the preceding history. Should we decide to investigate this case, we would have to account for more than one contact interval. Therefore, further decomposition may be required. To this end, another transition time, $t_2(x)$ should be brought into consideration and $T_2(t,t')$ derived through $T_1(t,t')$.

This iteration process can be extended to any finite number n of contact intervals if a sequence of transition times $-\infty < t_n < t_{n-1} < \ldots < t_2 < t_1 < t$ is considered and a set of $T_i(t,t')$ is derived recursively for use in an appropriate analog of (4.1.5). Such a generalization, however, leads to considerable mathematical and algorithmic complications. Since our attention is focussed on the case of an indentor moving in the same direction, we shall only employ (4.1.5) - (4.1.6) for the derivation of the main integral equation for $v(x,t)$.

4.2 The Main Integral Equation for v(x,t)

In the case of a single contact interval we can rewrite (4.1.5) as

$$v(x,t) = \int_{-\infty}^{t_1(x)} dt' \int_{C(t')} dx' K(x,x';t,t')v(x',t') + I(x,t), \quad x \in C(t), \tag{4.2.1}$$

where $I(x,t)$ is given by.

$$I(x,t) = \int_{t_1(x)}^{t} dt' l(t-t')u'(x,t') \tag{4.2.2}$$

and

$$K(x,x';t,t') = \frac{\sin\pi\theta e^{i\pi\theta} X(x,t')}{\pi X^+(x,t')(x'-x)} T_1(t,t';x) \tag{4.2.3}$$

Recall the expression for $X(z,t)$ as given by (3.2.37). Define

$$n(x,t) = [x-a(t)]^{1-\theta}[x-b(t)]^{\theta} \tag{4.2.4}$$

$$m(x,t) = [b(t)-x]^{\theta}[x-a(t)]^{1-\theta} \tag{4.2.5}$$

and observe that

$$X^+(x,t) = m(x,t)e^{i\pi\theta}, x \in C(t) \tag{4.2.6}$$

and

$$X(x,t) = \begin{cases} n(x,t), & x > b(t) \\ -n(x,t), & x < a(t) \end{cases} \tag{4.2.7}$$

Then:

$$K(x,x';t,t') = \mp \frac{\sin\pi\theta n(x,t')}{\pi m(x',t')(x'-x)} T_1(t,t';x), \tag{4.2.8}$$

where "$-$" relates to $x > b(t)$, "$+$" to $x < a(t)$.

Since the expression for $T_1(t,t';x)$ is known as long as the viscoelastic material is known, (4.2.3) involves only known quantities. Therefore, (4.2.1) combined with the subsidiary conditions, which for a single load take the form [45]:

$$\int_{a(t)}^{b(t)} \frac{dx v(x,t)}{m(x,t)} = 0 \tag{4.2.9}$$

$$\int_{a(t)}^{b(t)} \frac{dx x v(x,t)}{m(x,t)} = -W(t), \tag{4.2.10}$$

where, as before, $[a(t), b(t)] = C(t)$, yields a system of equations for determining $v(x,t)$ at any point x on the boundary, both inside and outside the contact interval.

In the frictionless case $\theta = \frac{1}{2}$ and so $\sin \pi\theta = 1$. Since the indentor is moving in the negative direction of the $x-$ axis and for any $t < t_1(x)$ we have $x < a(t)$, we must choose the positive sign in (4.2.7). Thereupon (4.2.1) becomes

$$v(x,t) = \frac{1}{\pi} \int_{-\infty}^{t_1(x)} dt' n(x,t') \int_{a(t')}^{b(t')} \frac{dx' v(x',t') T_1(t,t';x)}{(x'-x) m(x',t')}, \tag{4.2.11}$$

where $C(t') = [a(t'), b(t')]$ while (3.2.50) becomes

$$p(x,t) = -\frac{m(x,t)}{\pi} \int_{C(t)} dx' \frac{v(x',t)}{(x'-x) m(x',t)} \tag{4.2.12}$$

We shall further specialize to the case of a *standard linear solid*, for which the expression for $T_1(t,t';x)$ has a simple form and the main integral equation for $v(x,t)$ is amenable to further simplification.

4.3 The Main Integral Equation for v(x,t) for Standard Linear Solid

The standard linear model assumes [45]:

$$l(t) = l_0\, \delta(t) + l_1 e^{-\alpha t} \tag{4.3.1}$$

$$k(t) = k_0\, \delta(t) + k_1 e^{-\beta t} \tag{4.3.2}$$

$$k_0 = \tfrac{1}{l_0}; \quad k_1 = -\tfrac{l_1}{l_0^2}; \quad \beta = \alpha - \tfrac{k_1}{k_0}, \tag{4.3.3}$$

where k_0, k_1, l_0, l_1 are known real constants; $\alpha > 0, \beta > 0$ are relaxation and creep decay constants respectively related by (2.3.5). In terms of τ and τ'

$$\alpha = \tfrac{1}{\tau}, \quad \beta = \tfrac{1}{\tau'}. \tag{4.3.4}$$

Observe also that $\alpha > \beta$. Upon substituting the above expressions into (4.1.6), we obtain:

$$T_1(x,t,t') = \int_{t'}^{t_1(x)} dt'' \left[l_0 \delta(t-t'') + l_1 e^{-\alpha(t-t'')} \right] \left[k_0 \delta(t''-t') + k_1 e^{-\beta(t''-t')} \right] \tag{4.3.5}$$

Recall that $-\infty \leq t' \leq t_1(x) < t$. Clearly, $\delta(t-t'') = 0 \; \forall \; t'' \in [t', t_1(x)]$. Furthermore,

$$\int_{t'}^{t_1(x)} dt'' \, l_1 e^{-\alpha(t-t'')} k_0 \delta(t''-t') = k_0 l_1 e^{-\alpha(t-t')}. \tag{4.3.6}$$

Next,

$$\int_{t'}^{t_1(x)} dt'' \, l_1 e^{-\alpha(t-t'')} k_1 e^{-\beta(t''-t')} = l_1 k_0 e^{-\alpha(t-t_1(x))-\beta(t_1(x)-t')} - l_1 k_0 e^{-\alpha(t-t')} \tag{4.3.7}$$

in view of (4.3.3). By virtue of (4.3.6) and (4.3.7),

$$T_1(x,t,t') = k_0 \, l_1 e^{-\alpha(t-t_1(x))-\beta(t_1(x)-t')} \tag{4.3.8}$$

From (4.2.2) and (4.3.1) it follows that:

$$\begin{aligned} I(x,t) &= \int_{t_1(x)}^{t} dt' \, [\, l_0 \delta(t-t') + l_1 e^{-\alpha(t-t')}] u'(x,t') \\ &= l_0 \, u'(x,t) + l_1 \int_{t_1(x)}^{t} dt' \, e^{-\alpha(t-t')} u'(x,t') \end{aligned} \tag{4.3.9}$$

In the case of a cylindrical indentor whose profile is given by (2.2.1) moving with the speed $V(t)$ as described by (2.2.6), we have, upon recalling (4.2.2) and interchanging the order of integration in (4.2.1):

$$\begin{aligned} I(x,t) &= -\frac{1}{R} \left\{ \left(l_0 + \frac{1}{\alpha} l_1 \right) \left(x - \int_0^t d\tau \, V(\tau) \right) - \frac{1}{\alpha} l_1 e^{-\alpha(t-t_1(x))} \left(x - \int_0^{t_1(x)} d\tau \, V(\tau) \right) \right. \\ &+ \left. \frac{1}{\alpha} l_1 \int_{t_1(x)}^{t} d\tau \, e^{\alpha\tau} V(\tau) \right\} \end{aligned} \tag{4.3.10}$$

$$\begin{aligned} v(x,t) &= \frac{k_0 \, l_1}{\pi} e^{-\alpha t + (\alpha-\beta) t_1(x)} \int_{-\infty}^{t} dt' n(x,t') \int_{a(t')}^{b(t')} dx' \frac{e^{\beta t'} v(x',t')}{m(x',t')(x'-x)} \\ &+ I(x,t) \end{aligned} \tag{4.3.11}$$

It can be seen from both the general case (4.2.1) and the above equation that for any x such that $t_1(x) \leq t$ all quantities required to calculate $v(x,t)$ are already known. Here we are using the assumption that all previous history motion of the boundaries $a(t)$ and $b(t)$ can be retrieved. Thus the most curious part will pertain to the times t lying in the interval $[\, t_1(x), \, t\,]$ for which $a(t), b(t)$ are not yet determined.

Going back to (4.2.1), we can observe that this is a Fredholm-type equation with variable limits of integration. Due to the complicated nature of the kernel and the laws

according to which the contact region boundaries $a(t)$ and $b(t)$ change with time, the only feasible way of solving (4.2.1) in the absence of special simplifying assumptions is numerical integration. The kernel $K(x,x';t,t')$ possesses a non-integrable singularity at $x'=x$ as long as x belongs to the contact region. However, upon taking a closer look at the double integral in (4.2.1), we can conclude that unless $x=a(t_1(x))$, where t_1 is the transition time when the point x enters $C(t)$, the singularity in the integral kernel is of order $\frac{1}{2}$ at both $a(t)$ and $b(t)$. For convenience, we rewrite (4.2.1) as:

$$\begin{aligned} v(x,t) &= \int_{-\infty}^{t_1(x)} dt' \int_{a(t')}^{b(t')} dx'\, K(x,x';t,t')\, v(x',t') + I(x,t) \\ &= J_1(x,t) + I(x,t) \end{aligned} \tag{4.3.12}$$

$I(x,t)$ can easily be found using (4.3.10), provided $t_1(x)$ is known. Consider $J_1(x,t)$. Since we have assumed that up to the time $t_1(x)$ all previous history can be retrieved, $J_1(x,t)$ is completely determined by this history. In fact, for every $t' \in (-\infty; t_1(x)]$ $[a(t'), b(t')]$ is available and we can therefore explicitly carry out the integration. Bearing in mind that $a(-\infty)=a(0)\equiv -a_0$, $b(-\infty)=b(0)\equiv a_0$, we can further decompose $J_1(x,t)$ onto two parts as follows:

$$\begin{aligned} J_1(x,t) &= \int_{-\infty}^{0} dt' \int_{-a_0}^{a_0} dx'\, K(x,x';t,t')\, v(x',t') \\ &+ \int_{0}^{t_1(x)} dt' \int_{a(t')}^{b(t')} dx'\, K(x,x';t,t')\, v(x',t') \end{aligned} \tag{4.3.13}$$

From (3.2.33) we have for $t \in (-\infty, 0]$:

$$\begin{aligned} v(x',t) &= \int_{-\infty}^{t} dt' l(t-t')\, u'(x',t') = -\frac{x'}{R} \int_{-\infty}^{t} dt' \left[l_0\, \delta(t-t') + l_1 e^{-\alpha(t-t')} \right] \\ &= -\frac{x'}{R} \left[l_0 + \frac{1}{\alpha} l_1 \right] \end{aligned} \tag{4.3.14}$$

Therefore, for $x < -a_0$

$$\begin{aligned} \int_{-\infty}^{0} dt' \int_{-a_0}^{a_0} dx'\, K(x,x';t,t')\, v(x',t') &= \sqrt{x^2-a_0^2}\, \frac{k_0 l_1}{\pi} e^{-\alpha t + (\alpha-\beta) t_1(x)} \\ \times \int_{-\infty}^{0} dt' e^{\beta t'} \int_{-a_0}^{a_0} &\left[-\frac{x'}{R} \left(l_0 + \frac{1}{\alpha} l_1 \right) \right] \frac{dx'}{\sqrt{(a_0^2-x^2)}(x'-x)} \end{aligned}$$

$$= -\frac{k_0 l_1}{\beta R}\sqrt{x^2-a_0^2}e^{-\alpha t+(\alpha-\beta)t_1(x)}\left(l_0+\frac{1}{\alpha}l_1\right)\left(1+\frac{x}{\sqrt{x^2-a_0^2}}\right)$$

$$= -\frac{l_1}{\alpha R}e^{-\alpha t+(\alpha-\beta)t_1(x)}\left(x+\sqrt{x^2-a_0^2}\right) \tag{4.3.15}$$

Combining (4.3.10), (4.3.11) and (4.3.15), we have the following equation for the determination of $v(x,t)$ at $t > t_1$:

$$v(x,t) = \frac{k_0 l_1}{\pi}e^{-\alpha t+(\alpha-\beta)t_1(x)}\int_0^{t_1(x)}dt' n(x,t')\int_{a(t')}^{b(t')}dx'\frac{e^{\beta t'}v(x',t')}{m(x',t')(x'-x)}$$

$$- \frac{l_1}{\alpha R}e^{-\alpha t+(\alpha-\beta)t_1(x)}\left(x+\sqrt{x^2-a_0^2}\right)+I(x,t) \tag{4.3.16}$$

At time $t_0 = 0$ (4.2.10) yields:

$$W(0) = \frac{l_0+\frac{1}{\alpha}l_1}{R}\int_{-a_0}^{a_0}dx'\frac{x'^2}{\sqrt{a_0^2-x'^2}} = \pi\frac{l_0+\frac{1}{\alpha}l_1}{R}\frac{a_0^2}{2} \tag{4.3.17}$$

Hence,

$$a_0 = \sqrt{\frac{2RW(0)}{\pi\left(l_0+\frac{1}{\alpha}l_1\right)}}, \tag{4.3.18}$$

and is completely determined by R, α, l_0 and l_1. Note here, that $W(0)$ presents the initial normal load that was acting upon the indentor at t_0.

4.3.1 On the Singularities in the Main Integral Equation for v(x,t)

At first sight, (4.3.16) can cast a reasonable doubt on its integrability. In fact, $m(x',t')$ vanishes at both ends of the interval and $x'-x$ can turn out to be zero for $x \in [a(t'); b(t')]$. However, a scrupulous observer can conclude that the latter can only happen for a single point in time $t' = t_1(x)$, since $x = a(t_1(x))$. In this case $x = a(t')$. Fortunately, $n(a(t'),t') = 0$, which smears out the behaviour of the space integral in (4.3.16) at $t' = t_1(x)$. As for the other troublesome term, $m(x',t')$, a proper sequence of transformation of variables can remedy the problem. Clearly, putting

$$y = \frac{2}{b(t')-a(t')}x - \frac{b(t')+a(t')}{b(t')-a(t')} \tag{4.3.19}$$

maps the original interval $[a(t'); b(t')]$ onto $[-1; 1]$. Setting then $y = sin\, z$ eliminates the singularity.

In view of the above, we are left with a Fredholm-type equation (4.3.16), for which general Fredholm theory is applicable.

4.4 Steady-state Solution of the Main Integral Equation for v(x,t)

An important result which can serve as a model problem for the general problem is that for an indentor moving with a constant speed V. As before, we assume that the motion takes place in the negative direction of the x-axis. We shall only consider the frictionless case here.

We shall choose a new coordinate frame with the origin at the tip of the indentor. Let us assume that sufficient time has elapsed since the beginning of motion for transient effects to have vanished. This naturally leads to a conclusion that the contact interval has stabilized to be $[a_*; b_*]$. Then the current positions of the contact interval boundaries can be determined by:

$$a(t) = a_* - Vt, \quad b(t) = b_* - Vt \tag{4.4.1}$$

Since for any point with coordinate $x = a_* - Vt_1(x)$, solving for $t_1(x)$ yields

$$t_1(x) = -\frac{a_* + x}{V} \tag{4.4.2}$$

In view of the above considerations, we can view all our quantities depending on x and t as functions of a new variable $x + Vt$ as a whole.

Making a change of variables as follows:

$$x' \longrightarrow y' = x' + Vt', \quad x \longrightarrow y = x + Vt, \quad t' \longrightarrow z = x + Vt', \quad t'' \longrightarrow \xi = x + Vt'' \tag{4.4.3}$$

we arrive at:

$$v(y) \;=\; \int_{a_*}^{b_*} dy' K(y, y') v(y') + I(y), \tag{4.4.4}$$

where:

$$K(y,y') = \frac{1}{\pi}\int_{-\infty}^{a_*}\frac{dz}{V}\frac{T(y,z)n(z)}{(y'-z)m(y')} \tag{4.4.5}$$

$$T(y,z) = \int_{z}^{a_*}\frac{d\xi}{V}l\left(\frac{y-\xi}{V}\right)k\left(\frac{\xi-z}{V}\right) \tag{4.4.6}$$

$$I(y) = \int_{a_*}^{y}\frac{dz}{V}l\left(\frac{y-z}{V}\right)u'(z) \tag{4.4.7}$$

We shall now introduce a new scaled spatial variable

$$\tilde{x} = \frac{1}{b_*-a_*}[2x-(b_*+a_*)], \tag{4.4.8}$$

Clearly $\tilde{x}\in[-1;1]$ as long as $x\in[a_*,b_*]$. In view of this, we can rewrite (4.4.4) – (4.4.7) as

$$\tilde{v}(\tilde{x}) = \frac{b_*-a_*}{2V}\int_{-1}^{1}d\tilde{x}'\tilde{K}(\tilde{x},\tilde{x}')\tilde{v}(\tilde{x}')+\tilde{I}(\tilde{x}), \tag{4.4.9}$$

$$\tilde{K}(\tilde{x},\tilde{x}') = \frac{b_*-a_*}{\pi 2V}\int_{-\infty}^{-1}d\tilde{z}\frac{T(\tilde{x},\tilde{z})n(\tilde{z})}{(\tilde{x}'-\tilde{z})m(\tilde{x}')}$$

$$= \frac{b_*-a_*}{\pi 2V}\int_{-\infty}^{-1}d\tilde{z}\frac{\tilde{T}(\tilde{x},\tilde{z})\sqrt{|1-\tilde{z}^2|}}{(\tilde{x}'-\tilde{z})\sqrt{1-\tilde{x}'^2}} \tag{4.4.10}$$

$$\tilde{T}(\tilde{x},\tilde{z}) = \frac{b_*-a_*}{2V}\int_{\tilde{z}}^{-1}d\tilde{\xi}l\left[\frac{b_*-a_*}{2V}(\tilde{x}-\tilde{\xi})\right]k\left[\frac{b_*-a_*}{2V}(\tilde{\xi}-\tilde{z})\right] \tag{4.4.11}$$

$$\tilde{I}(\tilde{x}) = \frac{b_*-a_*}{\pi 2V}\int_{-1}^{\tilde{x}}d\tilde{z}l\left[\frac{b_*-a_*}{2V}(\tilde{x}-\tilde{z})\right]\tilde{u}'(\tilde{z}) \tag{4.4.12}$$

In the case of a cylindrical indentor:

$$\tilde{u}'(\tilde{z}) = e\tilde{z}+f = \tilde{d}(\tilde{z}),\quad x\in[a_*;b_*], \tag{4.4.13}$$

where e and f are (known) constants.

We can now require that time units be rescaled so that $\frac{b_*-a_*}{2V}=1$. This amounts to coopting new scaled time $\tilde{t}$ into the previous considerations as follows:

$$\tilde{t} = \frac{2Vt}{b_*-a_*}, \tag{4.4.14}$$

since multiplying the time units by a constant factor results in dividing the value of the speed by the same factor. Then, removing the tildes for the sake of brevity, we

can rewrite (4.4.9) – (4.4.12) as

$$v(x) = \int_{-1}^{1} dx' K(x,x') v(x') + I(x) \tag{4.4.15}$$

$$K(x,x') = \frac{1}{\pi} \int_{-\infty}^{-1} dz \frac{T(x,z)\sqrt{|1-z^2|}}{(x'-z)\sqrt{1-x'^2}} \tag{4.4.16}$$

$$T(x,z) = \int_{-z}^{-1} du l(x-u) k(u-z) \tag{4.4.17}$$

$$I(x) = \int_{-1}^{x} dz l(x-z) u'(z) \tag{4.4.18}$$

From the considerations analogous to those having lead to (4.3.8), we get for $T(x,z)$:

$$T(x,z) = \frac{1}{\alpha-\beta} k_1 l_1 \left[e^{-\alpha(x+1)+\beta(z+1)} \right] \tag{4.4.19}$$

Thus for $K(x,x')$

$$K(x,x') = \frac{k_1 l_1}{(\alpha-\beta)\sqrt{1-x'^2}} e^{-\alpha(x+1)+\beta} \int_{-\infty}^{-1} dz \frac{e^{\beta z}\sqrt{z^2-1}}{x'-z} \tag{4.4.20}$$

Consider the integral part of (4.4.20). Following the procedure discussed in [45], we arrive at:

$$\begin{aligned} K(x,x') &= \frac{k_1 l_1}{\pi(\alpha-\beta)\sqrt{1-x'^2}} e^{-\alpha(x+1)+\beta} \\ &\times \left\{ -\sqrt{1-x'^2}\beta e^{\beta x'} \int_{x'}^{1} dy \frac{e^{-\beta y} E(\beta,y)}{\sqrt{1-y^2}} + E(\beta,x) \right\} \\ &= \frac{k_1 l_1}{\pi(\alpha-\beta)} e^{-\alpha(x+1)+\beta} \left\{ -\beta e^{\beta x'} \int_{x'}^{1} dy \frac{e^{-\beta y} E(\beta,y)}{\sqrt{1-y^2}} + \frac{E(\beta,x)}{\sqrt{1-x'^2}} \right\} \end{aligned} \tag{4.4.21}$$

where:

$$E(\beta,y) = yK_0(\beta) - K_1(\beta), \tag{4.4.22}$$

K_0, K_1 are the modified Bessel functions. By virtue of (3.2.33),

$$v(x) = \int_{-\infty}^{x} dx' l(x-x') u'(x) \tag{4.4.23}$$

For a cylindrical indentor we have for the profile derivative:

$$u'(x) = -\frac{x}{R}, \tag{4.4.24}$$

or, in the dimensionless coordinates described by (4.4.8),

$$\tilde{u}'(\tilde{x}) = d_0 + d_1\tilde{x}, \tag{4.4.25}$$

where:

$$d_0 = -\tfrac{b_*+a_*}{2R}, \quad d_1 = -\tfrac{b_*-a_*}{2R} \tag{4.4.26}$$

In line with the previous discussion, we remove shall henceforth remove tildes from (4.4.26).

Bearing in mind the binomial representation of the derivative of the indentor profile given by (4.4.25), let us decompose $v(x)$ onto two parts as follows:

$$v(x) = q(x) + \Delta(x), \tag{4.4.27}$$

where:

$$q(x) = q_0 + q_1(x) = \int_{-\infty}^{x} dx' l(x-x')(d_0 + d_1 x'), \tag{4.4.28}$$

and, since for $x \in [a_*; b_*]$ $u'(x) \equiv d_0 + d_1 x$,

$$\Delta(x) = \int_{-\infty}^{-1} dx' l(x-x') \left[u'(x') - (d_0 + d_1 x')\right] \tag{4.4.29}$$

We shall further denote $d(x) \equiv d_0 + d_1 x$ for convenience. From (4.3.1) we observe:

$$\Delta(x) = l_1 e^{-\alpha x} \int_{-\infty}^{-1} dx' e^{\alpha x'} [u'(x') - d(x')] \tag{4.4.30}$$

Therefore, by (4.4.21) and (4.4.30):

$$\begin{aligned}
\int_{-1}^{1} dx' K(x,x')\Delta(x') &= \frac{k_1 l_1^2}{\pi(\alpha-\beta)} \int_{-1}^{1} dx' \left\{ \left[-\beta e^{\beta x'} \int_{x'}^{1} dy e^{-\beta y} \frac{E(\beta,y)}{\sqrt{1-y^2}} + \frac{E(\beta,x)}{\sqrt{1-x'^2}} \right] \right. \\
&\times \left. e^{-\alpha x'} \int_{-\infty}^{-1} dz e^{\alpha z} [u'(z) - d(z)] \right\} \\
&= \frac{k_1 l_1^2}{\pi(\alpha-\beta)} e^{-\alpha(x+1)+\beta} \int_{-\infty}^{-1} dz e^{\alpha z} [u'(z) - d(z)] \\
&\times \left(\frac{\alpha \chi(\beta,\alpha) e^{\alpha-\beta}}{\alpha-\beta} \right),
\end{aligned} \tag{4.4.31}$$

where:

$$\chi(\beta,\alpha) = -\left[I_0(\alpha) K_1(\beta) + I_1(\alpha) K_0(\beta) \right], \tag{4.4.32}$$

I_0, I_1, K_0, K_1 are the modified Bessel functions. Subsidiary conditions (4.2.9) and (4.2.10) in our new dimensionless variables reduce to:

$$-\frac{1}{\pi}\int_{-1}^{1} dx \frac{q(x)}{m(x)} = l_1 \int_{-\infty}^{-1} dx' e^{\alpha x'}[u'(x') - d(x')] I_0(\alpha) \tag{4.4.33}$$

$$-\frac{1}{\pi}\int_{-1}^{1} dx \frac{xq(x)}{m(x)} = \frac{W_1}{\pi} - l_1 \int_{-\infty}^{-1} dx' e^{\alpha x'}[u'(x') - d(x')] I_1(\alpha), \tag{4.4.34}$$

where:

$$W_1 = \frac{2W}{b_* - a_*} \tag{4.4.35}$$

is the non-dimensionalized counterpart of W.

We now proceed to evaluate the integral on the right hand side of (4.4.28):

$$\begin{aligned}\int_{-\infty}^{x} dx' l(x - x')(d_0 + d_1 x') &= \int_{-\infty}^{x} \left[l_0 \delta(x - x') + l_1 e^{-\alpha(x-x')}\right][d_0 + d_1(x')] \\ &= d_0\left(l_0 + \frac{l_1}{\alpha} - d_1 \frac{l_1}{\alpha^2}\right) + d_1\left(l_0 + \frac{l_1}{\alpha}\right) x \end{aligned} \tag{4.4.36}$$

Equating the like power terms in the expression resulting from combining the latter equation with (4.4.28), we obtain:

$$q(x) = q_0 + q_1(x) \tag{4.4.37}$$

$$q_0 = d_0\left(l_0 + \frac{l_1}{\alpha}\right) - d_1 \frac{l_1}{\alpha^2} \tag{4.4.38}$$

$$q_1 = d_1\left(l_0 + \frac{l_1}{\alpha}\right) \tag{4.4.39}$$

As shown in [45], for a standard linear solid

$$l_1 \int_{-\infty}^{-1} dx' e^{\alpha x'}[u'(x') - d(x')] = \frac{K_1(\beta) q_1 \left(1 - \frac{\beta}{\alpha}\right)}{\beta \chi(\beta, \alpha)} \tag{4.4.40}$$

Therefore for a cylindrical indentor when $q(x) = q_0 + q_1(x)$ (4.4.33) and (4.4.34) reduce respectively to:

$$-q_0 = \frac{K_1(\beta) q_1 \left(1 - \frac{\beta}{\alpha}\right)}{\beta} \chi(\beta, \alpha) I_0(\alpha) \tag{4.4.41}$$

$$-\frac{1}{2} q_1 = \frac{W_1}{\pi} - \frac{K_1(\beta) q_1 \left(1 - \frac{\beta}{\alpha}\right)}{\beta \chi(\beta, \alpha)} I_1(\alpha) \tag{4.4.42}$$

Recall now that the positive decay constants α and β are defined in dimensionless coordinates as $\alpha = \frac{1}{\tau}$ and $\beta = \frac{1}{\tau'}$ respectively, where τ is the relaxation decay time, τ' is the creep decay time. As prescribed by (4.4.14), in dimensionless coordinates (omitting tildes for simplicity):

$$\alpha = \frac{b_* - a_*}{2V\tau}, \quad \beta = \frac{b_* - a_*}{2V\tau'} \tag{4.4.43}$$

With the help of (4.4.26), we can express α and β in terms of d_1 as

$$\alpha = -\frac{d_1 R}{V\tau}, \quad \beta = -\frac{d_1 R}{V\tau'} \ , \tag{4.4.44}$$

and, employing the above relationship, transform (4.4.42) into an implicit equation for d_1:

$$A(d_1) = -\frac{B}{d_1} - C(d_1)d_1, \tag{4.4.45}$$

where:

$$A(d_1) = -\frac{1}{2}\left(l_0 + \frac{l_1}{\alpha}\right) \tag{4.4.46}$$

$$B(d_1) = -\frac{W}{\pi R} \tag{4.4.47}$$

$$C(d_1) = -\frac{k_1(\beta)I_1(\alpha)}{\beta\chi(\beta,\alpha)}\left(l_0 + \frac{l_1}{\alpha}\right)\left(1 - \frac{\beta}{\alpha}\right), \tag{4.4.48}$$

α and β being function of d_1 as prescribed by (4.4.43).

Equation (4.4.45) provides a means for finding d_1, whereupon q_1 can be found from (4.4.39), q_0 from (4.4.41) and d_0 from (4.4.38). Once both d_0 and d_1 have been determined, the calculation of a_* and b_* from (4.4.26) proves to be a trivial exercise. However, there exist certain computational difficulties associated with solving (4.4.45). Firstly, $C(d_1)$ is dependent on Bessel functions and therefore in its computation the computational behaviour of the latter must be taken into consideration. Secondly, d_1 is normally a small number compared with unity and therefore may amplify the error if put in the denominator. Therefore we suggest an alternative form of (4.4.45):

$$A(d_1)d_1 = -B - C(d_1)d_1^2 \tag{4.4.49}$$

We can also rewrite (4.4.48) as

$$C(d_1) = -\frac{1}{\frac{I_0(\alpha)}{I_1(\alpha)} + \frac{K_0(\beta)}{K_1(\beta)}} \left(l_0 + \frac{l_1}{\alpha}\right)\left(1 - \frac{\beta}{\alpha}\right) \tag{4.4.50}$$

In the latter form it is clear that $\lim_{d_1 \to 0} C(d_1) = 0$.

We can now give an expression for the hysteretic friction. Recalling (3.3.9), we can write in the dimensionless coordinates:

$$f_H = \frac{1}{W_1} \int_{-1}^{1} dx p(x) u'(x), \tag{4.4.51}$$

where W_1 is given by (4.4.35) and, in view of (4.4.26), $W_1 = -\frac{W}{d_1 R}$. Equation (4.4.25) yields:

$$f_H = \frac{1}{W_1} \int_{-1}^{1} dx p(x)(d_0 + d_1 x) \tag{4.4.52}$$

Now recall that $\int_{-1}^{1} dx p(x) = W_1$ and so

$$f_H = d_0 + \frac{d_1}{W_1} \int_{-1}^{1} dx x p(x) \tag{4.4.53}$$

Interchanging the order of integration in (4.2.12) and dropping the time dependency, we proceed to obtain from (4.4.53):

$$f_H = d_0 + \frac{d_1}{W_1} \int_{-1}^{1} \frac{dx v(x)}{m(x)} \frac{1}{\pi} \int_{-1}^{1} \frac{m(x')x'}{x' - x} \tag{4.4.54}$$

After evaluating the inner integral in the above equation, we conclude:

$$f_H = d_0 - \frac{1}{W_1} \int_{-1}^{1} \frac{dx v(x) x^2}{m(x)}, \tag{4.4.55}$$

bearing in mind the solvability condition (4.2.9) in its steady-state form. Decomposition (4.4.27) and the expression for $\triangle x$ (4.4.30) allow us to conclude that $q(x)$ vanishes for $x \in [-1; 1]$. After evaluating the integral in (4.4.55) and recalling the properties of the Hilbert transform and Bessel functions as in [45], we arrive at:

$$f_H = d_0 - \frac{\pi d_1^2 R}{2W} \frac{K_1(\beta) q_1 \left(1 - \frac{\beta}{\alpha}\right)}{\beta \chi(\beta, \alpha)} I_2(\alpha), \tag{4.4.56}$$

where $I_2(\alpha)$ is the modified Bessel function of the second kind.

Chapter 5

Numerical Algorithm

5.1 Numerical Methods for Solving Integral Equations of Linear Viscoelasticity

Equation (4.3.16) together with the subsidiary conditions (4.2.9) and (4.2.10), presents a challenging computational problem. To gain some insights on how to deal with technical difficulties arising in the process of its solution, let us briefly review the spectrum of numerical methods available for solving the integral equations of linear viscoelasticity in general. We shall start with a general overview and then restrict our discussion to the solution of Volterra–Fredholm equations, to which (4.3.16) belongs.

Numerical methods for solving some of the contact problems of linear viscoelasticity can be classified with respect to the adopted formulation of the problem as shown in Figure 5.1. If the governing equations are cast into the *variational* form, a variety of methods can be applied. Kalker [71] developed a method for solving the viscoelastic rolling contact problem using the so called *influence function methods*, which bear resemblance to the *finite element method*. The results obtained with the help of his *CONTACT* code are reasonably accurate, however, the method applies only to the steady-state rolling contact. An interesting generalization of the variational method using *mathematical programming* has been proposed by Goldshtein *et al.* [49] for the elastic contact. The generalization of this method to the viscoelastic contact problem,

however, may prove computationally challenging. *An iteration method* proposed by Pavlov and Svetashkov [104] deals with a general class of viscoelastic boundary value problems in the quasi-static approximation. The authors prove a theorem assuring the convergence of the introduced iteration process and formulate *an approximate correspondence principle* enabling them to construct a viscoelastic solution from its known elastic prototype. The application of this analysis is restricted to problems with fixed boundaries.

The adoption of the *differential form* of the constitutive equations opens the door to a plethora of numerical methods aimed at solving partial differential equations. Volkov [123] proposed a finite difference algorithm based on *Newton's method* to investigate the propagation of a plane wave in a viscoelastic medium. Though the author's considerations differ from the rolling contact problem, the computational aspect of his treatment of moving boundaries is quite relevant. A numerical solution of the penetrating contact problem was constructed by Khludneva [74] with the help of *penalty functions*. The author investigated the deformation of a circular viscoelastic plate by a rigid axisymmetric indentor. The introduction of a penalty function allowed the author to account for non-linearity in the boundary conditions. Merzhievsky and Reznyansky [91] applied the *moving mesh method* devised by S.K. Godunov [39] to the free boundary value problem of the loading of a metal specimen. Though the approach in question was used to investigate crack propagation, it seems technically possible to extend Godunov's algorithm to the rolling contact problem. It is unclear, however, whether the unknown contact interval boundaries can be handled by the above mentioned technique.

Although *the finite element method (FEM)* has proved to be an indispensable tool in solving elastic contact problems (see, e.g., [71], [75], [101]), its application to viscoelasticity is hindered by substantial complications arising from the hereditary effects incorporated into the constitutive equations. Nevertheless, Harrison *et al.* [61] managed to apply FEM to the modelling of the viscoelastic response of polymers for some simple geometric shapes. The use of FEM was facilitated by the fact that all considered bodies could easily be triangulated (see, e.g., [86]).

A detailed comparison of the numerical results obtained through the application

of FEM to the viscoelastic large strain problem with the analytic solutions available in certain special cases can be found in [110]. A simplified treatment of the contact problem using the adaptive FEM was presented in [80]. The authors employed the Winkler model to investigate the bending of viscoelastic beams and plates. The problem was treated in its *variational formulation* by predominantly analytical means, i.e., no computational results were supplied. Korobeinikov and Alyokhin [78] presented a concise overview of the *Lagrange multiplier* and *penalty function* methods for the quasi-static contact problem. The formulation adopted by the authors allowed for iterations in time until the difference between two consecutively obtained solutions had become sufficiently small. It has also been observed that a solution to the dynamic problem exhibited oscillations attributed to the inaccurate representation of higher modes of the solution. A comparison between the analytic and numerical solutions of the contact problem revealed satisfactory agreement between the two.

Another group of techniques relates to the *integral formulation* of the viscoelastic contact problem. Among the most widely used are *the Nyström method* and the *collocation method* [117]. The application of the first to the solution of the Volterra-Fredholm equation of the second kind is discussed in [60]. The authors presented, along with theoretical results concerning the existence and uniqueness of the solution of a difference analog of the original problem, some numerical examples for continuous kernels and fixed spatial domains. The utilization of the Nyström method, however, does not seem plausible for moving boundary problems, especially those involving singular integral kernels.

A treatise of non-linear Volterra integral equations was presented by Brunner [13] and Brunner and Yatsenko [12]. Both of these articles dealt with the one-dimensional case, nevertheless, it seems possible to extend the approach developed by the authors to more complicated problems. In [13] the *iterated collocation* technique was devised for a Volterra equation with a constant time delay. Global convergence and local superconvergence of the proposed algorithm were investigated and the estimates for the speed of convergence were provided. In [12] the results of the previously cited paper were extended to an equation with a variable time delay. The existence and uniqueness of the solution were proved for a specific type of Volterra equations and the

results were shown to be smooth. A numerical example of the *discrete time collocation* technique shows excellent agreement between the exact and numerical solutions for the chosen trial function.

The viscoelastic contact problems can also be formulated as *integro-differential* equations. Among the techniques used for solving the latter, we can briefly mention *the ray method* [108] and *the deciphering method* [72]. The use of the above in application to the rolling contact problem is limited due to the specific nature of the underlying algorithms. Of some interest to us is also *the freezing method* developed by Movlyankulov [97] and Movlyankulov and Filatov [96]. It deals with the dynamic nonlinear viscoelastic problems in the small viscosity approximation and bears some resemblance to the estimates provided in [43], [45] and [47]. The method employs *the Taylor expansion* of the unknown function and involves only linear terms. The results presented in [97] and [96] are analytical in nature.

To conclude the review of numerical methods, we mention a general treatment of a viscoelastic integro-differential equation by Fabiano and Ito [30], an algorithm by Ladopoulos [81] for evaluating multi-dimensional integrals of linear viscoelasticity with singularities and a concise but comprehensive review of presently available numerical techniques for solving viscoelastic contact problems by Janovsky *et al.* [66].

Throughout this thesis, however, we have adopted *the integral form* of the viscoelastic integral equations as the one that reflects the physical nature of the problem the best. Even though some of the above mentioned numerical methods account for moving and free boundaries, none of them is fully suitable for a comprehensive treatment of the main integral equation (4.3.16) subjected to the subsidiary conditions (4.2.9) and (4.2.10). We shall therefore develop an algorithm specifically tailored to our needs in line with the general approach mentioned in [45]. The description and justification of this algorithm will comprise the rest of this chapter.

5.2 General Algorithm

The general equation (4.3.16) and the subsidiary conditions (4.2.9), (4.3.18) present a system of three equations in three unknowns: $a(t), b(t)$ and $v(x,t)$. Traditional

methods of solving such systems (see, e.g., [5], [114]) cannot handle the unknown contact interval boundaries at an arbitrary time t. Moreover, the dependency of the upper limit of time integration on the space variable x provides yet another obstacle. A general algorithm described below employs a fully explicit scheme outlined in [45]. We begin with the initial solution given by (4.3.18), which yields:

$$a_0 = -\sqrt{\frac{2RW(0)}{\pi\left(l_0 + \frac{l_1}{\alpha}\right)}}, \tag{5.2.1}$$

where the negative sign is taken because the indentor is moving in the negative direction of the $x-$axis. Adding (4.3.14) and noticing the symmetry of the initial contact interval, we obtain the starting point for the iterative procedure: $v^{(0)} = v(x,0)$.

To construct an algorithm allowing us to evaluate $v^{(k)}(x,t)$, we must discretize both the spatial and the temporal domain. At $t = t_0 = 0$, when the motion has started, we can use a uniform spatial grid. For further time steps we shall use an unequally spaced mesh for the reasons explained below. The temporal grid is naturally chosen to be adaptive to accommodate the change in the indentor velocity.

To explain the essence of the algorithm in greater detail, we first turn our attention to time $t_0 = 0$. From (4.3.14), for any x inside the initial contact interval $C(t) = [a_0, b_0]$ ($b_0 = -a_0 > 0$)the value of $v(x,t)$ can be found analytically. Hence, we can discretize $[a_0, b_0]$ uniformly as $a_0 = x_1(0) < x_2(0) < ... < x_n(0) = b_0$, where $x_i(0) - x_{i-1}(0) = h_0 \forall i = 1, 2, ..., n$, and compute $v(x_i(0), t_0)$.

As the indentor starts moving, the contact interval changes from $[a_0, b_0]$ to $[a(t), b(t)]$. To account for the transient nature of the problem, we must discretize the temporal domain appropriately. Because the speed of the indentor is dependent on time, it is natural to suggest an adaptive time mesh. Let us suppose that the first time step, $\triangle t_0$, has been chosen to satisfy:

$$\triangle t_0 \leq D_0 \frac{h}{V(\triangle t_0)}, \tag{5.2.2}$$

where h is the size of the spatial mesh at at $t_0 = 0$, $V(\triangle t_0)$ is the speed of the indentor at $t = \triangle t_0$ (recall that $V(t)$ is known for all t) and D_0 is a constant determined by trial and error. A rationale for such a restriction on $\triangle t_0$ will be given shortly.

At time $t_{(1)} = t_0 + \triangle t_0 = \triangle t_0$ (we put parentheses around the subindex to avoid confusing $t_{(1)}$ with $t_1(x)$) the new contact interval boundaries $a(t_{(1)})$ and $b(t_{(1)})$ are yet undetermined. In view of this, we first make an initial guess about their values as follows:

$$\begin{cases} a^{(1)}(t_{(1)}) &= a_0 + \frac{1}{2}V(t_{(1)})\triangle t_0 \\ b^{(1)}(t_{(1)}) &= b_0 + \frac{1}{2}V(t_{(1)})\triangle t_0 \end{cases} \tag{5.2.3}$$

(recall here, that $V(t) < 0 \, \forall t$). The choice of $\triangle t_0$ governed by (5.2.2) ensures that $a^{(1)}(\triangle t_0) < a_0$ and $b_0 > b^{(1)}(\triangle t_0) > x_{n-1}(0)$, as shown in Figure 5.1, while an example of $\triangle t_1$ not obeying (5.2.2) is presented in Figure 5.2. The latter choice of the first time step leads to a substantially more complicated computational algorithm and therefore should be avoided.

Observe that $x_i(0) \in [a^{(1)}(t_{(1)}), b^{(1)}(t_{(1)})]$, $i = 1, 2, ..., n-1$. For consistency, we denote: $x_0^{(1)}(t_{(1)}) = a^{(1)}(t_{(1)}), x_1^{(1)}(t_{(1)} = x_1(0), ..., x_{n-1}^{(1)}(t_{(1)}) = x_{n-1}(0), x_n^{(1)}(t_{(1)}) = b^{(1)}(t_{(1)})$ and thus obtain a spatial (non-uniform) mesh for $[a^{(1)}(t_{(1)}), b^{(1)}(t_{(1)})]$. From (4.3.16) it follows that

$$v(x_i^{(1)}(t_{(1)}), t_{(1)}) = I(x_i^{(1)}(t_{(1)}), t_{(1)}), \quad i = 1, .., n-1, n \tag{5.2.4}$$

Remember, that the exact $a(t_{(1)}$ is not yet known and hence $t_1(a(t_{(1)}))$ is still undetermined, while $t_1(x_i^{(1)}(t_{(1)})) = -\infty$ for $i = 1, 2, ..., n$ since $x_i^{(1)}(t_{(1)} \in [a_0, b_0] \forall i = 1, 2, ..., n$. Now, equipped with the values of $v(x_i^{(1)}(t_{(1)}), t_{(1)})$ for all $i = 1, 2, ..., n$, we can proceed to extrapolate $v(a^{(1)}(t_{(1)}), t_{(1)})$. If we assume that $a^{(1)}(t_{(1)})$ is in fact the real front boundary of the contact interval at time $t_{(1)}$, then $v(x,t) \in C^\infty[a^{(1)}(t_{(1)}), b^{(1)}(t_{(1)})]$. Using a cubic spline with $x_i^{(1)}(t_{(1)})$ as knots, we are then justified to compute $v(a^{(1)}(t_{(1)}), t_{(1)})$, bearing in mind that the distance travelled by the indentor during the time step $\triangle t_0$ is small compared to the length of the contact interval $b^{(1)}(t_{(1)}) - a^{(1)}(t_{(1)})$.

To satisfy the subsidiary conditions (4.2.9) and (4.2.10), we construct the cost function:

$$f(a(t_{(1)}), b(t_{(1)})) = \left[\int_{a(t_{(1)})}^{b(t_{(1)})} dx' \, \frac{v(x', t_{(1)})}{m(x', t_{(1)})}\right]^2 + \left[\int_{a(t_{(1)})}^{b(t_{(1)})} dx' \, \frac{x' v(x', t_{(1)})}{m(x', t_{(1)})} + W(t_{(1)})\right]^2 \tag{5.2.5}$$

Our object now is to minimize the value of f by choosing the appropriate $a(t_{(1)})$ and $b(t_{(1)})$. This can be accomplished with the help of the quasi-Newton finite gradient method. For the $k-$th choice of $a(t_{(1)})$ and $b(t_{(1)})$ we can compute $v(a^{(k)}(t_{(1)}), t_{(1)})$ and $v(b^{(k)}(t_{(1)}), t_{(1)})$ using the cubic spline technique described above. Notice here, that the spline coefficients need only be determined once, at the start of this iterative procedure. The spatial integrals involved in (5.2.5) can be evaluated numerically using a combination of modified Clenshaw-Curtis and Gauss-Kronrod formulas used in an IMSL routine DQDAWS [122]. This routine ensures sufficient accuracy and efficiency of the numeric quadrature.

Keeping in mind that $n(a(t_{(1)}), t_{(1)}) = 0$, as follows from (4.2.4), we can observe that the suggested discretization of (4.3.16) results in $v(a^{(k)}(t_{(1)}), t_{(1)})$ depending only on $v(x_i(t_{(1)}), t_{(1)})$, $i = 1, 2, ..., n$, but not on itself. This makes the difference scheme under consideration fully explicit. An attempt to introduce an implicit scheme would necessitate the introduction of at least two unknown contact intervals at any given time step, which would complicate the algorithm immensely. In our explicit scheme $v(a(t_{(1)}), t_{(1)})$ and $v(b(t_{(1)}), t_{(1)})$ can be computed can be computed from (4.2.8) as soon as estimates for $a(t_{(1)})$ and $b(t_{(1)})$ that minimize $f(a(t_{(1)}), b(t_{(1)}))$ are found from (5.2.5).

Now let us suppose that we have computed $v(x_i(t_j), t_j)$, where $i = 0, 1, 2, ..., n-1, n$ and $t_j = t_{j-1} + \triangle t_{j-1}$ so that $a(t_j) = x_0(t_j) < x_1(t_j) < ... < x_{n-1}(t_j) < x_n(t_j) = b(t_j)$ We can safely assume that the mesh is uniform, i.e., $x_i(t_j) - x_{i-1}(t_j) = h_j \, \forall i = 1, 2, ..., n$, where h_j is the size of the mesh (at time t_j). If this is not so, we can rediscretize $[a(t_j), b(t_j)]$ to make the mesh uniform and then compute $v(x_i(t_j), t_j)$ at all the regular mesh points. We now restrict the $j-$th time step, $\triangle t_j$, to obey:

$$\Delta t_i < D_j \frac{2 \min_{i=\overline{1,n}} |x_i - x_{i-1}|}{V(t_j) + V(t_j + \triangle t_j)}, \tag{5.2.6}$$

where D_j is a constant determined by trial and error. The above relationship ensures the same "non-overlapping" condition as the one described for the first discrete time, $t_{(1)}$. Denote: $t_{j+1} = t_j + \triangle t_j$. Upon this, we can make an initial guess about the boundaries of the new contact interval, $a^{(1)}(t_{j+1})$ and $b^{(1)}(t_{j+1})$. Denoting $x_0^{(1)}(t_{j+1}) =$

$a^{(1)}(t_{j+1}), x_1^{(1)}(t_{j+1}) = x_1(t_j), ..., x_{n-1}^{j+1}(t_{j+1}) = x_{n-1}(t_j), x_n^{(1)}(t_{j+1}) = b^{(1)}(t_{j+1})$, we compute $v(x_i^{(1)}, t_{j+1}) \forall i = 0, 1, ..., n-1, n$. The computation of $v(x_i^{(1)}, t_{j+1}) \forall i = 1, ..., n-1$ is possible through the direct use of (4.3.16), because for each $x_i^{(1)}$, $i = 1, ..., n-1$ the corresponding $t_1(x_i^{(1)}) \, i = 1, ..., n-1$ is known from the previous history of motion (see Figure 5.3) and hence $a^{(1)}(t_1(x_i^{(1)}))$ and $b^{(1)}(t_1(x_i^{(1)}))$ are also known. To obtain $v(b^{(1)}(t_{j+1}), t_{j+1})$ we can use cubic spline interpolation as described previously, while the computation of $v(a^{(1)}(t_{j+1}), t_{j+1})$ requires extrapolation. Subsequently, the same optimization procedure as described for $t_{(1)}$ can be applied to determine the values of $a(t_{j+1})$ and $b(t_{j+1})$ delivering the minimum to $f(a(t_{j+1}), b(t_{j+1})$ in (5.2.5), i.e., ensuring that the subsidiary conditions (4.2.9) and (4.2.10) are satisfied. The transition from t_j to t_{j+1} is illustrated in Figure 5.3.

It appears desirable to obtain a heuristic uniform upper bound for D_j for all t_j. A universal estimate $D = max_{j=1,2,...} D_j$ that guarantees both stability and efficiency of the algorithm was found to be 0.3. An initial trial time step $\triangle t_1$ was chosen to be 0.01 before the condition (5.2.2) was applied.

Since for $v(x,t)$ is infinitely smooth inside $C(t)$, the error arising from approximating $v(x, t_{i+1})$ by a cubic spline is $O(h^4)$ for all interior points [10]. Thus, for a sufficiently large number of spatial mesh points inside the contact interval, we can expect the error in estimating $v(a^{(i+1)}, t_{i+1})$ and $v(b^{(i+1)}, t_{i+1})$ to be negligible. As a rule of thumb, we chose 51 mesh points (50 intervals) to provide a good compromise between the speed and accuracy of the algorithm.

5.3 Treatment of Integral Singularities

The integrand in (4.3.16) possesses integrable singularities at $x = a(t'), x = b(t')$ that can be handled, e.g., by employing Gaussian type quadrature formulas [23, 29, 112]. Another singularity occurs when t' in the time integral becomes equal to $t_1(x)$. In this case $a(t') = a(t_1(x)) = x$ and the inner integrand becomes undefined at $a(t')$. However,

$$\lim_{t' \to t_1(x)} n(x,t') \int_{a(t')}^{b(t')} dx' \frac{v(x',t')}{m(x',t')(x'-x)} = E, \tag{5.3.1}$$

where E is finite and so no non-integrable singularity arises. However, in choosing an appropriate quadrature formula to evaluate the temporal integral in (4.3.16), it is desirable to avoid handling the values of $v(x,t)$ at $t = t_1(x)$. To this end, we apply the trapezoid formula for $t \in [0, t_i]$ and the rectangle formula for $t \in [t_i, t_{i+1}]$ as follows:

$$\int_0^{t_1(x)} dt' f(t') \approx \sum_{k=1}^{i} \frac{f(t_k) + f(t_{k-1})}{2}(t_k - t_{k-1}) + f(t_i)(t_1(x) - t_i), \tag{5.3.2}$$

where

$$f(t') = n(x,t')e^{\beta t'} \int_{a(t')}^{b(t')} dx' \frac{v(x',t')}{m(x',t')(x'-x)} \tag{5.3.3}$$

A consequence of this is that the iterative expression for $v(a_{i+1}, t_{i+1})$ does not contain a_{i+1}, t_{i+1}, but only earlier values. This is true in any case for a point in the interior of the contact interval. Thus the iteration scheme is entirely explicit, in contrast with that which would emerge from a standard Fredholm-type equation [5], [22].

To evaluate $p(x_j^{(i)}, t_i)$ using (4.2.12) and the known values of $v(x_j^{(i)}, t_i)$ we have to eliminate a first-order singularity in the integrand. Utilizing the Kantorovich method [22] and bearing in mind the differentiability of $v(x,t)$, we obtain:

$$p(x,t) = -\frac{m(x,t)}{\pi}\left\{\int_{a(t)}^{b(t)} \frac{dx'[v(x',t) - v(x,t)]}{m(x',t)(x'-x)} + v(x,t)\int_{a(t)}^{b(t)} \frac{dx'}{m(x',t)(x'-x)}\right\} \tag{5.3.4}$$

However, the second term in (5.3.4) is equal to zero, whereas

$$\lim_{x' \to x} \frac{v(x',t) - v(x,t)}{x' - x} = v'(x,t) \tag{5.3.5}$$

and $p(x_j^{(i)}, t_j)$ can thus be numerically evaluated for any $(x_j^{(i)}, t_i)$ without difficulty. Thereupon the hysteretic friction can be computed from (3.3.11).

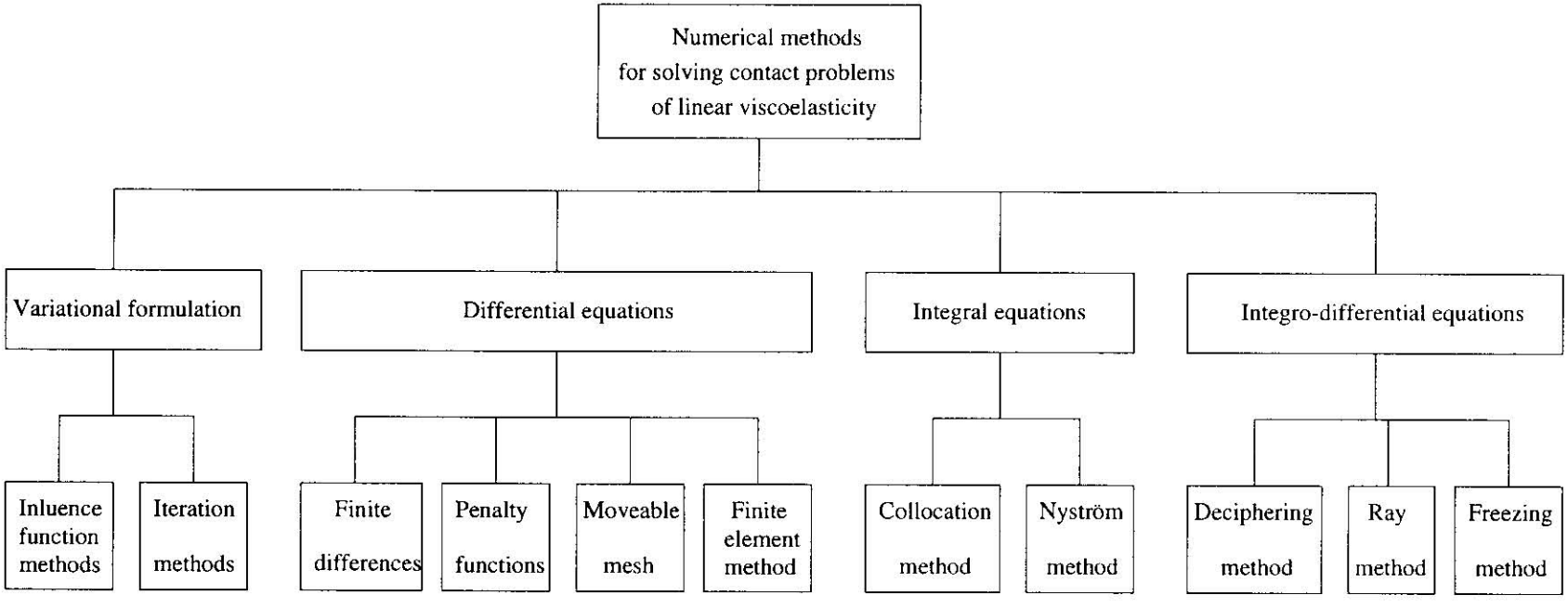

Figure 5.1: Numerical methods for solving contact problems of linear viscoelasticity.

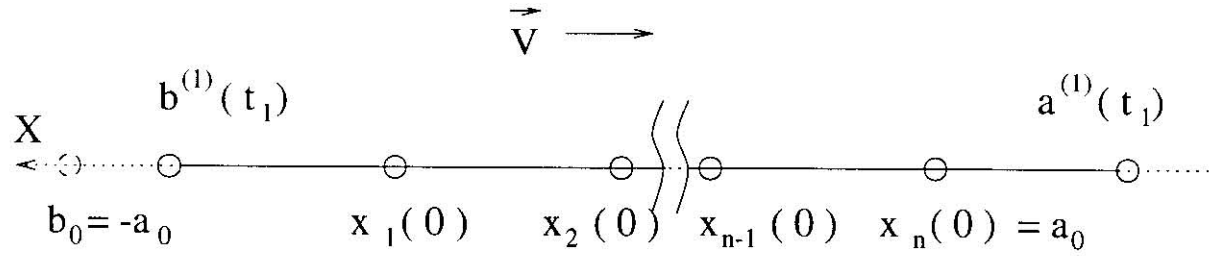

Figure 5.1: Schematic representation of the discretization procedure for the spatial domain: $t_1 = \triangle t_0$: an appropriate choice of $\triangle t_0$

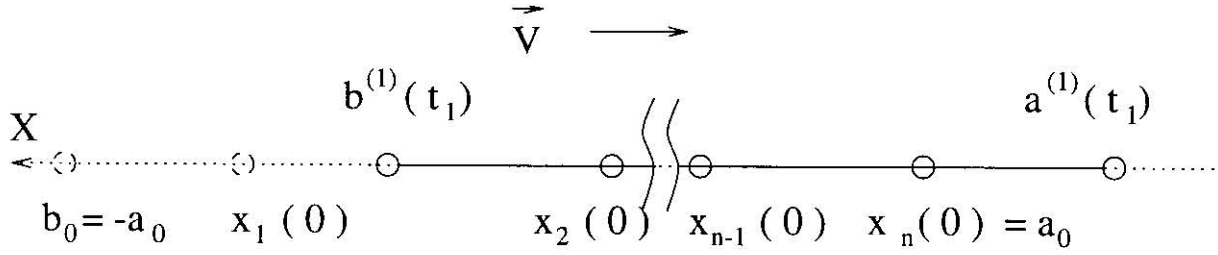

Figure 5.2: Schematic representation of the discretization procedure for the spatial domain: $t_1 = \triangle t_0$: an inappropriate choice of $\triangle t_0$

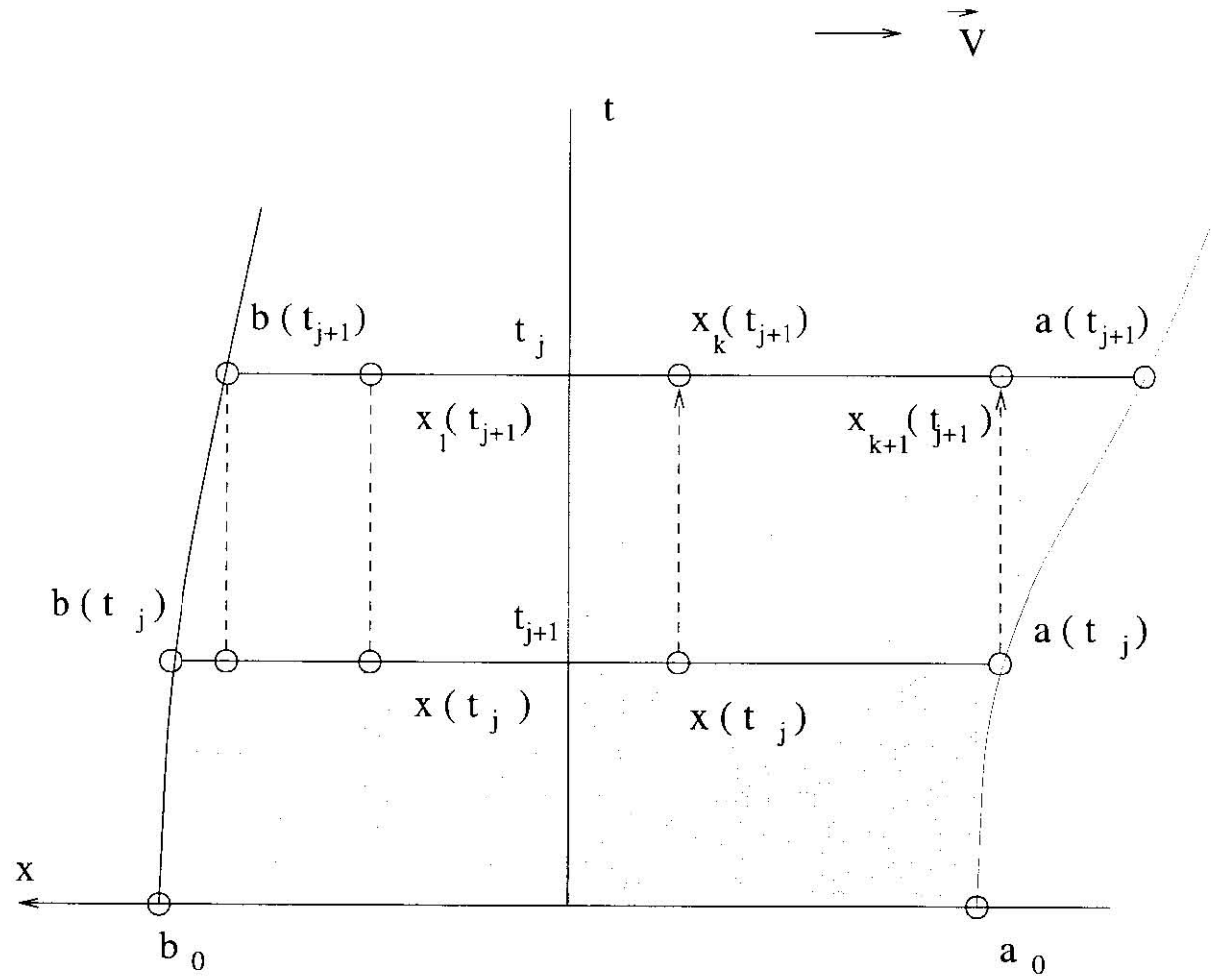

Figure 5.3: Transition from t_j to t_{j+1}: $[a(t_j), b(t_j)]$ – contact interval at time t_j, $[a(t_{j+1}), b(t_{j+1})]$ – contact interval at time t_{j+1}, $x_i(t_j)$ – mesh points at time t_j, $x_i(t_{j+1})$ – mesh points at time t_{j+1}, $\vec{V}$ – velocity of the indentor. Filled region represents the history of motion.

Chapter 6

Results and Discussion

6.1 Introductory Remarks

The computational realization of the algorithm described in Section 5 was carried out on a networked SUN SPARC 20 workstation with available 163 Mb RAM and two 150 MHz CPU. The program required 18 – 20 Mb of operating memory and a single computational run at the given level of discretization extended from 50 to 250 hours of CPU time, depending on the chosen pattern of speed / loading variation. Such a substantial difference in CPU time can be explained bearing in mind that for high speed / loading amplitude, smaller time steps are required, which leads to substantial increase in the computation time. The choice of IMSl as a computational library is justified by its accessibility, reliability and efficiency for large scale computations (as in [15]).

For the discretization of the spatial domain we chose $NX = 51$ mesh points, whereas the time domain had up to $NT = 3000$ mesh points. The radius R of the indentor was taken to be 10 units of length, while α (given by (4.3.4)) equalled 0.1 inverted units of time. The speed V of the indentor was measured in units of length divided by units of time, so that $\frac{R\alpha}{V}$ presented a dimensionless parameter. We also take care of the sign of $V(t)$ so that $V(t)$ is positive (recall that the indentor is moving in the negative direction of the x axis).

Recalling (2.3.4), we can factor out G_0 to obtain:

$$G(t) = G_0 \left(1 + \frac{G_1}{G_0} e^{-\alpha t}\right). \tag{6.1.1}$$

Clearly, for theoretical purposes the value of G_0 can be scaled to unity and therefore it is the dimensionless ratio $\frac{G_0}{G_1}$ that determines the degree of viscoelasticity of the material. If $\frac{G_1}{G_0} = 0$, the material is purely elastic. As $\frac{G_1}{G_0}$ grows, the viscoelastic properties of the material become more and more pronounced. In view of this, we are justified in modelling the problem numerically for certain benchmark values of $\frac{G_1}{G_0}$ and drawing conclusions based on the results of these numerical experiments. Observe also that (2.3.6) implies

$$\frac{\alpha}{\beta} = 1 + \frac{G_1}{G_0}, \tag{6.1.2}$$

thus prescribing β as soon as α (or τ) and $\frac{G_1}{G_0}$ have been chosen.

Detailed graphs are provided for the histories of contact interval width, indentor tip shift (the calculation of the latter quantity is explained below) and hysteretic friction for a viscoelastic material with $\frac{G_1}{G_0} = \frac{1}{4}$. The normalized speed is added to each graph to facilitate the comparison between the changes in the computed quantities and the motion pattern of the indentor.

To facilitate the comparison between the transient and the steady-state cases, we combine the graphs of the solution of the transient problem produced by the numerical algorithm described in Chapter 5 with the graphs of the solution of the steady-state problem with the same parameters obtained through the analytical considerations of Section 4.4. However, one should bear in mind that this combination is somewhat artificial. The steady-state quantities represent the *steady-state* solution (i.e., $t \to \infty$) and therefore depend *on speed only.* The transient quantities are functions of *time.*

On each of the graphs in this chapter representing the histories of contact interval width, indentor tip shift and hysteretic friction the subindex T corresponds to the transient solution and S corresponds to the steady-state solution. The quantities C_T and C_S are the normalized lengths of the transient and steady-state contact intervals respectively computed as $C_S(V(t)) = (b_S(V(t)) - a_S(V(t)))/(2R)$, $C_T(t) = (b_T(t) - a_T(t))/(2R)$, h_T; h_S and h_T are the indentor tip shifts: $h_T(t) = -(a_T(t) + b_T(t) -$

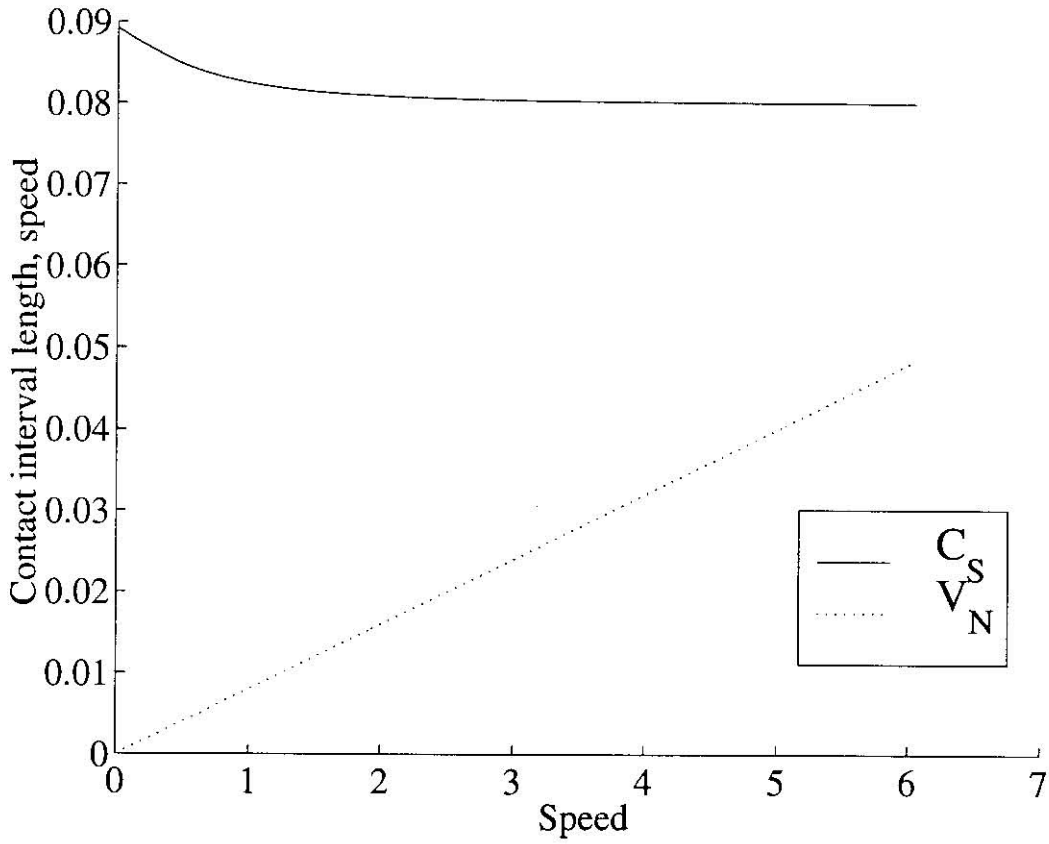

Figure 6.1: Dependence of the contact interval length on speed in the steady-state problem: $\frac{G_1}{G0} = \frac{1}{4}$.

$2x_0(t))/(b_T(t) - a_T(t))$, $h_S(V(t)) = -(a_S(V(t)) + b_S(V(t)))/(b_S(V(t)) - a_S(V(t)))$, where $x_0(t)$ is the current position of the indentor tip, $V(t)$ is the current magnitude of the speed of the indentor. Transient and steady-state coefficients of hysteretic friction f_{H_T} and f_{H_S} are computed with the help of (3.3.11). The normalized speed is $V_N(t) = V(t)/(K\alpha R)$, where $K = 10$ for the graphs containing C_S and C_T, h_S and h_T, while $K = 100$ for the graphs containing f_{H_S} and f_{H_T}. The magnitude of the velocity V has been scaled to conveniently fit its plot on the graphs. In our subsequent discussion we shall assume that all quantities have been normalized as described above.

The graphs of the steady-state contact interval C_S, indentor tip shift h_S and hysteretic friction f_S are plotted *as functions of* V in figures 6.1, 6.2 and 6.3 respectively for $\frac{G_1}{G0} = \frac{1}{4}$. In view of the considerations presented above, we assign the following meaning to the graphs further in this chapter containing transient quantities together with the steady-state quantities. For any given time t the graph of a transient quantity plotted against time represents *the actual value* of this quantity at this time. The value of the corresponding "benchmark" steady-state quantity plotted on the same graph is in fact the value of this quantity for the current value of *speed* $V(t)$. For example, the graphs of h_T, h_S and V_N in Figure 6.5 can for time $t_* = 2$ be interpreted as follows. For this moment in time the transient solution f_{H_T} is approximately equal to 7×10^{-3}. This is the value of f_{H_T} for the viscoelastic material impacted upon by a rolling indentor which started its motion from rest at $t_0 = 0$ and accelerated to the speed $V_N(t_*)$ as described by (6.2.1). The normalized speed of the indentor, $V(2)/(K\alpha R)$ equals approximately 0.8. For this value of speed the steady-state ($t \to \infty$) value of the hysteretic friction f_{H_S} is just under 6×10^{-3}.

Cumulative graphs of the histories of contact interval width, indentor tip shift and hysteretic friction for viscoelastic materials with $\frac{G_1}{G_0} = \frac{1}{4}$, $\frac{G_1}{G_0} = \frac{1}{2}$ and $\frac{G_1}{G_0} = 1$ are presented further in the chapter. The corresponding steady-state values are not shown on these graphs for the sake of clarity. In each case snapshots of pressure distribution are displayed at several instances in time allowing one to observe the development of asymmetry in this distribution and the establishment of the steady-state régime where applicable. On these graphs the contact interval has been rescaled to $[-1, 1]$ to

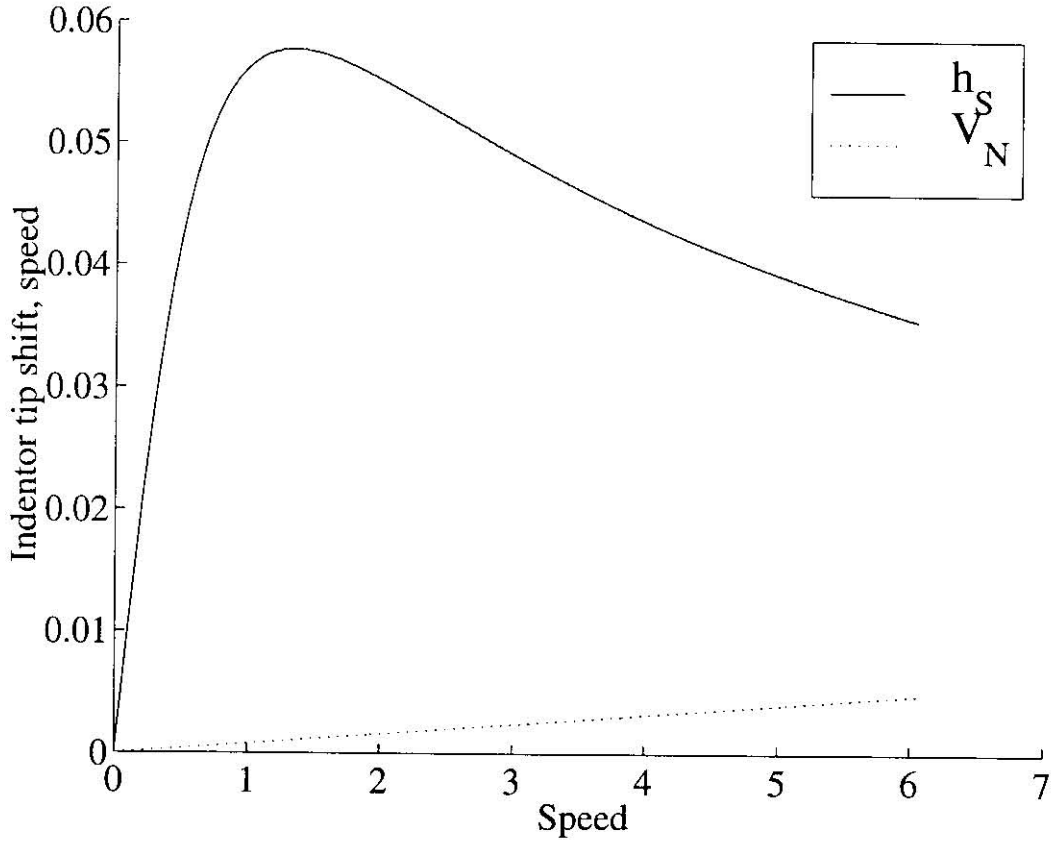

Figure 6.2: Dependence of the indentor tip shift on speed in the steady-state problem: $\frac{G_1}{G0} = \frac{1}{4}$.

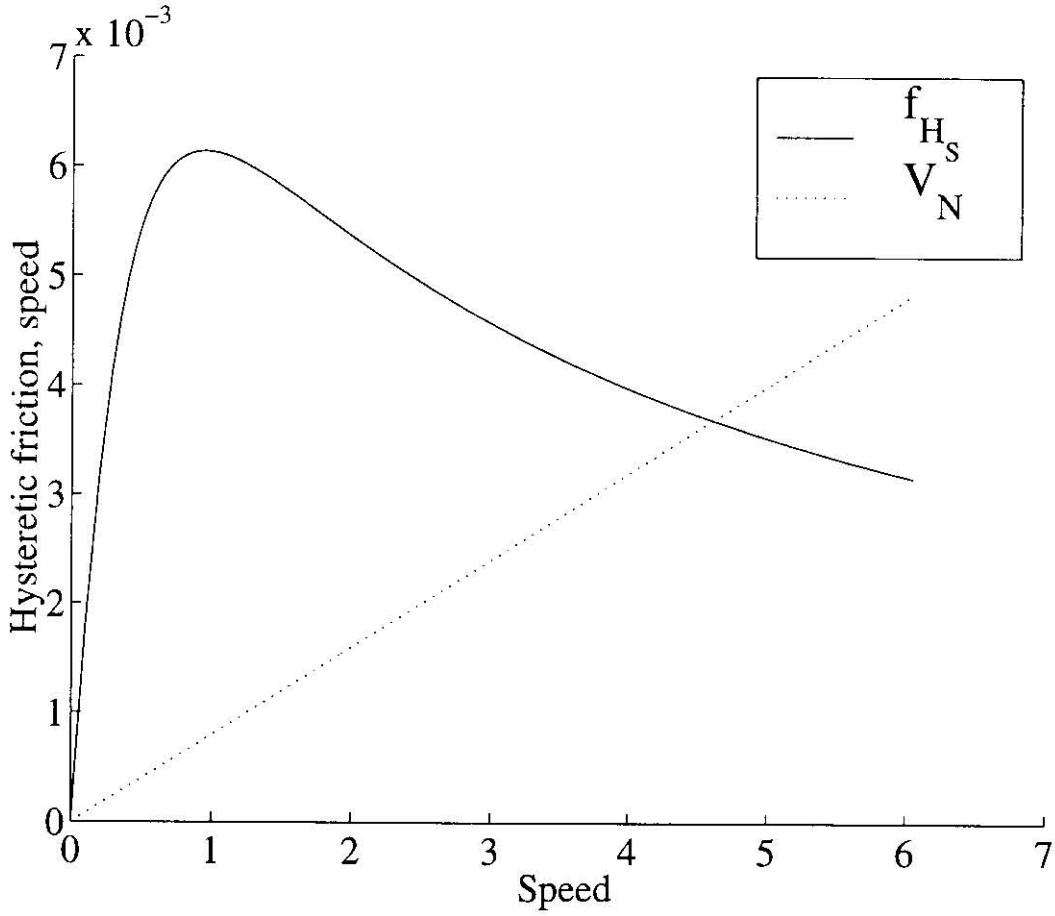

Figure 6.3: Dependence of the hysteretic friction on speed in the steady-state problem: $\frac{G_1}{G0} = \frac{1}{4}$.

facilitate the comparison of pressure distributions for unequal contact intervals (recall that the length of the contact interval changes with time as the indentor moves). The discussion of each case concludes with the graphs of the three components of the stress tensor: σ_{11}, σ_{12} and σ_{22} at one (fixed, but different in each case) moment of time. Only the viscoelastic material with $\frac{G_1}{G_0} = \frac{1}{4}$ has been chosen to illustrate these stress distributions. Other values of viscoelasticity do not generate qualitatively different pictures. Each stress distribution is presented at a fixed instance of time.

6.2 Trial Case: Acceleration to a Constant Speed

As our first example we choose

$$V(t) = \begin{cases} \sin t, & 0 \leq t < \frac{\pi}{2} \\ 1, & t \geq \frac{\pi}{2} \end{cases} \tag{6.2.1}$$

The length of the contact interval and the shift of the indentor tip are each plotted against time in Fig. 6.4. The hysteretic friction and the speed of the indentor are shown in Figure 6.5. As the indentor starts moving, the length of the contact interval starts to decrease. This length exceeds the length of the contact interval for the same value of V in the steady-state case up to $t \approx 3$, after which point the two lengths become indistinguishable. The indentor tip shift also starts growing at the beginning, then reaches its maximum at $t \approx 1.8$ and then declines to its steady-state value. Observe that initially (up to $t \approx 1.3$) $h_T < h_S$, though later $h_T > h_S$ (the two coalesce at $t \approx 5$). The hysteretic friction f_{H_T} exhibits behaviour similar to that of h_T. Its value stays less than f_{H_S} (for the same speeds) until $t \approx 1$, after which time f_{H_T} becomes greater than f_{H_S} up to $t \approx 4$. After this latter moment, however, f_{H_T} becomes smaller than f_{H_S}, as predicted by Golden and Graham [43]. The difference, nevertheless, is very small.

We should also point out that a "hump" in the graph of f_{H_S} occurs in full compliance with the behaviour of f_{H_S} as a function of speed as shown in Figure 6.3. An increase in the speed of the indentor leads to an increase in the hysteretic friction until the latter reaches its maximum and thereafter begins to decline.

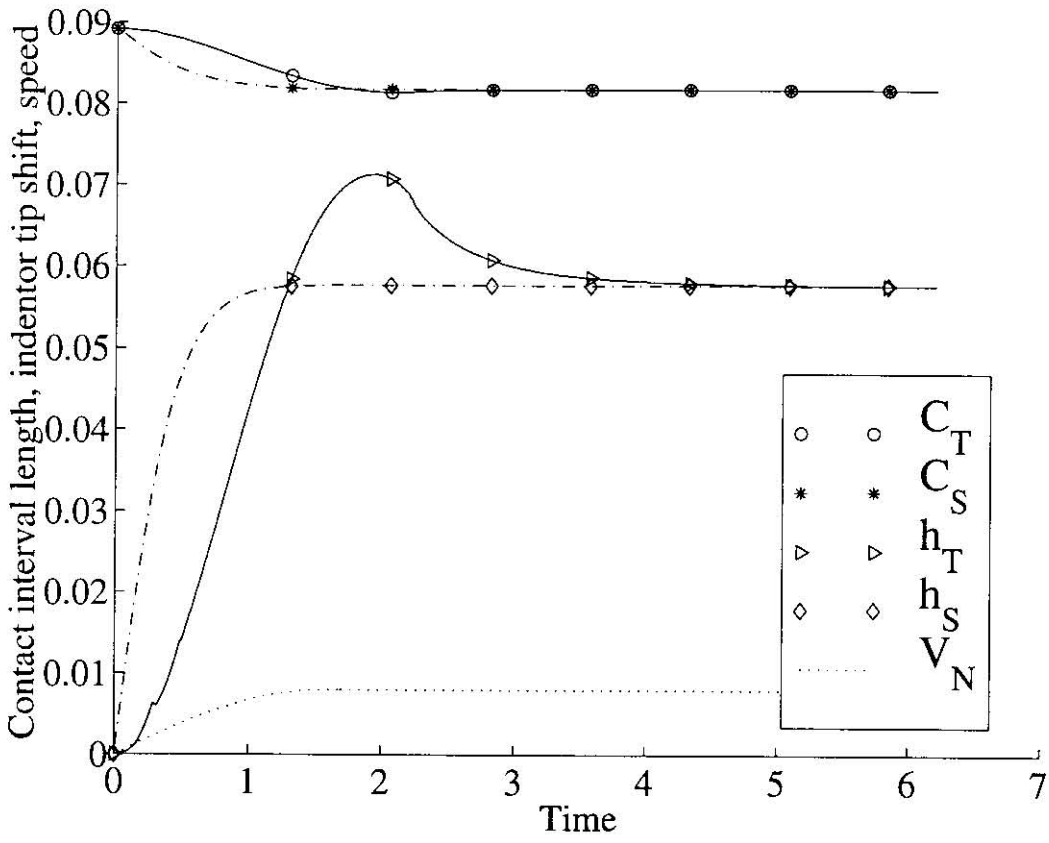

Figure 6.4: Indentor accelerating to a constant speed $V = 1$ as given by (6.2.1). History of contact interval length, indentor tip shift and speed. The solid lines indicate the transient solution and the broken lines indicate the steady-state solution. The dotted line indicates the speed. $\frac{G_1}{G_0} = \frac{1}{4}$

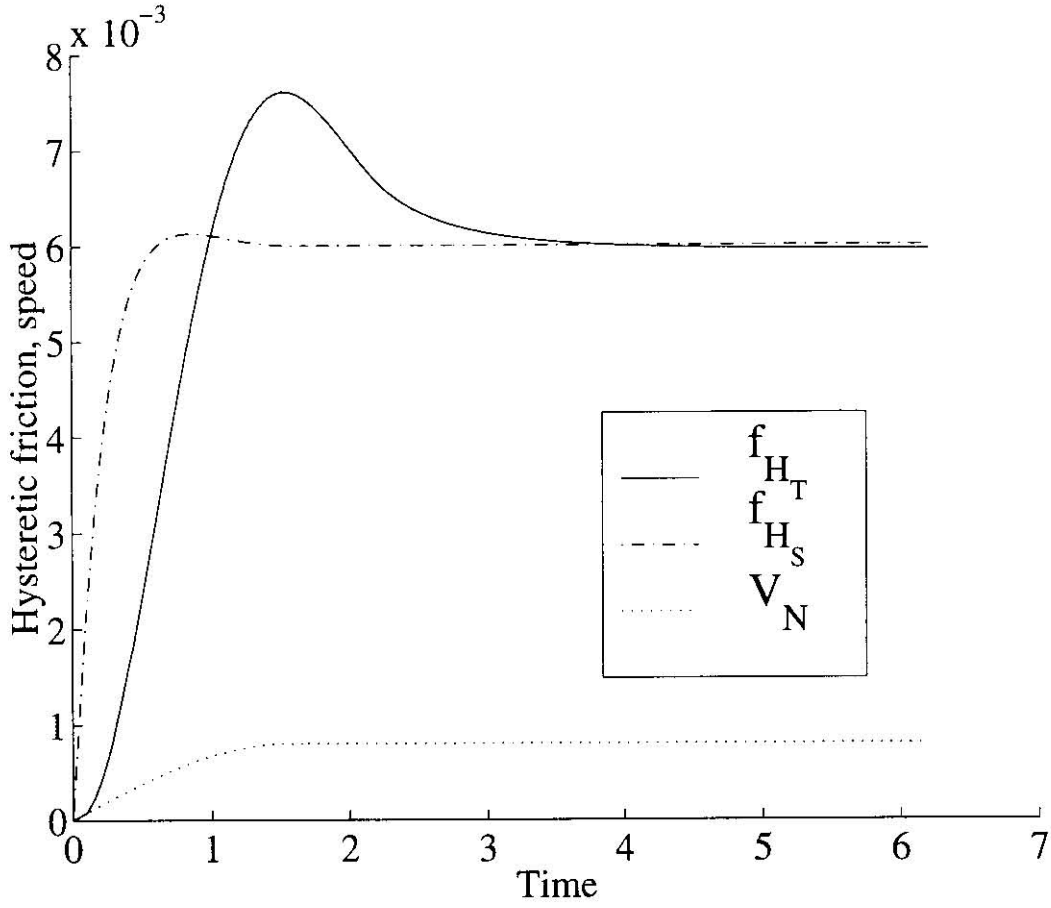

Figure 6.5: Indentor accelerating to a constant speed $V = 1$ as given by (6.2.1). History of hysteretic friction and speed. The solid lines indicate the transient solution and the broken lines indicate the steady-state solution. The dotted line indicates the speed. $\frac{G_1}{G_0} = \frac{1}{4}$

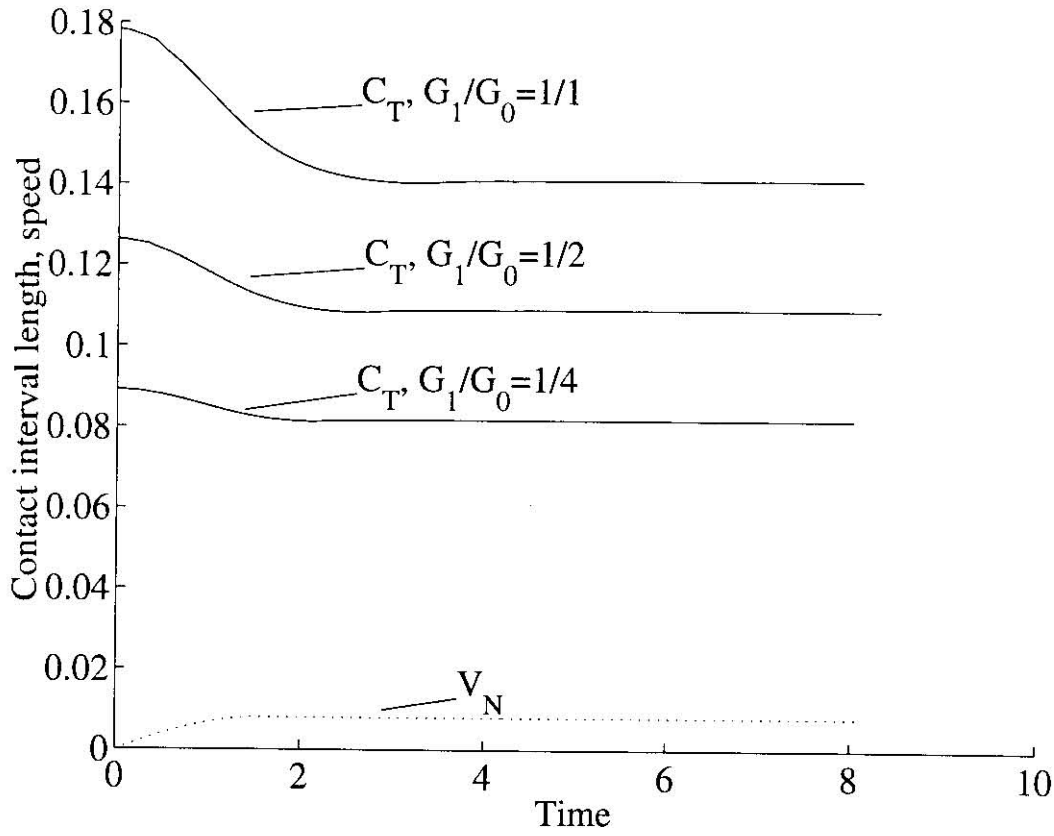

Figure 6.6: Indentor accelerating to a constant speed $V = 1$ as given by (6.2.1). History of contact interval length and speed. $\frac{G_1}{G_0} = \frac{1}{4}$, $\frac{G_1}{G_0} = \frac{1}{2}$, $\frac{G_1}{G_0} = 1$

Cumulative graphs of the histories of the contact interval length and hysteretic friction for viscoelastic materials with $\frac{G_1}{G_0} = \frac{1}{4}$, $\frac{G_1}{G_0} = \frac{1}{2}$ and $\frac{G_1}{G_0} = 1$ are given in Figure 6.6 and Figure 6.7 respectively. One can observe that a higher dimensionless ratio $\frac{G_1}{G_0}$ (i.e., more pronounced viscoelasticity of the material) leads to a larger contact interval length and higher hysteretic friction. Also, the minima of C_T and f_{H_T} are reached later in the history of motion for higher values of $\frac{G_1}{G_0}$.

The histories of pressure distribution for the same materials are given in Figures 6.8, 6.9 and 6.10. The graphs of pressure distribution for the times when transient effects are most evident contain a hump which moves toward the end of the contact interval as time elapses. This hump is also more clearcut for higher values of $\frac{G_1}{G_0}$. We suggest the following explanation of this phenomenon. When the indentor starts moving, the first two terms in (4.3.16) used to calculate $v(x,t)$ become different from zero for the front part of the contact interval ($x < a_0$). In the rear part of the contact interval ($b(t) > x > a_0$) $v(x,t)$ is still equal to $I(x,0)$. Once the indentor has completely moved out of the initial contact interval $[a_0, b_0]$, $v(x,t)$ is fully governed by (4.3.16) with non-zero first terms and the hump disappears. Since the value of the pressure is closely related to that of $v(x,t)$, the change from a linear to nonlinear dependence in $v(x,t)$ results in a sharp (though still smooth) change in $p(x,t)$. Physically the observed phenomenon may be explained from the fact that the indentor starts moving instantly and at $t_0 = 0$ the pressure is instantly redistributed. As t grows, the pressure distribution approaches its steady-state value in full compliance with the results of Fan, Golden and Graham [31].

The distributions of stress components for the material with $\frac{G_1}{G_0} = \frac{1}{4}$ are presented in Figures 6.11 – 6.13 for a large time ($t > 8$). Observe that the influence of the indentor rapidly diminishes as we move deeper inside the half-space for all three components of σ. The first component, σ_{11}, has a hump for small y under the contact interval, which is surrounded by two troughs along the x axis. The second component, σ_{12}, is antisymmetric about the indentor tip and has pronounced peaks underneath the contact interval boundaries for small y, which is the consequence of the adopted assumption about zero tangential forces on the boundary. The lines of equal value for the third component, σ_{22}, are similar to the pictures for an elastic material presented

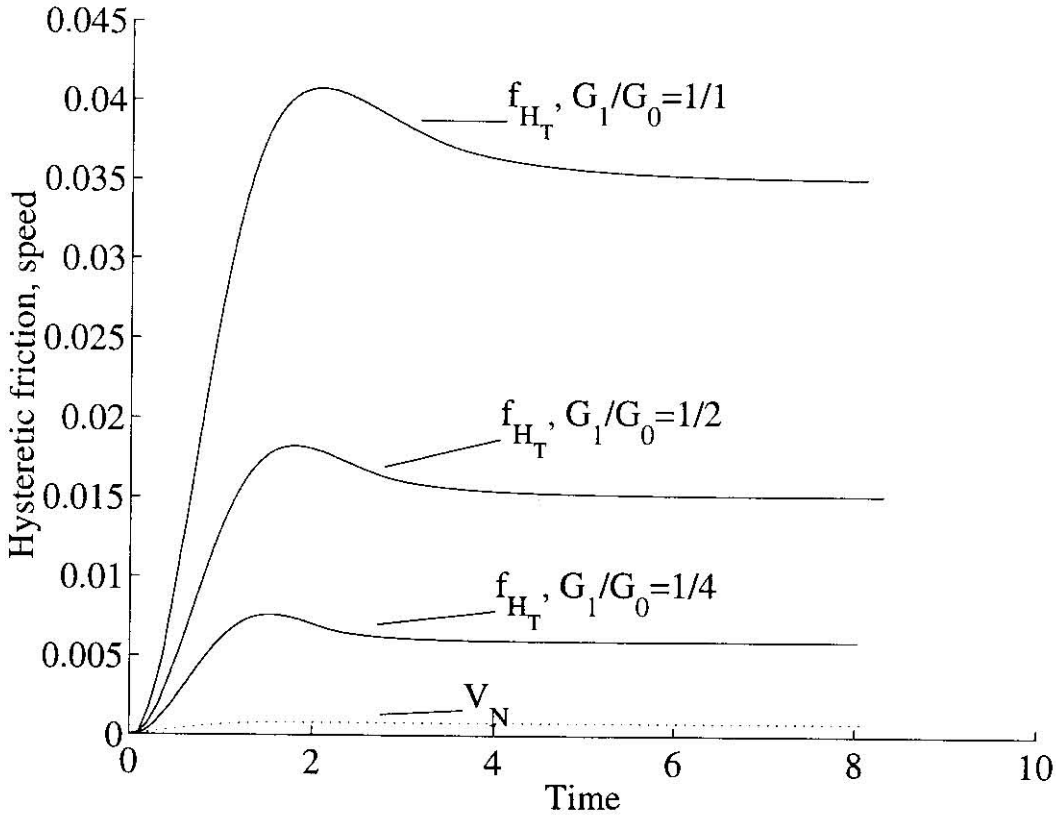

Figure 6.7: Indentor accelerating to a constant speed $V = 1$ as given by (6.2.1). History of hysteretic friction and speed. $\frac{G_1}{G_0} = \frac{1}{4}$, $\frac{G_1}{G_0} = \frac{1}{2}$, $\frac{G_1}{G_0} = 1$

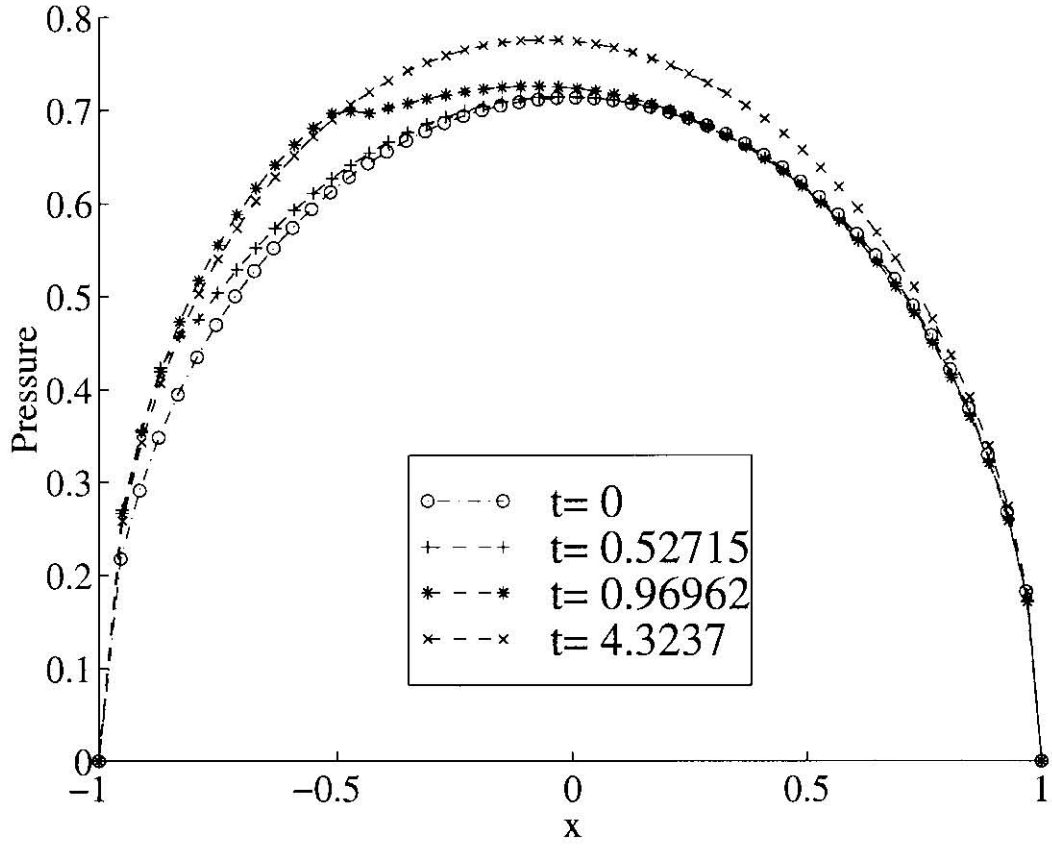

Figure 6.8: Indentor accelerating to a constant speed $V = 1$ as given by (6.2.1). History of pressure distribution. $\frac{G_1}{G_0} = \frac{1}{4}$

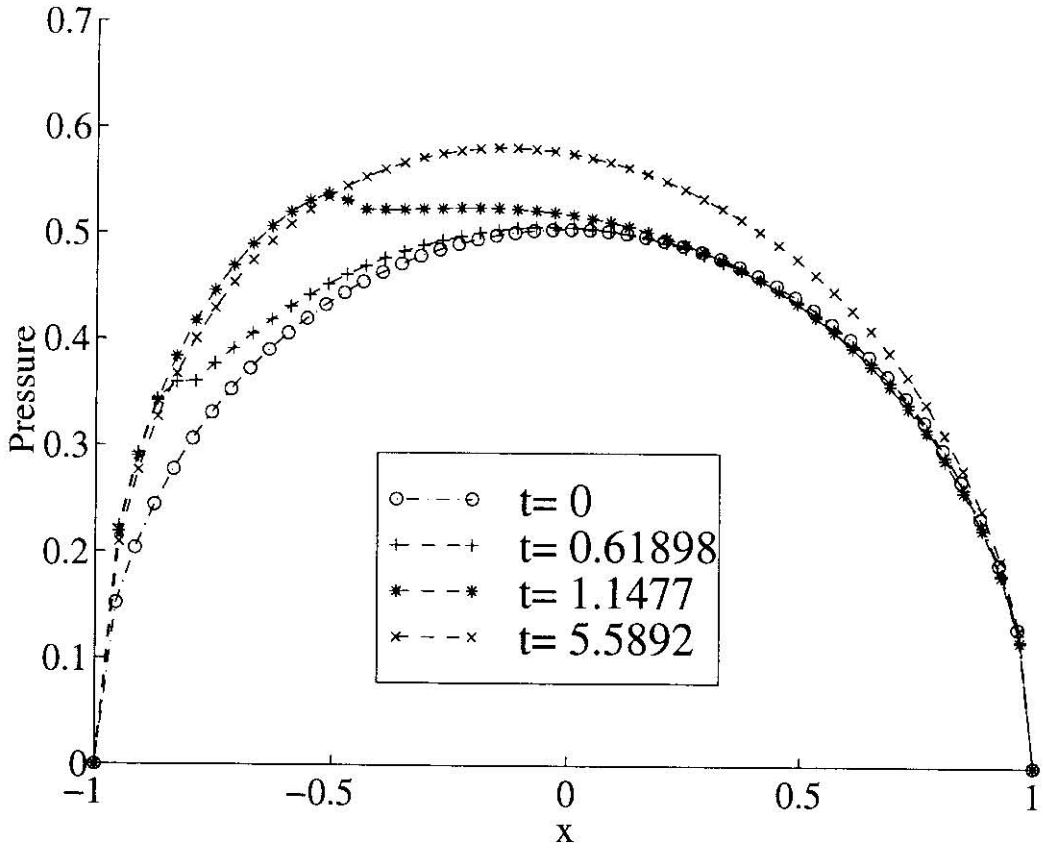

Figure 6.9: Indentor accelerating to a constant speed $V = 1$ as given by (6.2.1). History of pressure distribution. $\frac{G_1}{G_0} = \frac{1}{2}$

by Timoshenko and Goodier [118]. Overall, the graphs of pressure distribution are in good agreement with elastic data [87, 70, 71].

6.3 Constant Acceleration

We now choose $V = t$ for $t \geq 0$ and $V = 0$ for $t < 0$. The length of the contact interval and the shift of the indentor tip are each plotted against time in Fig. 6.14.

The hysteretic friction and the speed of the indentor are shown in Figure 6.15.

The contact interval length eventually tends to a stable value which corresponds to the "high speed" elastic limit as described in [31]. The hysteretic friction, however, increases to its maximum value and then decreases steadily tending to zero. Observing the curve in Figure 6.15, we can see a time delay between the steady-state peak of the hysteretic friction and its transient counterpart. Initially, the transient hysteretic friction is less than the steady-state value, but becomes larger soon after the time corresponding to the peak in the steady-state value. Following the peak in the transient value of the hysteretic friction, the difference between it and its steady-state counterpart steadily declines to zero, as do both quantities at large speeds. Observe that the history of the indentor tip shift mimics the history of the hysteretic friction here and in all cases described below. This is an expression of the fact that hysteretic friction is related to the uneven pressure distribution inside $C(t)$ and the indentor tip shift is a measure of such asymmetry.

It is also interesting to observe that while the transient contact interval length C_T coalesces with its steady-state counterpart C_S after $t \approx 3$, the indentor tip shifts h_S and h_T are different throughout the observed history. In other words, even though $C_T = C_S$ for $t > 3$, the indentor tip in the transient case is positioned differently inside the contact interval with respect to the front and rear boundaries then in the steady-state case. The difference in shapes of pressure distribution between the transient and the steady-state cases accounts for the difference in hysteretic friction.

Cumulative graphs of the histories of the contact interval length and hysteretic friction for viscoelastic materials with $\frac{G_1}{G_0} = \frac{1}{4}$, $\frac{G_1}{G_0} = \frac{1}{2}$ and $\frac{G_1}{G_0} = 1$ are given in Figure 6.16 and Figure 6.17 respectively.

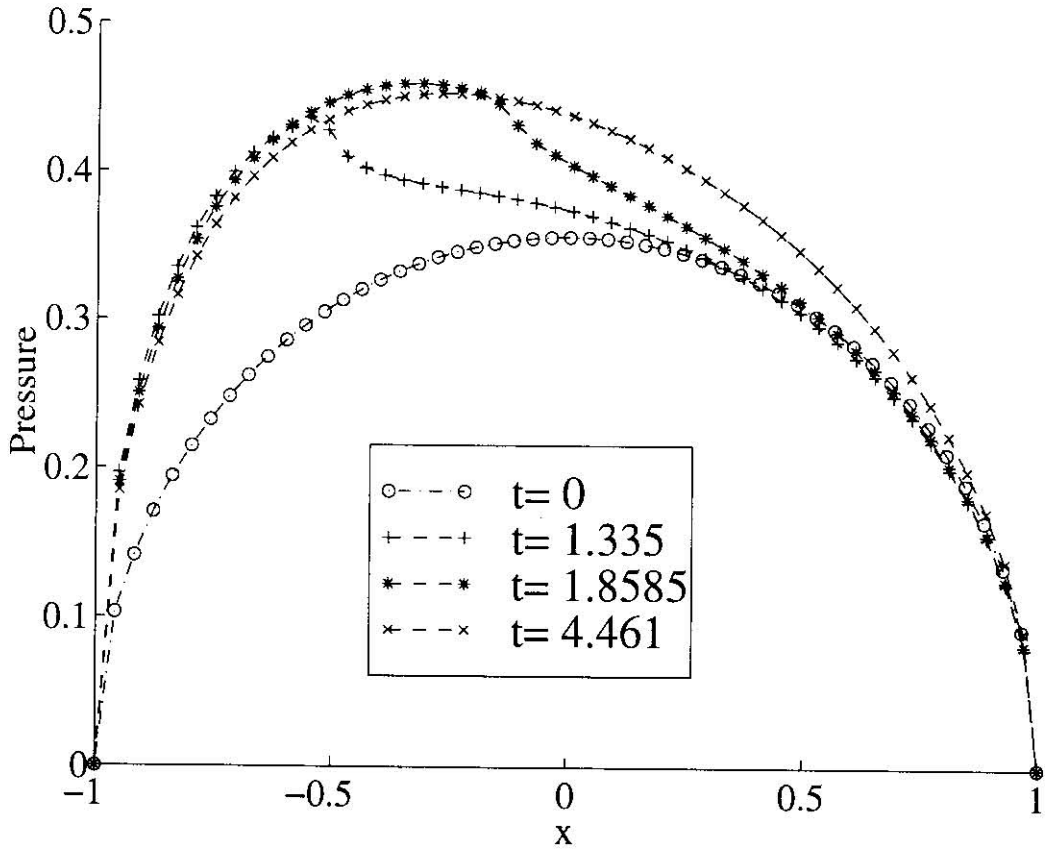

Figure 6.10: Indentor accelerating to a constant speed $V = 1$ as given by (6.2.1). History of pressure distribution. $\frac{G_1}{G_0} = 1$

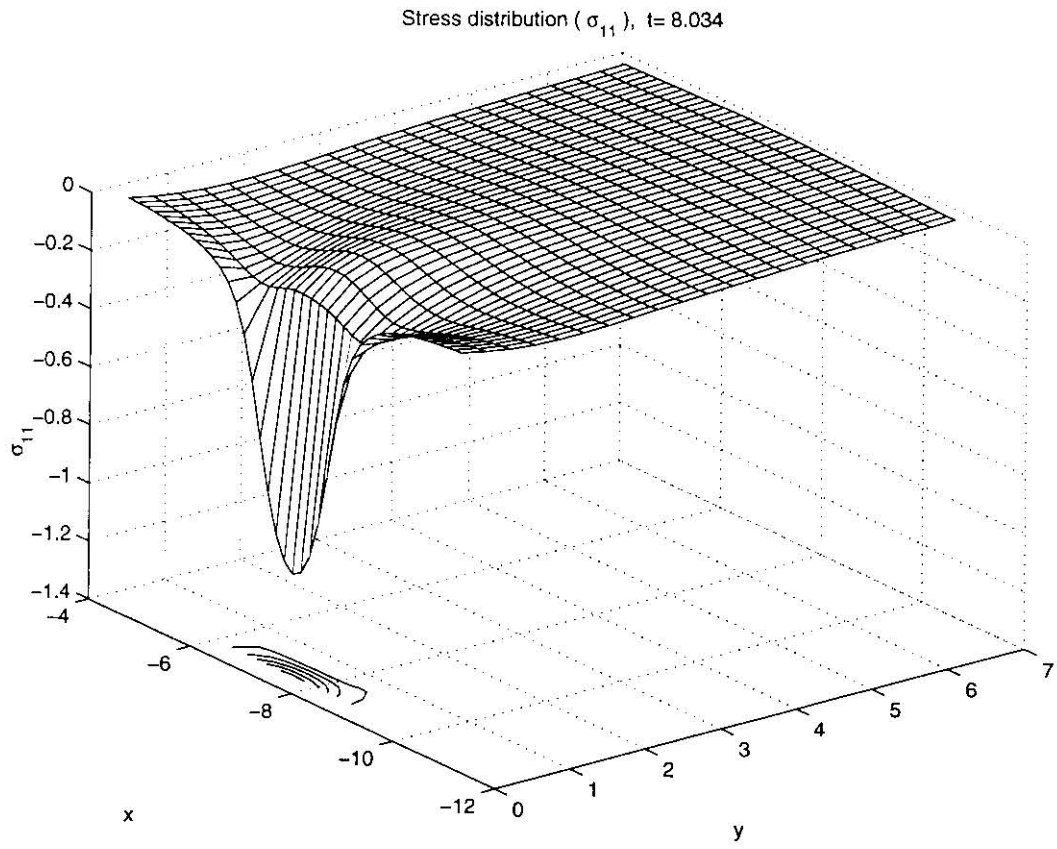

Figure 6.11: Indentor accelerating to a constant speed $V = 1$ as given by (6.2.1). Stress distribution: σ_{11}. $\frac{G_1}{G_0} = \frac{1}{4}$

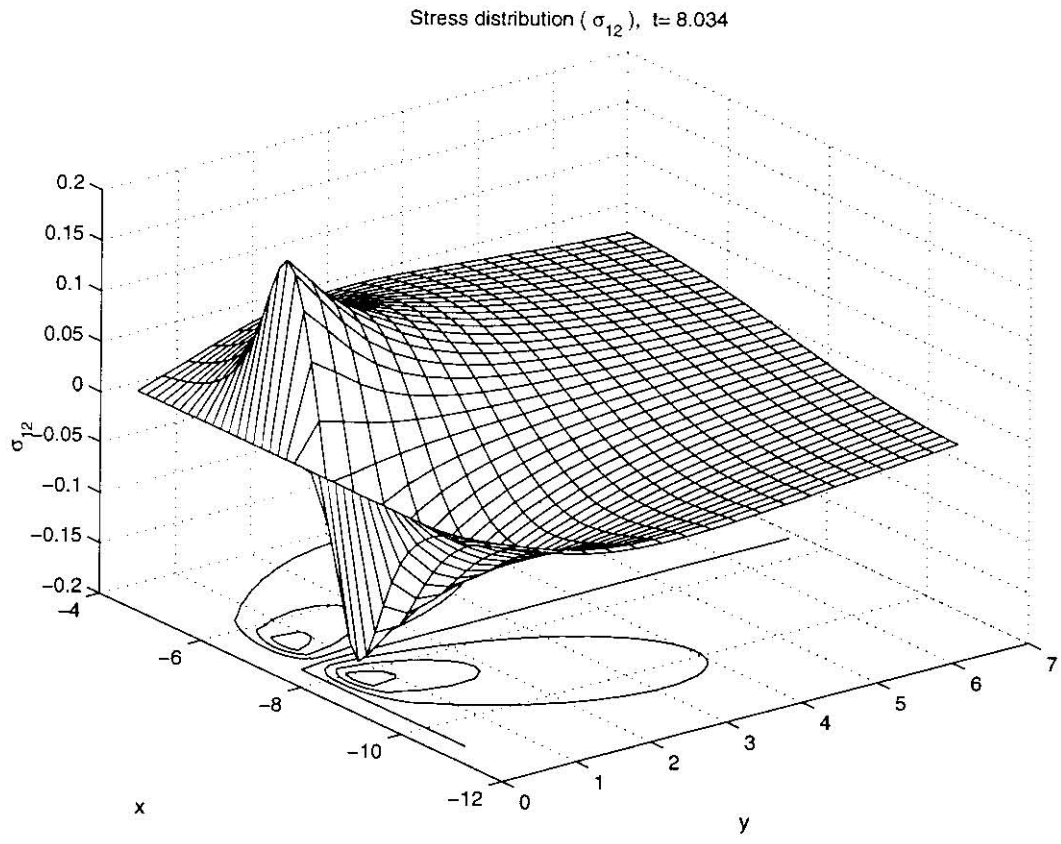

Figure 6.12: Indentor accelerating to a constant speed $V = 1$ as given by (6.2.1). Stress distribution: σ_{12}. $\frac{G_1}{G_0} = \frac{1}{4}$

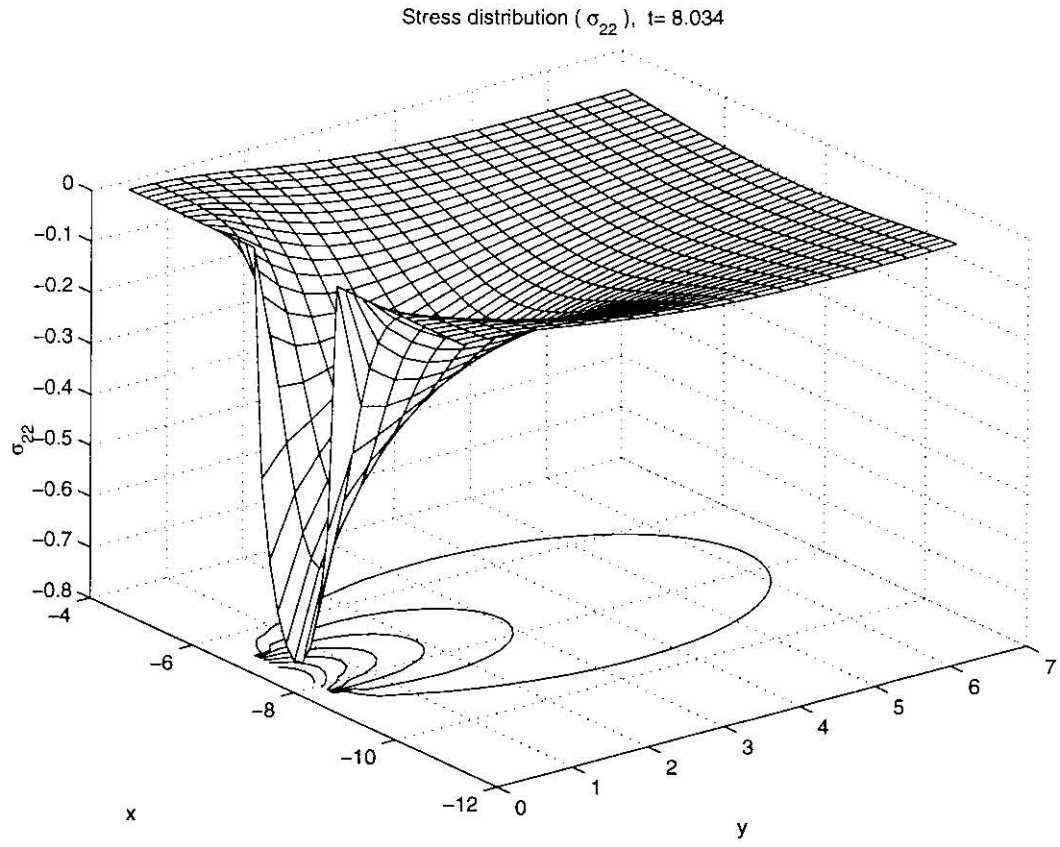

Figure 6.13: Indentor accelerating to a constant speed $V = 1$ as given by (6.2.1). Stress distribution: σ_{22}. $\frac{G_1}{G_0} = \frac{1}{4}$

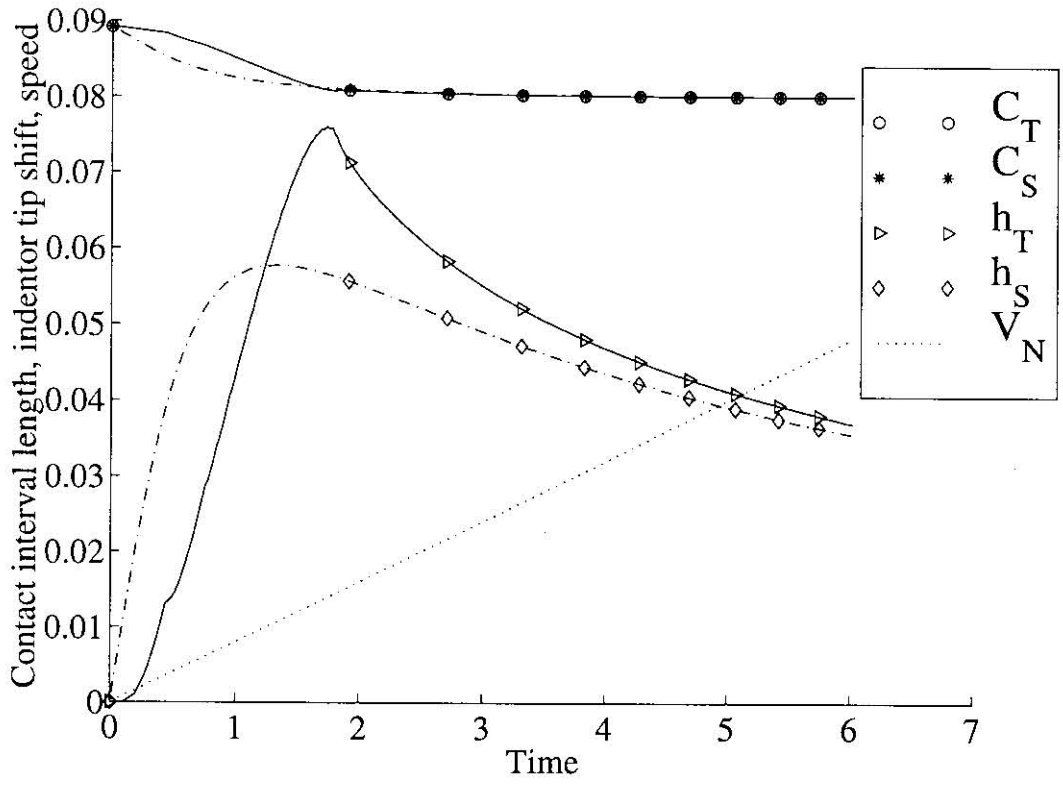

Figure 6.14: Constantly accelerating indentor: $V = t$. History of contact interval length, indentor tip shift and speed. The solid lines indicate the transient solution and the broken lines indicate the steady-state solution. The dotted line indicates the speed. $\frac{G_1}{G_0} = \frac{1}{4}$

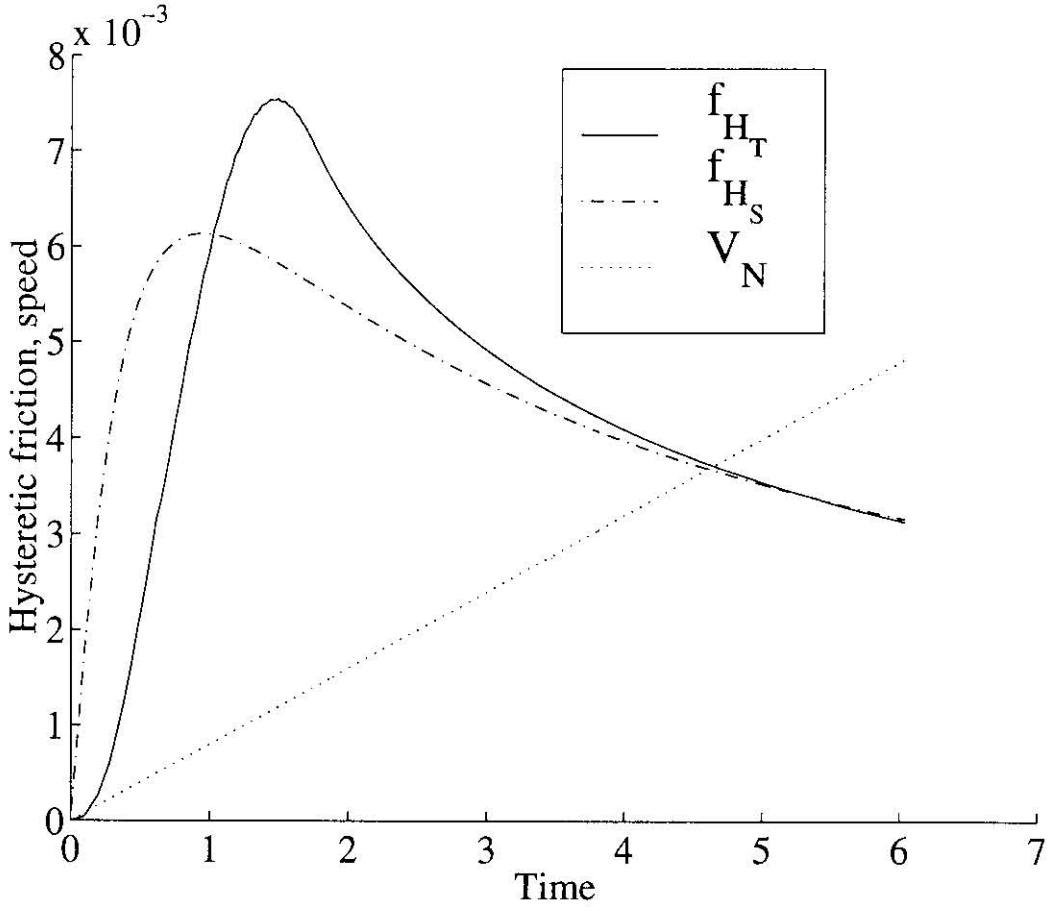

Figure 6.15: Constantly accelerating indentor: $V = t$. History of hysteretic friction and speed. The solid lines indicate the transient solution and the broken lines indicate the steady-state solution. The dotted line indicates the speed. $\frac{G_1}{G_0} = \frac{1}{4}$

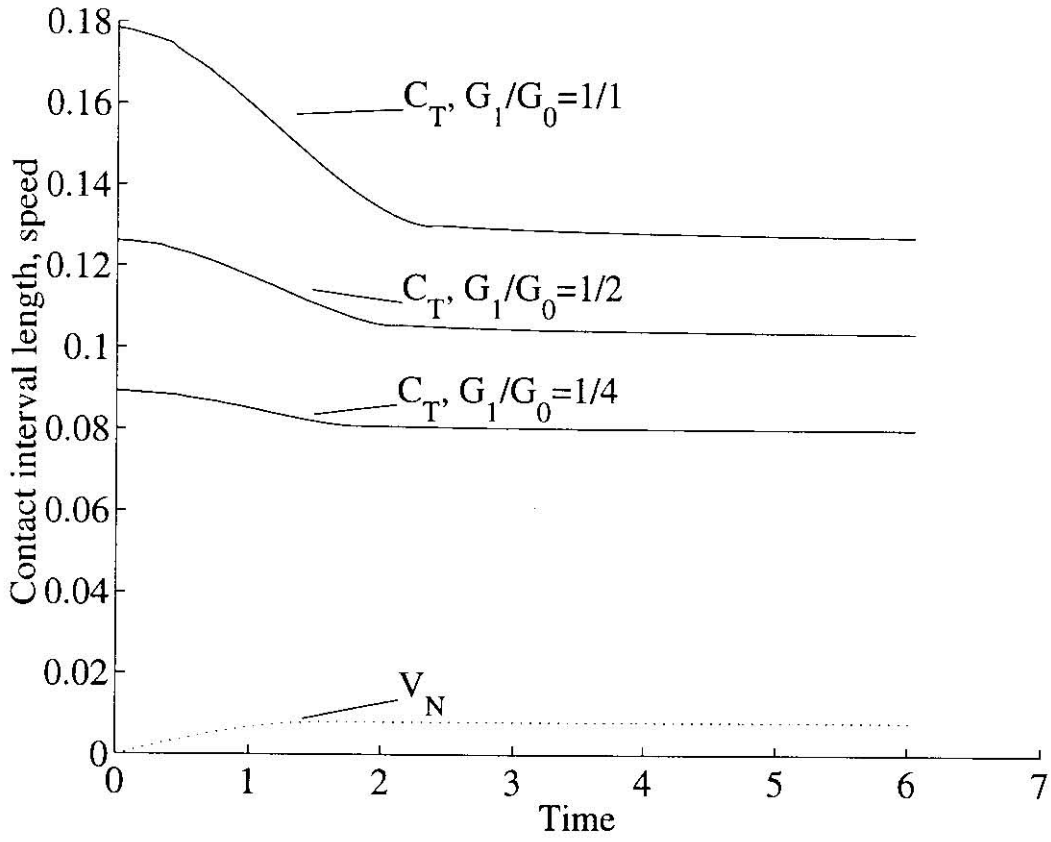

Figure 6.16: Constantly accelerating indentor: $V = t$. History of contact interval length and speed. $\frac{G_1}{G_0} = \frac{1}{4}$, $\frac{G_1}{G_0} = \frac{1}{2}$, $\frac{G_1}{G_0} = 1$

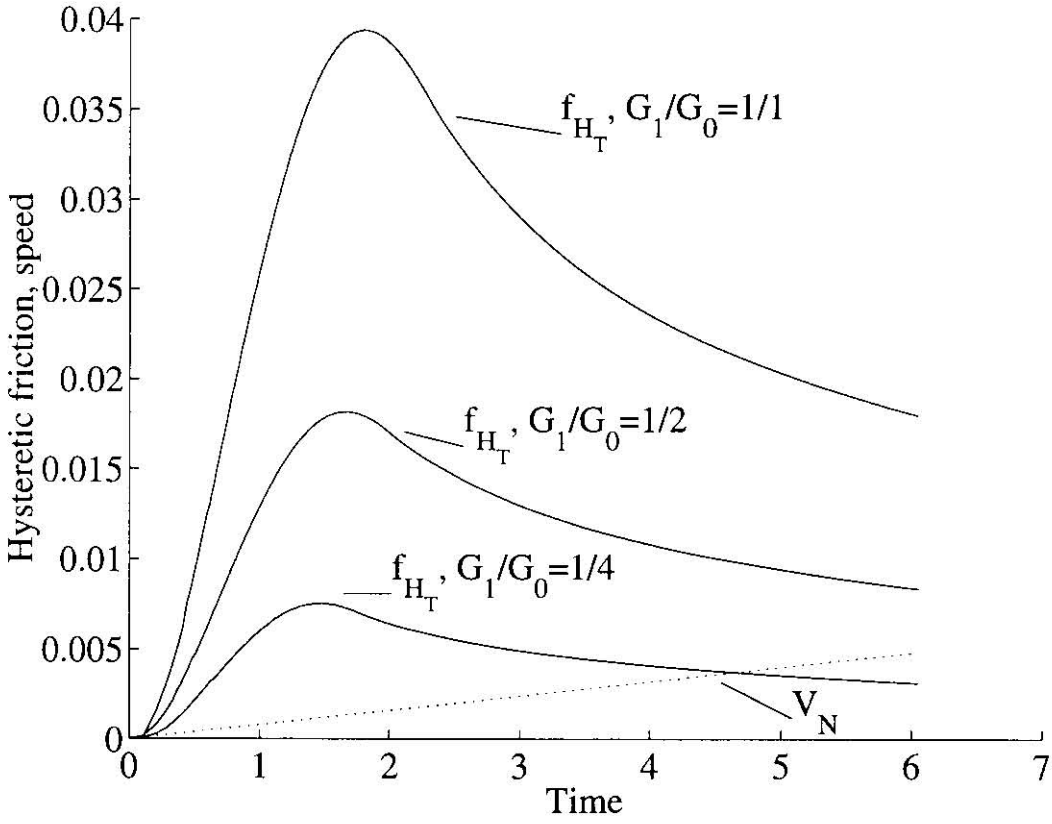

Figure 6.17: Constantly accelerating indentor: $V = t$. History of hysteretic friction and speed. $\frac{G_1}{G_0} = \frac{1}{4}$, $\frac{G_1}{G_0} = \frac{1}{2}$, $\frac{G_1}{G_0} = 1$

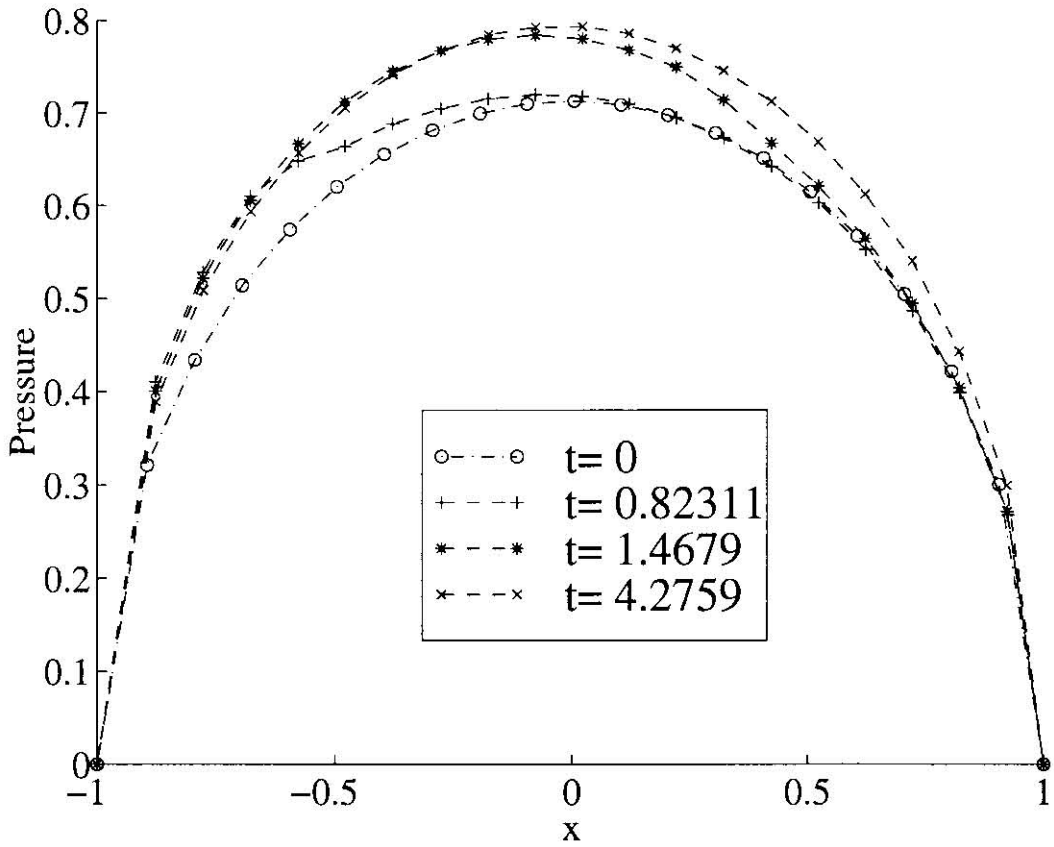

Figure 6.18: Constantly accelerating indentor: $V = t$. History of pressure distribution. $\frac{G_1}{G_0} = \frac{1}{4}$

The histories of pressure distribution for the same materials are given in Figures 6.18, 6.19 and 6.20.

The distributions of stress components for the material with $\frac{G_1}{G_0} = \frac{1}{4}$ are presented in Figures 6.21 - 6.23.

6.4 Acceleration Followed by Deceleration

We now consider the case of an indentor accelerating smoothly from rest to a prescribed speed V_1 and then, after a period of constant velocity motion, decelerating to the speed V_2 (which is substantially less than V_1). As an example, we consider

$$V(t) = \begin{cases} \sin t, & 0 \leq t < \frac{\pi}{2} \\ 1, & \frac{\pi}{2} \leq t < 5 \\ 1 + 0.9 \sin(t + \pi - 5), & 5 \leq t < 5 + \frac{\pi}{2} \\ 0.1, & t > 5 + \frac{\pi}{2} \end{cases} \tag{6.4.1}$$

The results are presented in Figures 6.24, 6.25. We can observe the characteristic trough in the length of the contact interval after the initial period of acceleration. Thereupon, for the constant speed motion the lengths of the contact interval for the transient and the steady-state case merge and for the deceleration phase the transient contact interval length lags behind the steady-state case catching up to the latter shortly after the speed has become constant. The behaviour of the hysteretic friction is a mirror image of that of the contact interval length in that for those periods of time when the transient contact interval length exceeds its steady-state counterpart, the transient hysteretic friction is smaller than the steady-state one. It is also interesting to notice that, even though at the beginning of the deceleration period the transient hysteretic friction is slightly smaller than the steady-state one, by the end of this period it is larger.

Cumulative graphs of the histories of the contact interval length and hysteretic friction for viscoelastic materials with $\frac{G_1}{G_0} = \frac{1}{4}$, $\frac{G_1}{G_0} = \frac{1}{2}$ and $\frac{G_1}{G_0} = 1$ are given in Figure 6.26 and Figure 6.27 respectively. For comparison, we also provide the steady-state solutions corresponding to the same values of the viscoelastic ratios. As one

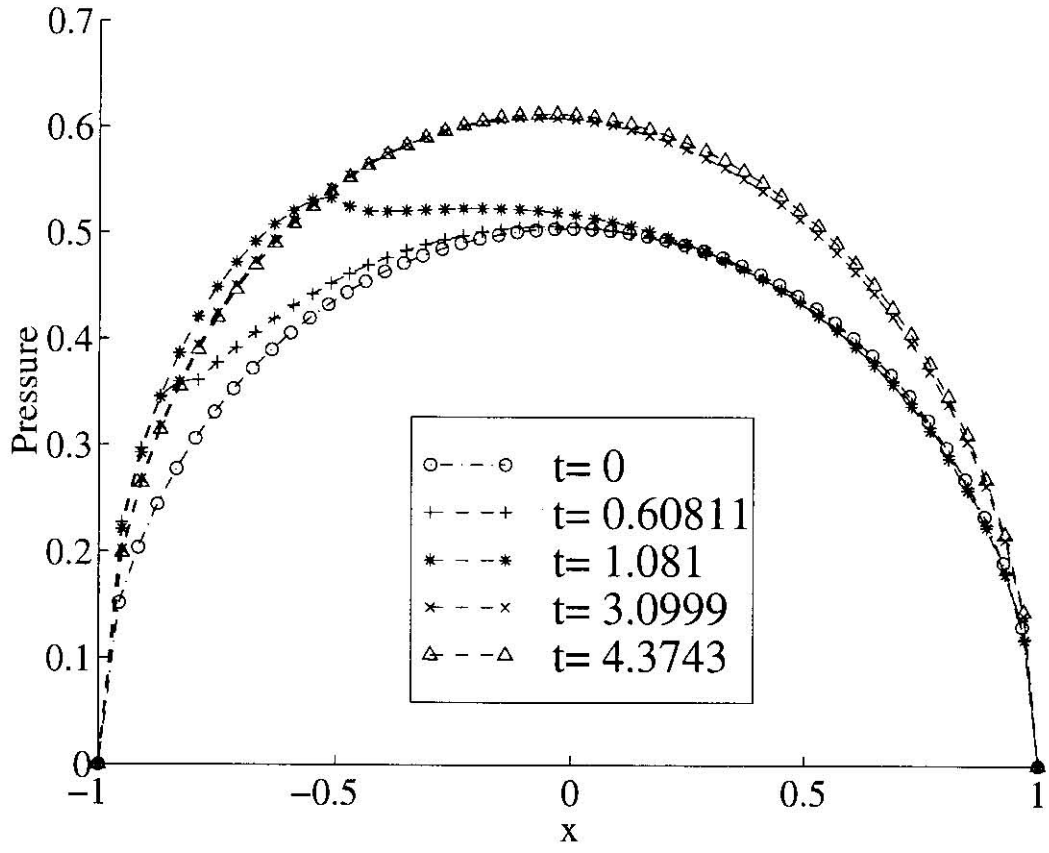

Figure 6.19: Constantly accelerating indentor: $V = t$. History of pressure distribution. $\frac{G_1}{G_0} = \frac{1}{2}$

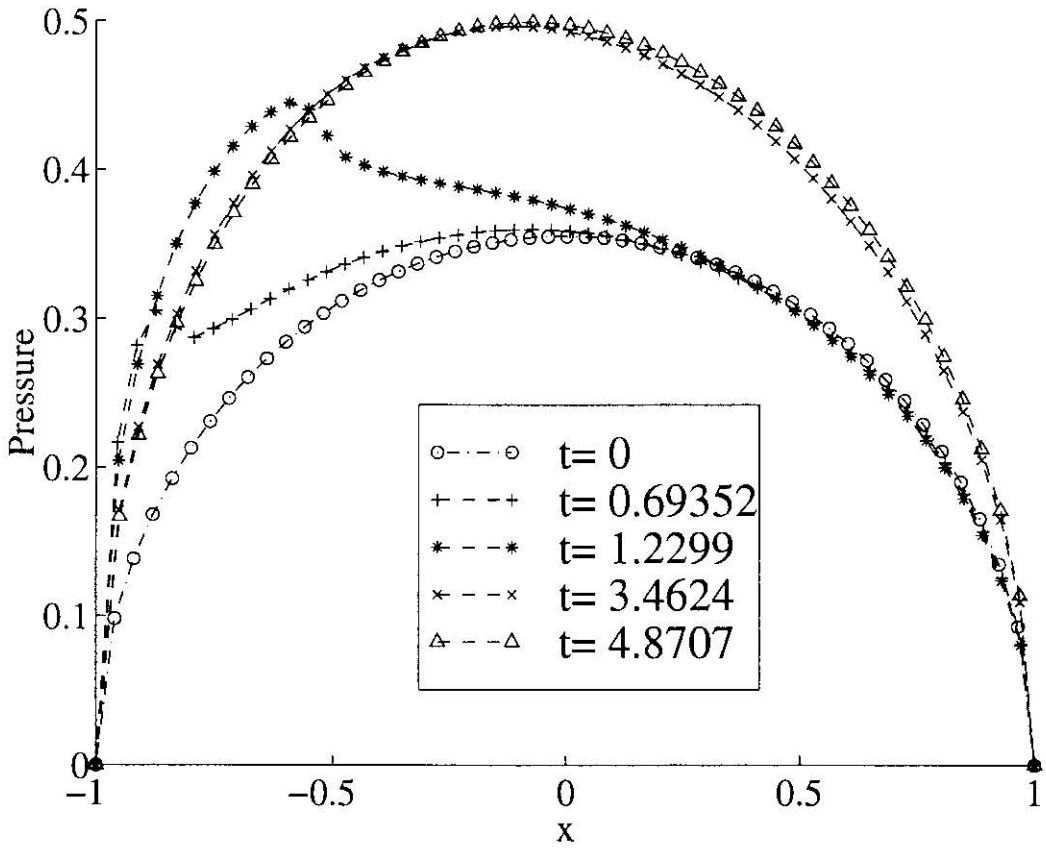

Figure 6.20: Constantly accelerating indentor: $V = t$. History of pressure distribution. $\frac{G_1}{G_0} = 1$

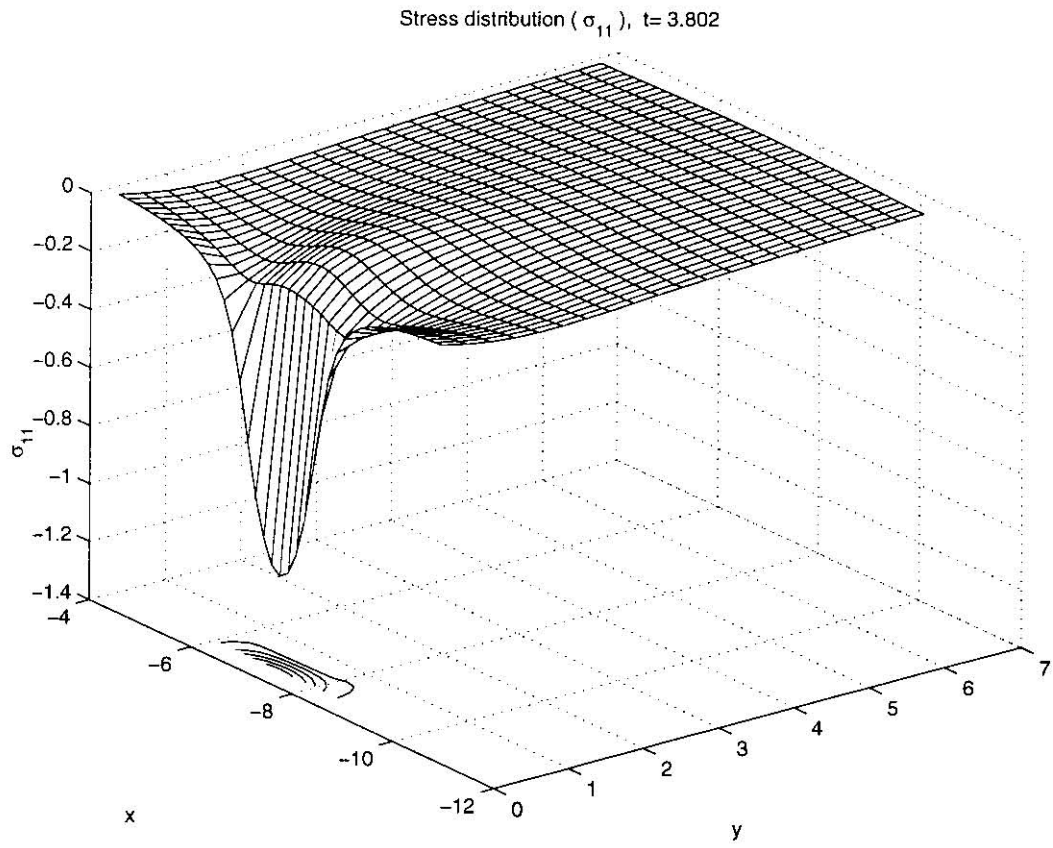

Figure 6.21: Constantly accelerating indentor: $V = t$. Stress distribution: σ_{11}. $\frac{G_1}{G_0} = \frac{1}{4}$

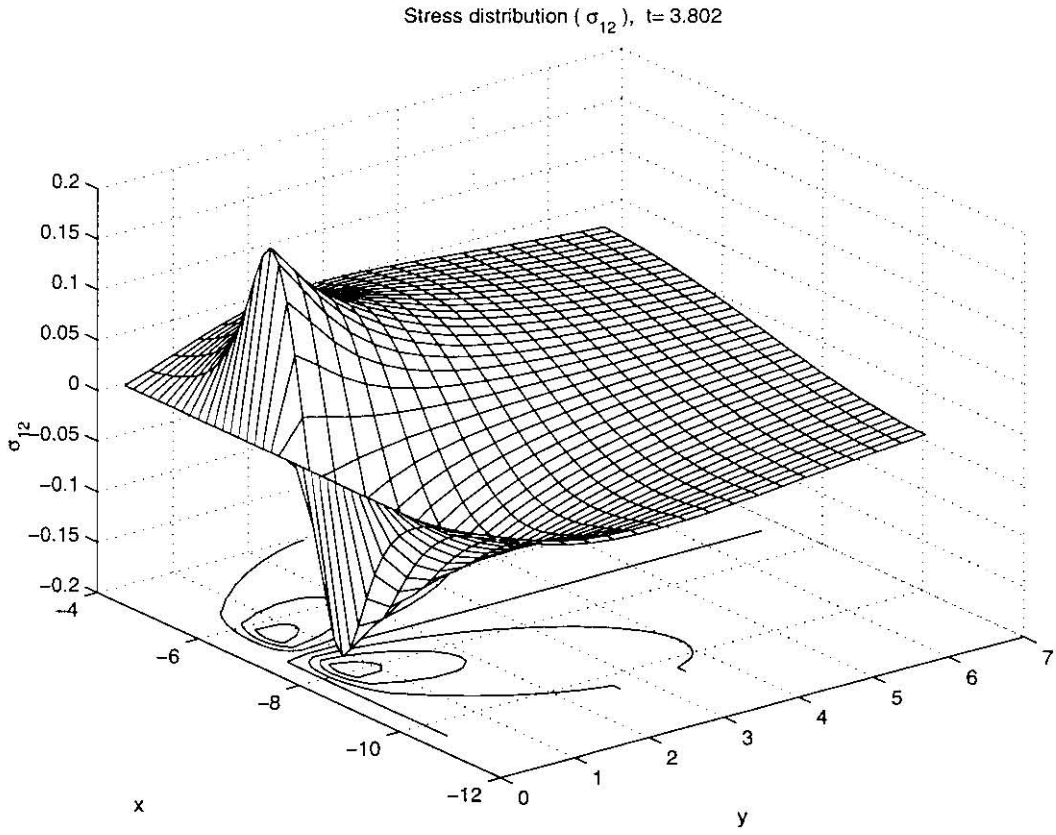

Figure 6.22: Constantly accelerating indentor: $V = t$. Stress distribution: σ_{12}. $\frac{G_1}{G_0} = \frac{1}{4}$

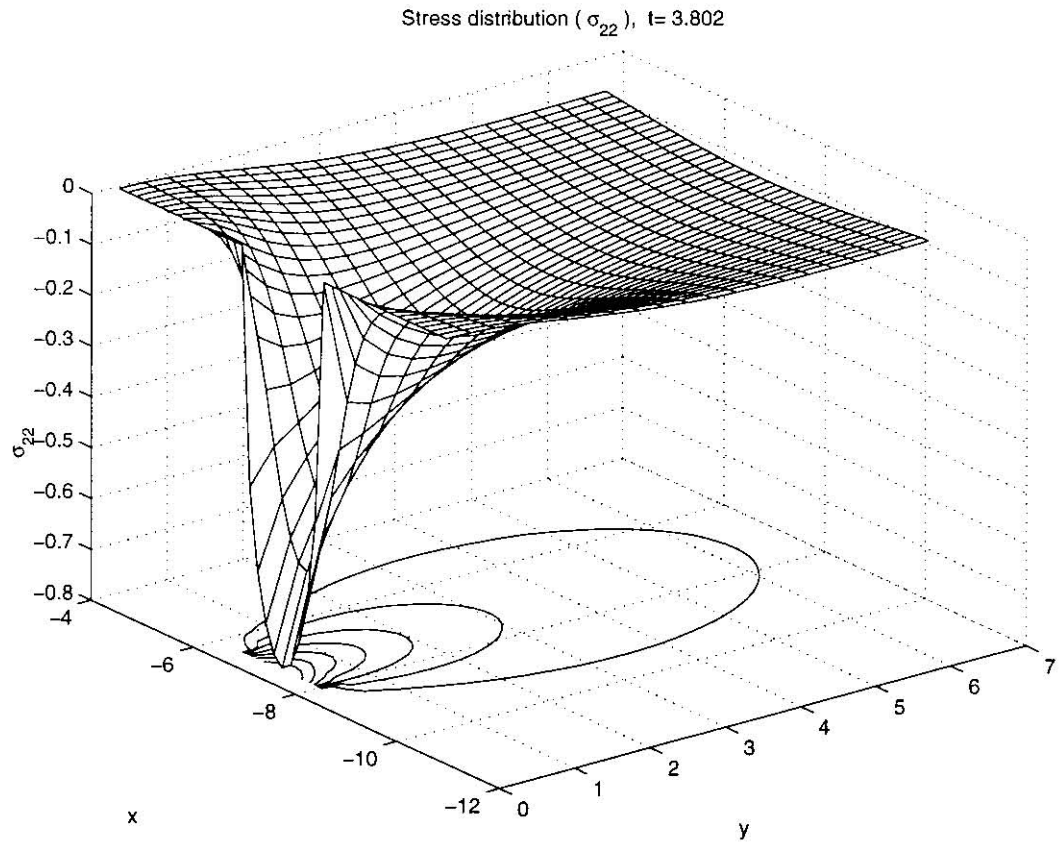

Figure 6.23: Constantly accelerating indentor: $V = t$. Stress distribution: σ_{22}. $\frac{G_1}{G_0} = \frac{1}{4}$

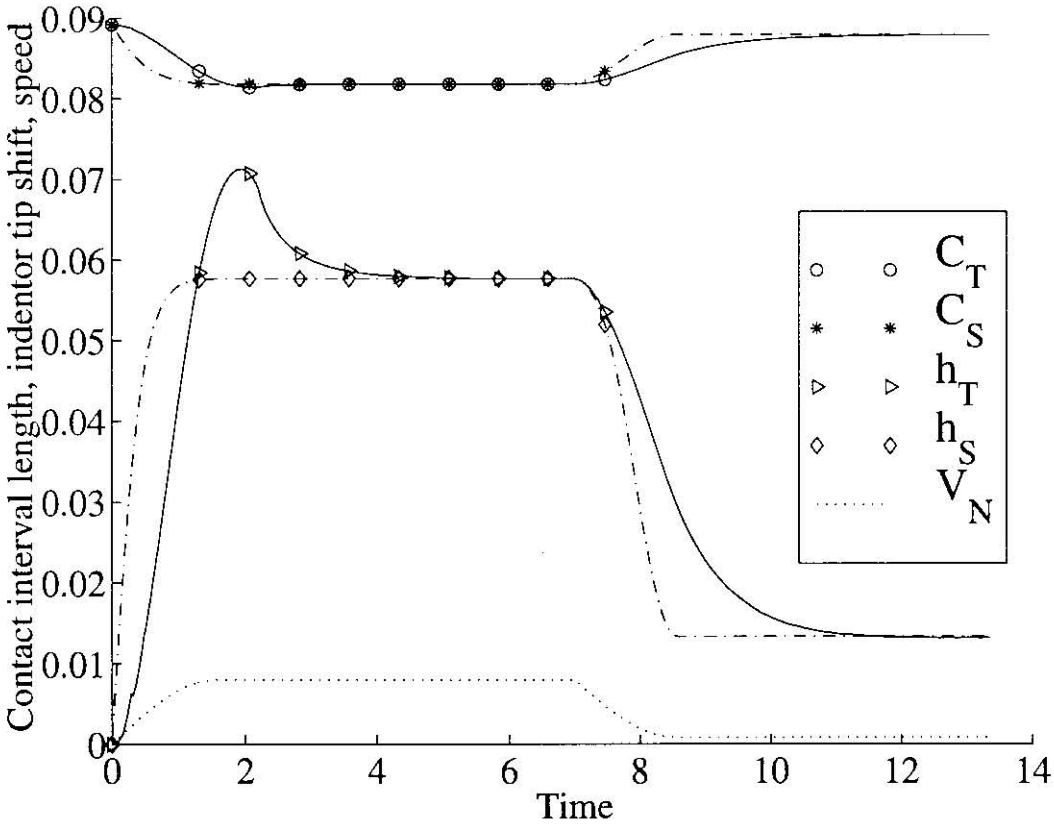

Figure 6.24: Alternately accelerating and decelerating indentor with $V(t)$ varying as described by (6.4.1). History of contact interval length, indentor tip shift and speed. The solid lines indicate the transient solution and the broken lines indicate the steady-state solution. The dotted line indicates the speed. $\frac{G_1}{G_0} = \frac{1}{4}$.

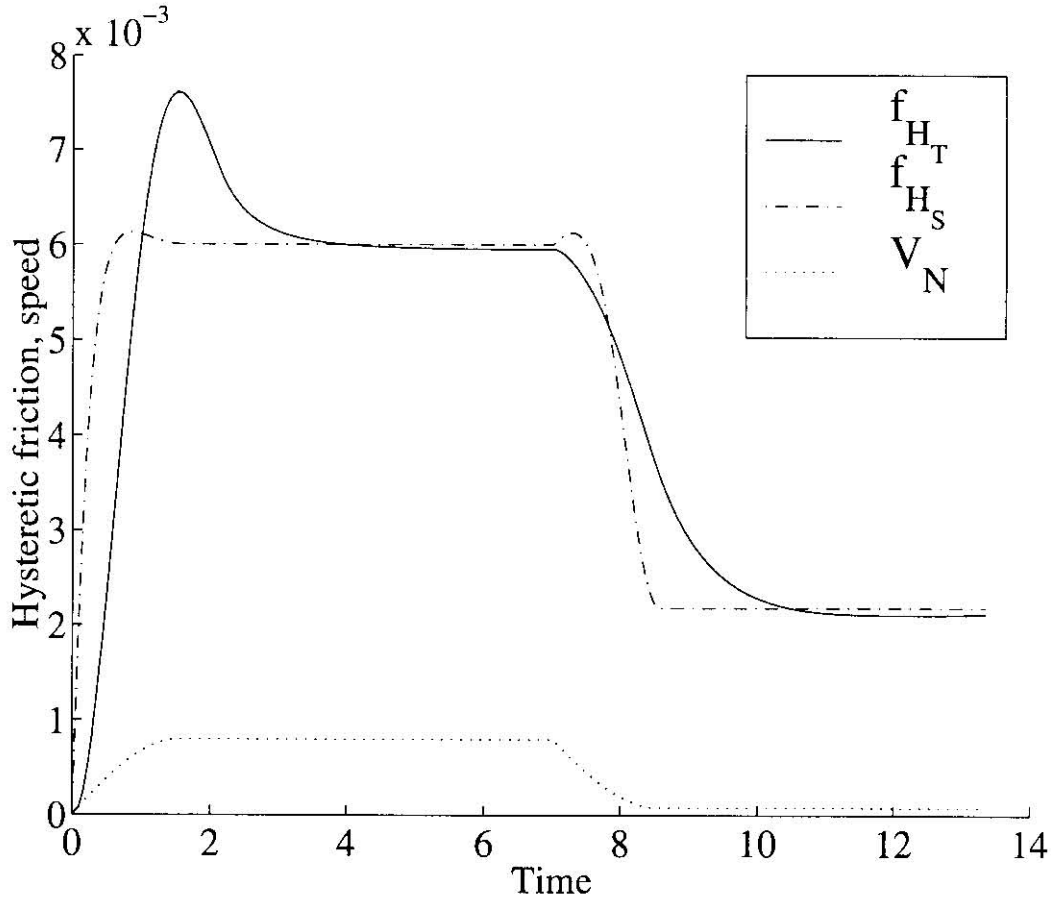

Figure 6.25: Alternately accelerating and decelerating indentor with $V(t)$ varying as described by (6.4.1). History of hysteretic friction and speed. The solid lines indicate the transient solution and the broken lines indicate the steady-state solution. The dotted line indicates the speed. $\frac{G_1}{G_0} = \frac{1}{4}$.

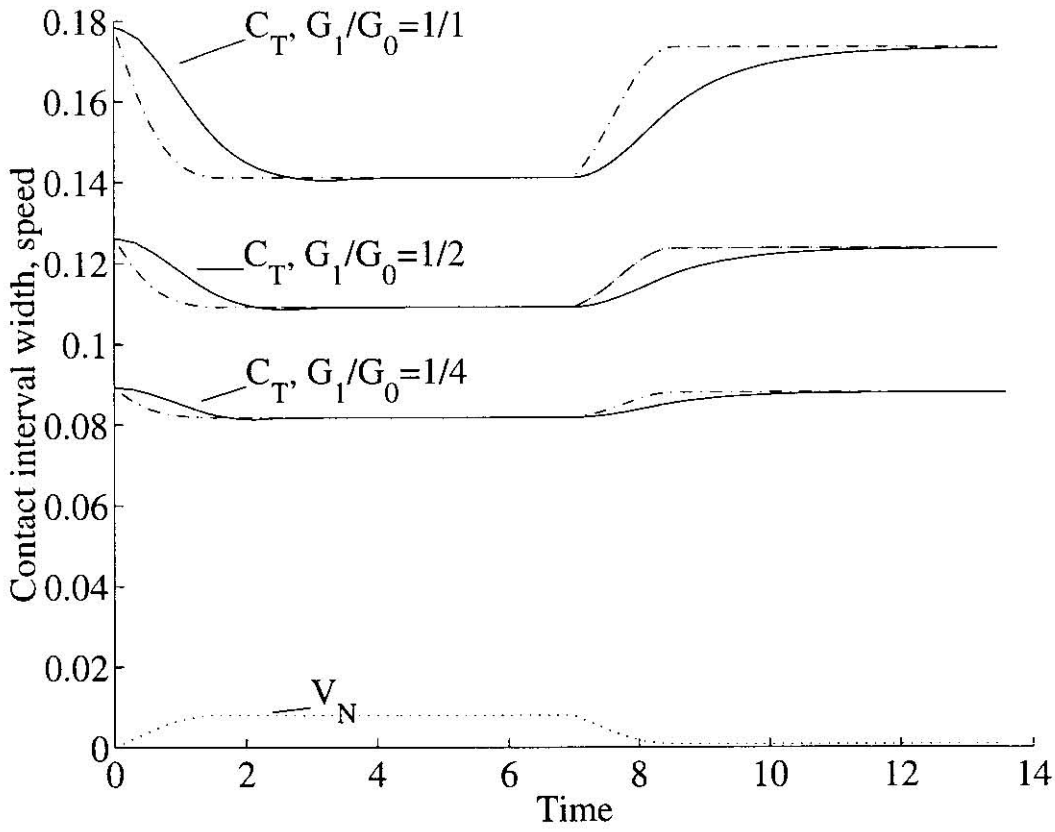

Figure 6.26: Alternately accelerating and decelerating indentor with $V(t)$ varying as described by (6.4.1). History of contact interval length and speed. The solid lines indicate the transient solution and the dash-dotted lines indicate the steady-state solution. The dotted line indicates the speed. $\frac{G_1}{G_0} = \frac{1}{4}$, $\frac{G_1}{G_0} = \frac{1}{2}$, $\frac{G_1}{G_0} = 1$

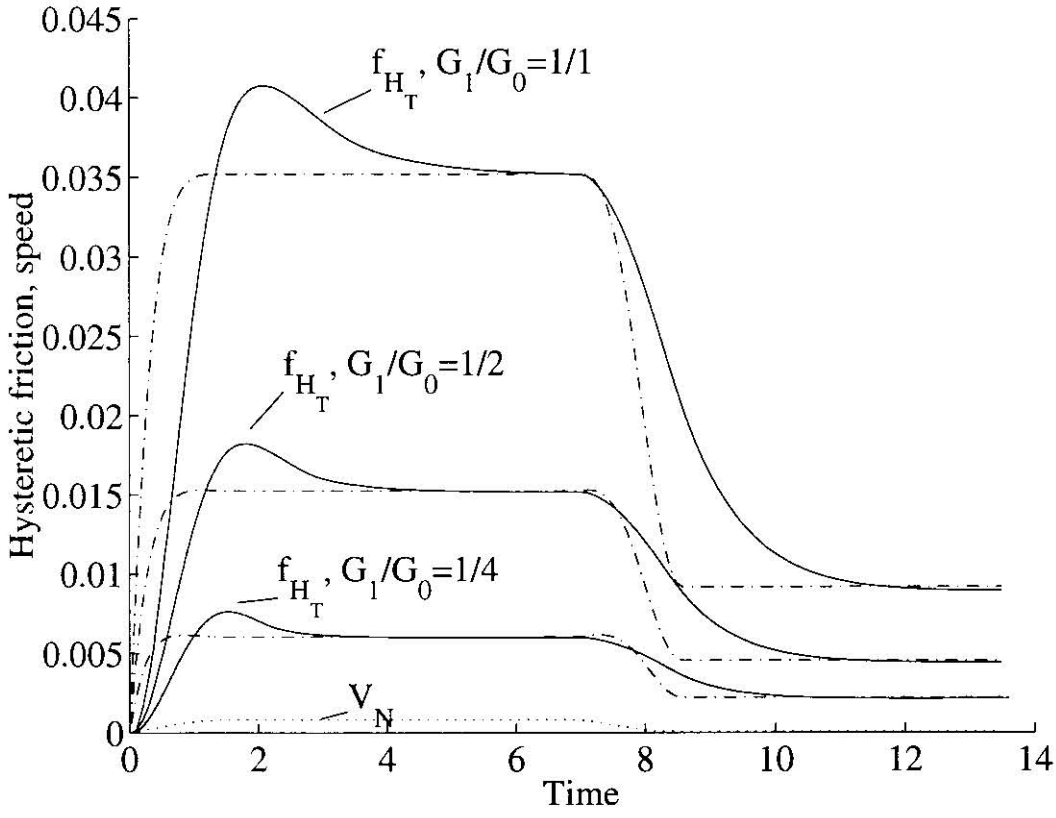

Figure 6.27: Alternately accelerating and decelerating indentor with $V(t)$ varying as described by (6.4.1). History of hysteretic friction and speed. The solid lines indicate the transient solution and the dash-dotted lines indicate the steady-state solution. The dotted line indicates the speed. $\frac{G_1}{G_0} = \frac{1}{4}$, $\frac{G_1}{G_0} = \frac{1}{2}$, $\frac{G_1}{G_0} = 1$

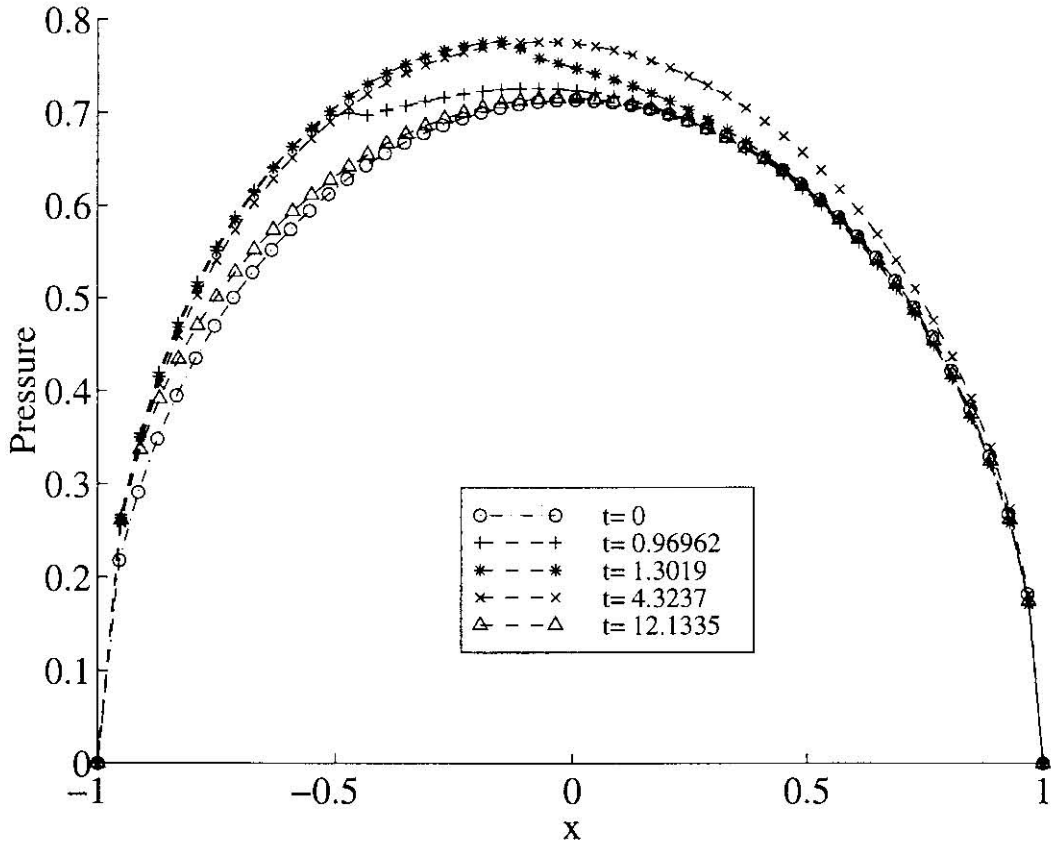

Figure 6.28: Alternately accelerating and decelerating indentor with $V(t)$ varying as described by (6.4.1). History of pressure distribution. $\frac{G_1}{G_0} = \frac{1}{4}$

can observe, for materials with more pronounced viscoelastic properties the transient solutions approaches the steady-state solutions later than for slightly viscoelastic materials.

The histories of pressure distribution for the same materials are given in Figures 6.28, 6.29 and 6.30.

The distributions of stress components for the material with $\frac{G_1}{G_0} = \frac{1}{4}$ are presented in Figures 6.31 - 6.33.

6.5 Periodically Varying Speed: $V = 1 + 0.9 \sin t$

For the first example in the case of a periodically varying speed, we consider:

$$V(t) = A + B \sin t, \tag{6.5.1}$$

where $A > B > 0$. Three combinations of A and B were tried: $A = 1.0, B = 0.9$, $A = 1.0, B = 0.25$ and $A = 0.5, B = 0.25$. The graphs for the first set of values are presented. These are the most interesting results that were obtained.

Consider the case of a relatively high average speed with periodic variations of large amplitude about this value: $A = 1, B = 0.9$ (see Figures 6.34, 6.35).

The length of the transient contact interval follows its steady-state counterpart, but with a delay. The steady-state hysteretic friction is almost sinusoidal. However, the neighbourhood of the peak is "inverted", i.e., the friction decreases as the normalized speed $\frac{V}{100\alpha R}$ increases to values above 0.01. This is in line with the fact that for the steady-state problem the hysteretic friction reaches its peak at medium velocities and decreases as speed deviates to either side of these values (see [65], [45], [31], [47],).

The transient hysteretic friction, however, presents a totally different picture. After a sharp increase corresponding to the accelerating indentor, it starts to decrease after the normalized speed $\frac{V}{100\alpha R}$ becomes greater than 0.01. The rate of decrease slows down shortly after the speed reaches its maximum. The hysteretic friction attempts to stabilize at a certain level. As the speed further continues to decline, the hysteretic friction drops rapidly and then starts to increase with the beginning of a

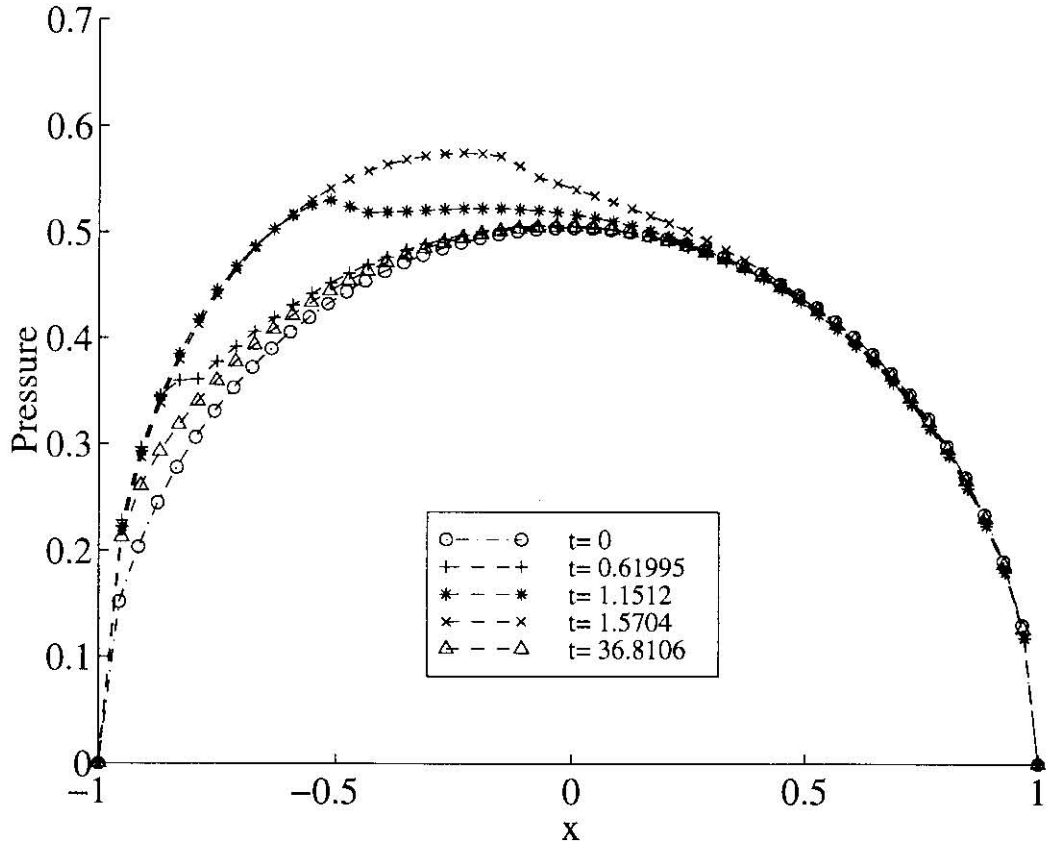

Figure 6.29: Alternately accelerating and decelerating indentor with $V(t)$ varying as described by (6.4.1). $\frac{G_1}{G_0} = \frac{1}{2}$

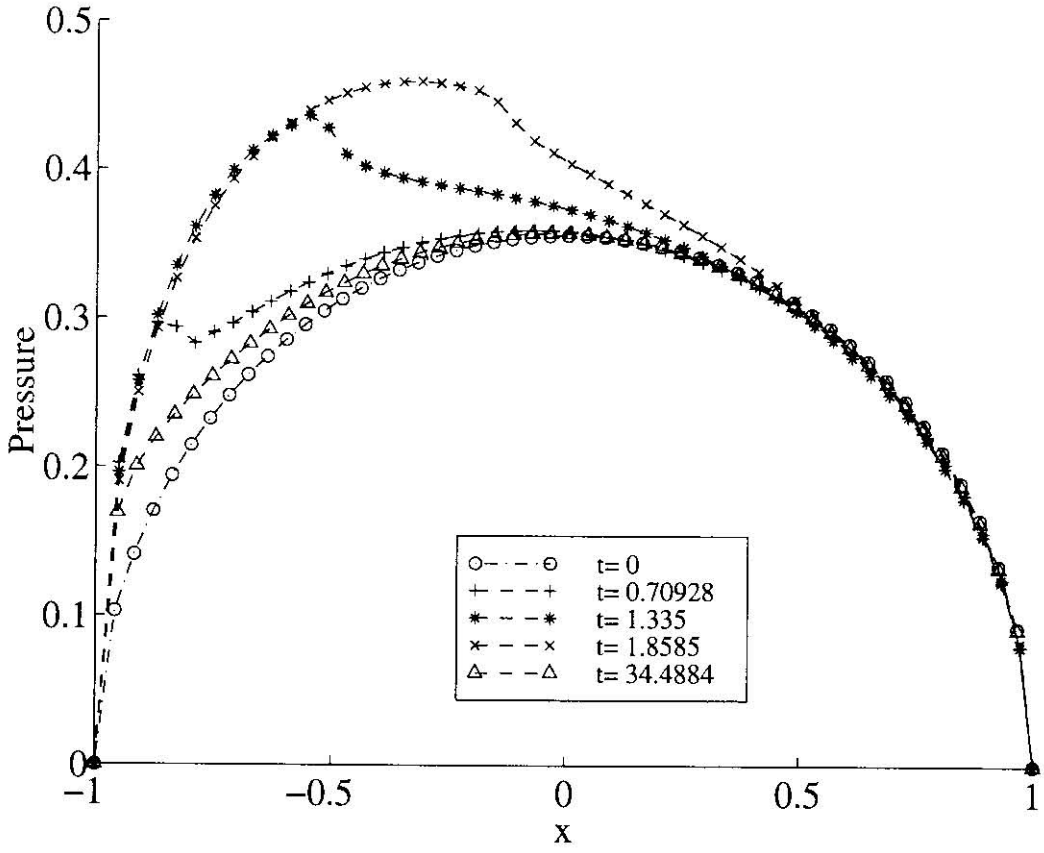

Figure 6.30: Alternately accelerating and decelerating indentor with $V(t)$ varying as described by (6.4.1). History of pressure distribution. $\frac{G_1}{G_0} = 1$

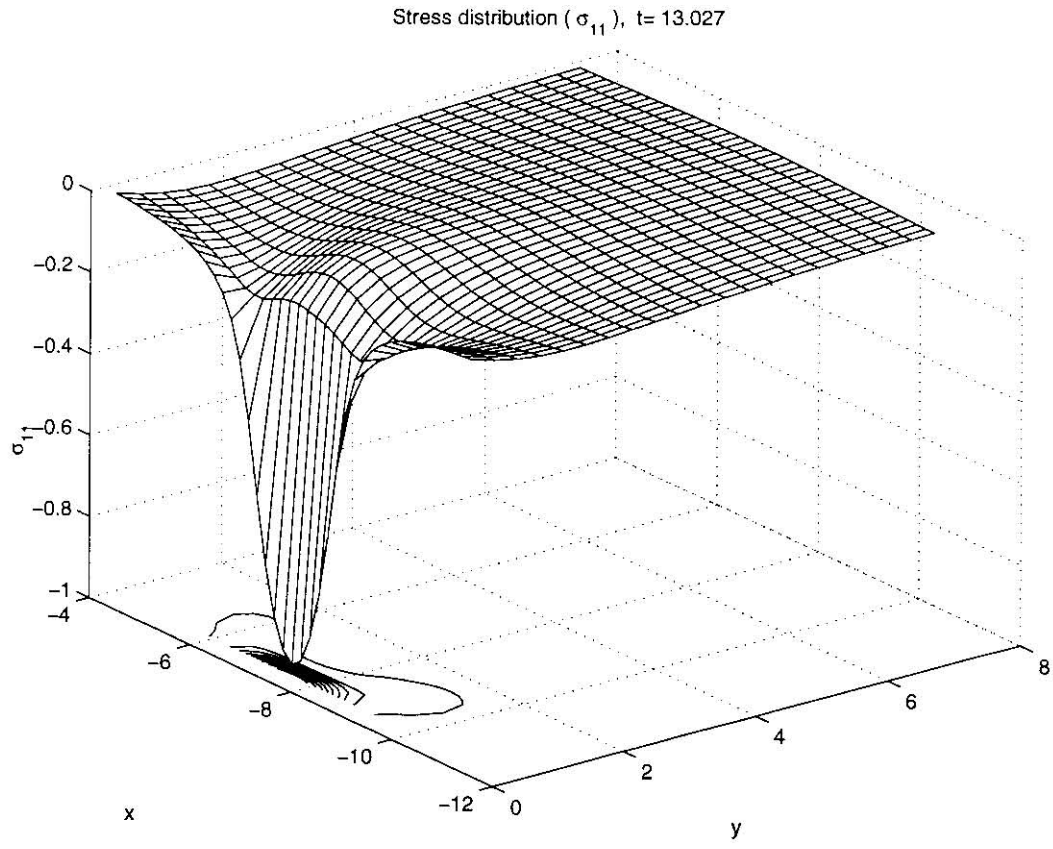

Figure 6.31: Alternately accelerating and decelerating indentor with $V(t)$ varying as described by (6.4.1). Stress distribution: σ_{11}. $\frac{G_1}{G_0} = \frac{1}{4}$

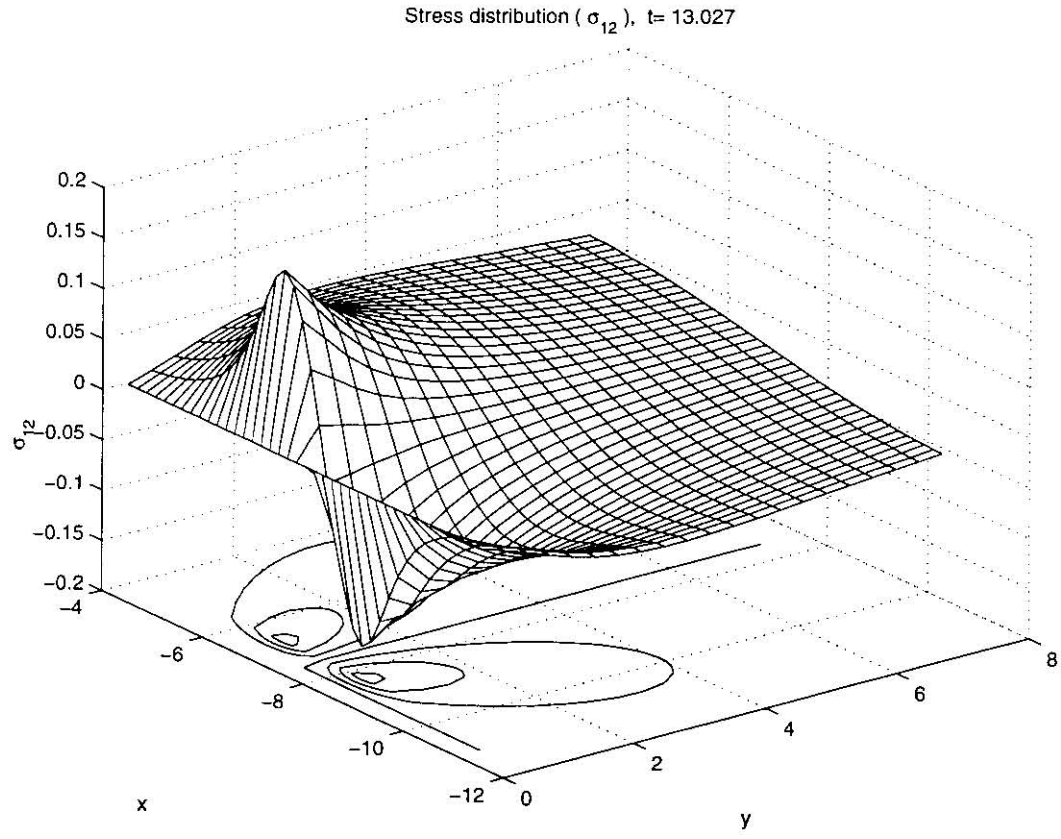

Figure 6.32: Alternately accelerating and decelerating indentor with $V(t)$ varying as described by (6.4.1). Stress distribution: σ_{12}. $\frac{G_1}{G_0} = \frac{1}{4}$

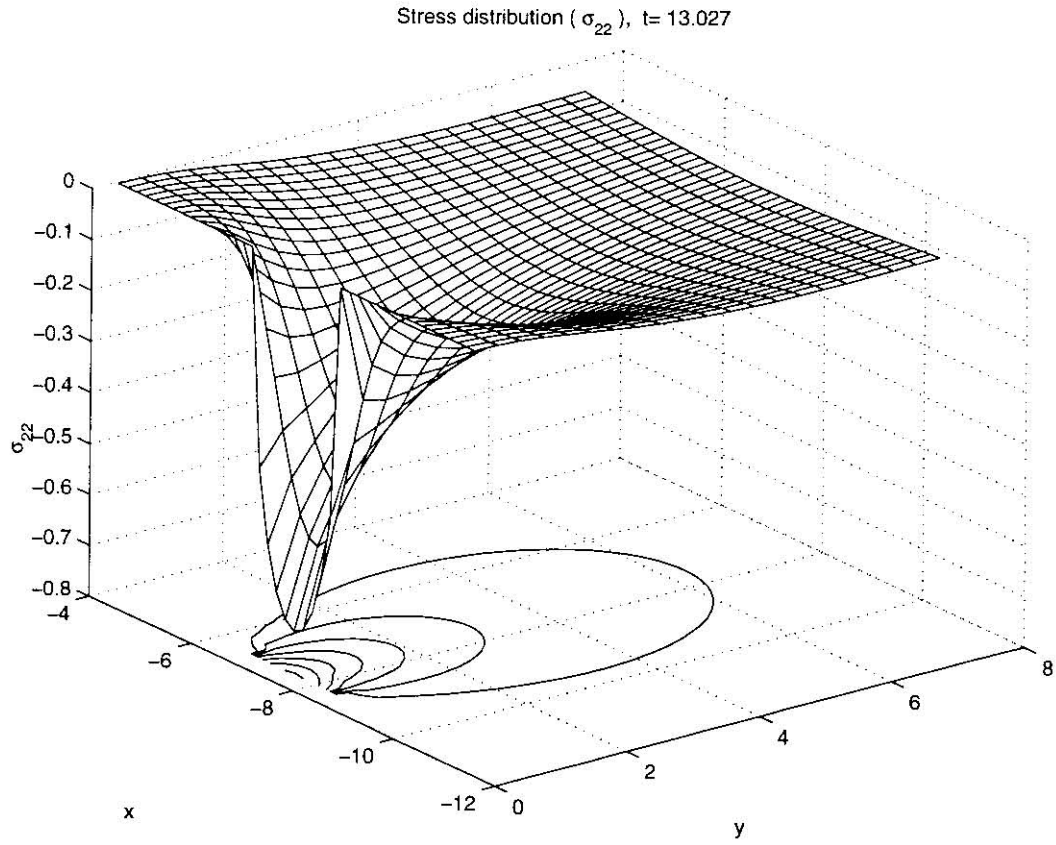

Figure 6.33: Alternately accelerating and decelerating indentor with $V(t)$ varying as described by (6.4.1). Stress distribution: σ_{22}. $\frac{G_1}{G_0} = \frac{1}{4}$

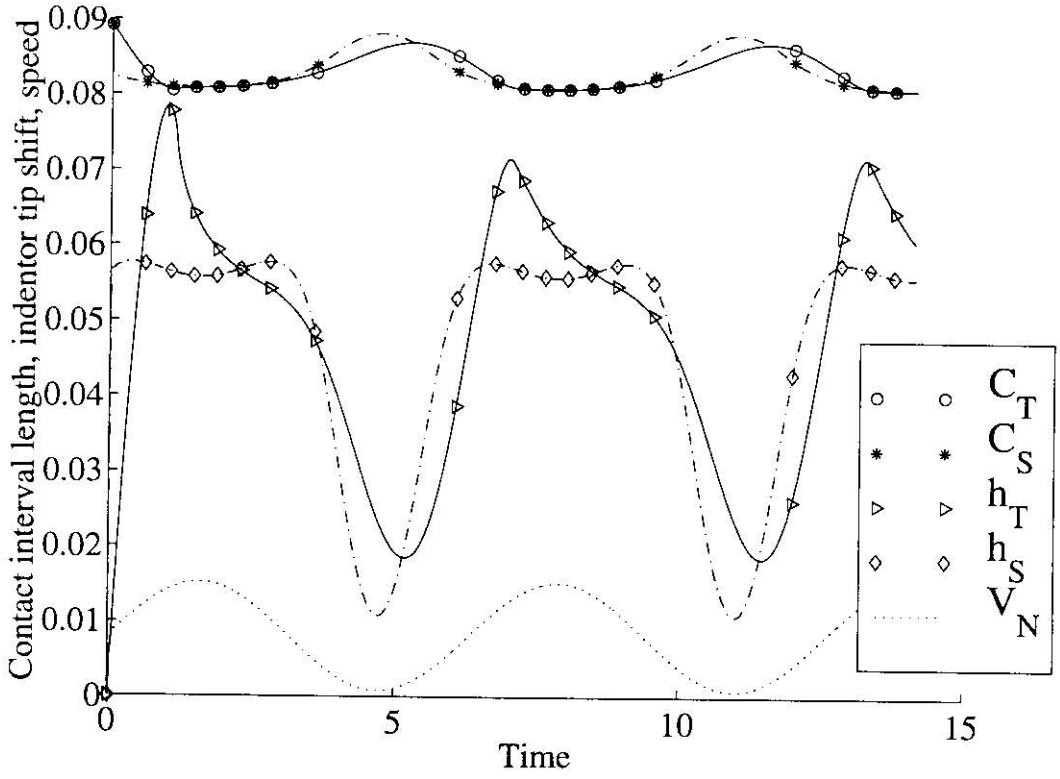

Figure 6.34: Periodically accelerating indentor: $V(t) = 1 + 0.9\sin(t)$. History of contact interval length, indentor tip shift and speed. The solid lines indicate the transient solution and the broken lines indicate the steady-state solution. The dotted line indicates the speed. $\frac{G_1}{G_0} = \frac{1}{4}$.

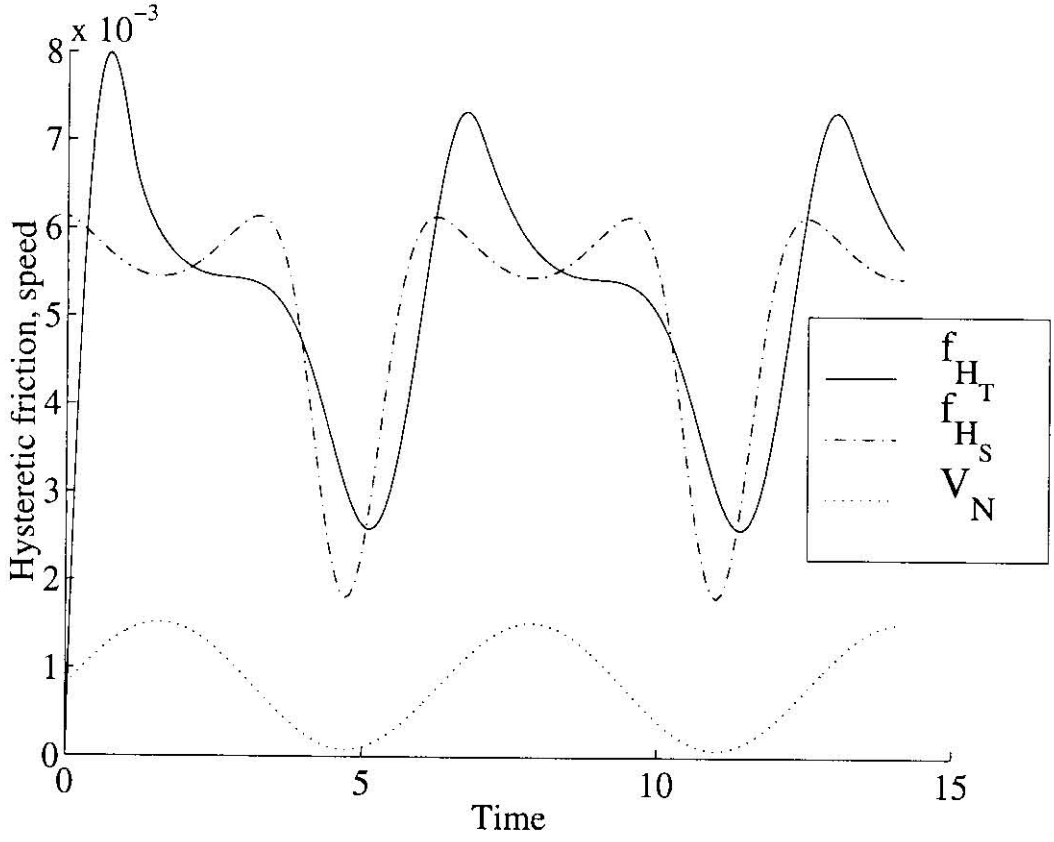

Figure 6.35: Periodically accelerating indentor: $V(t) = 1 + 0.9\sin(t)$. History of hysteretic friction and speed. The solid lines indicate the transient solution and the broken lines indicate the steady-state solution. The dotted line indicates the speed. $\frac{G_1}{G_0} = \frac{1}{4}$.

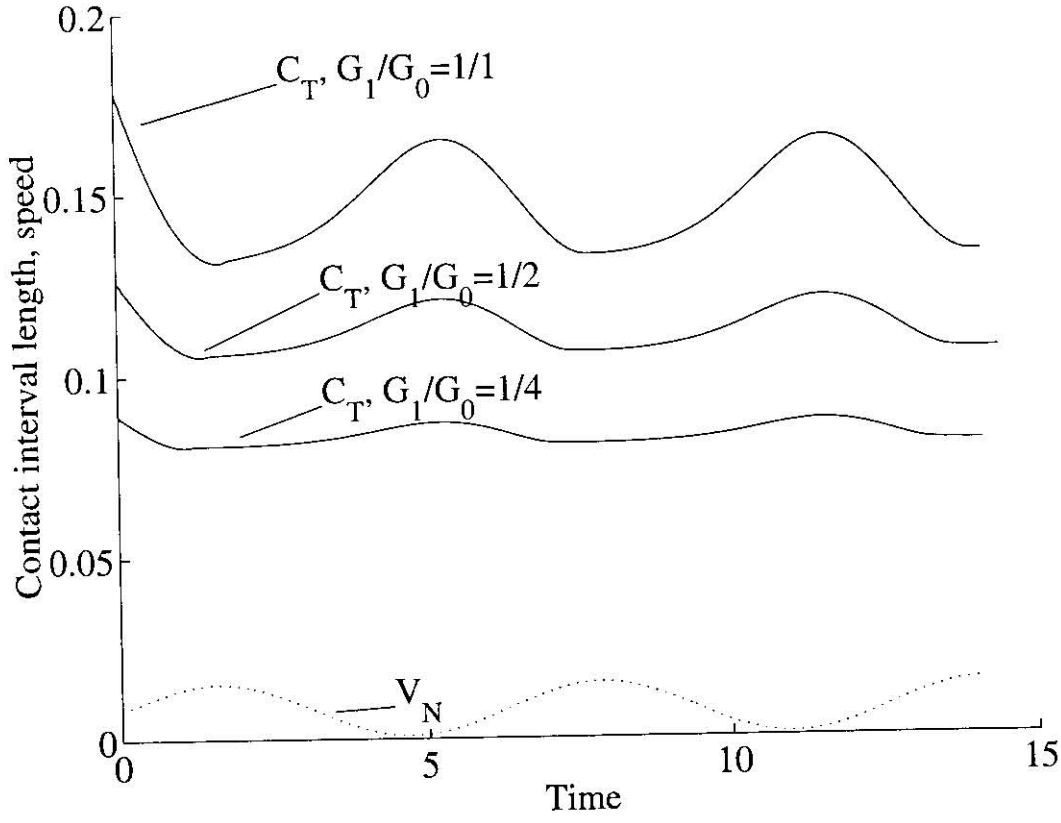

Figure 6.36: Periodically accelerating indentor: $V(t) = 1 + 0.9\sin(t)$. History of contact interval length and speed. $\frac{G_1}{G_0} = \frac{1}{4}$, $\frac{G_1}{G_0} = \frac{1}{2}$, $\frac{G_1}{G_0} = 1$

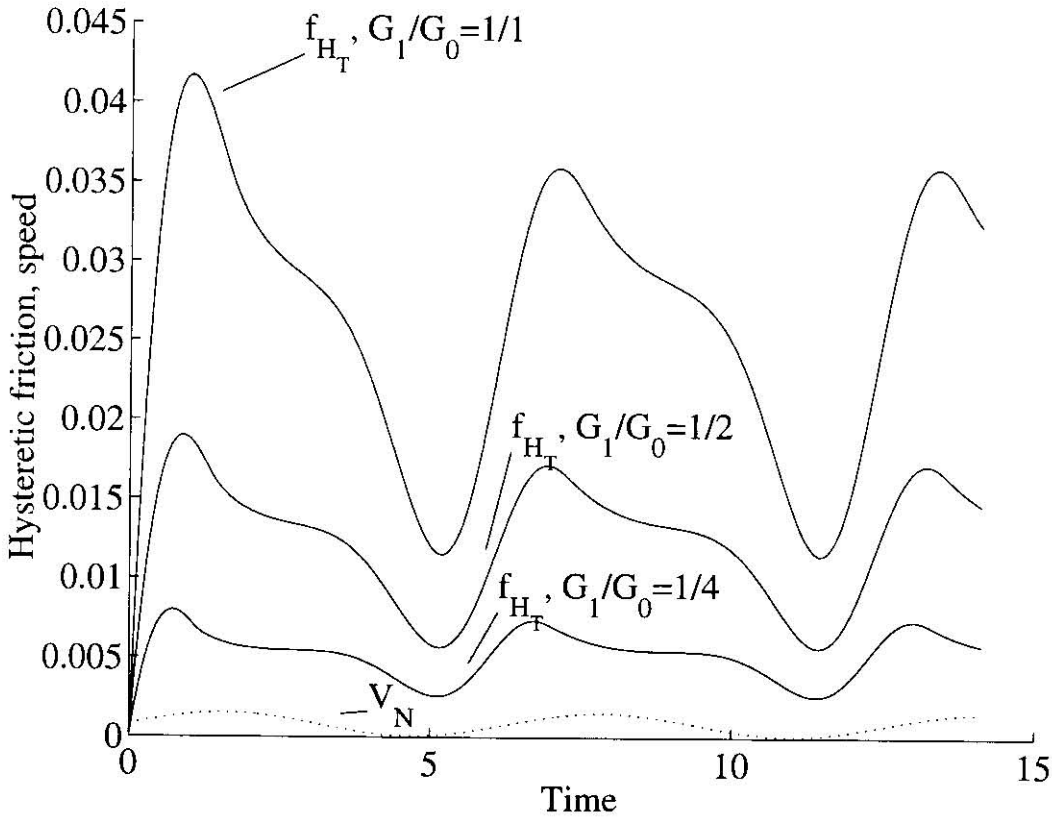

Figure 6.37: Periodically accelerating indentor: $V(t) = 1 + 0.9\sin(t)$. History of hysteretic friction and speed. $\frac{G_1}{G_0} = \frac{1}{4}$, $\frac{G_1}{G_0} = \frac{1}{2}$, $\frac{G_1}{G_0} = 1$

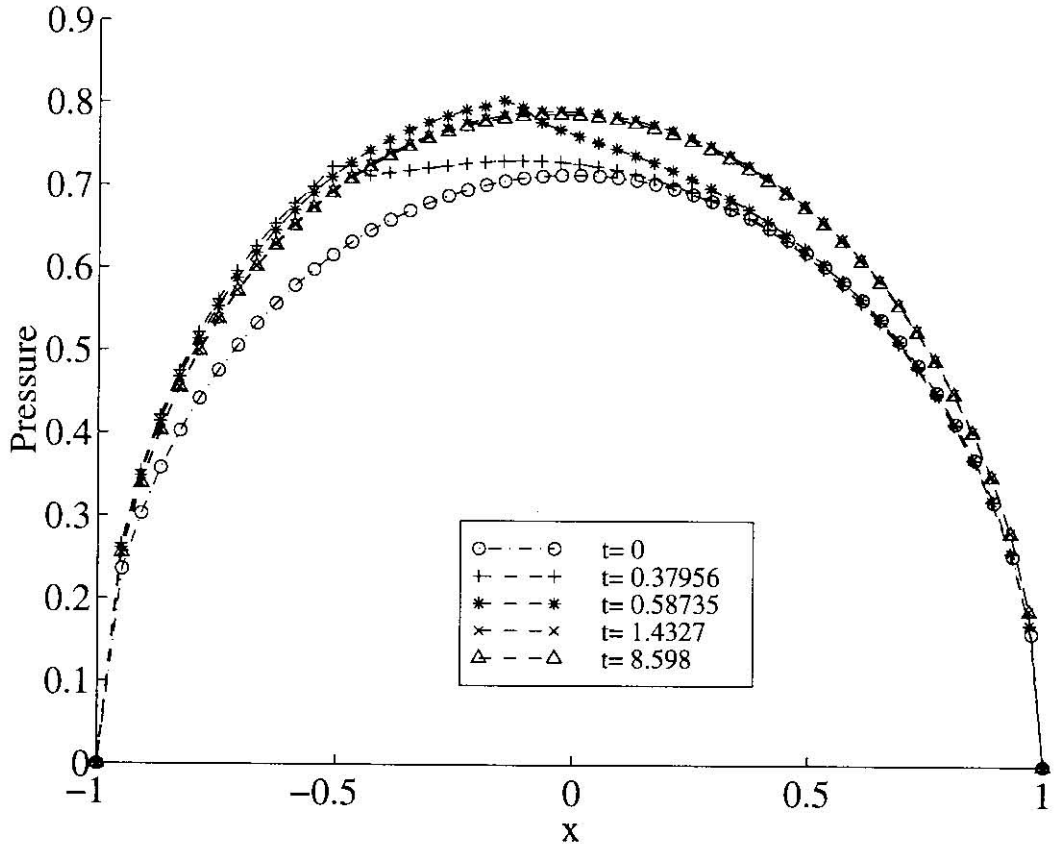

Figure 6.38: Periodically accelerating indentor: $V(t) = 1 + 0.9\sin(t)$. History of pressure distribution. $\frac{G_1}{G_0} = \frac{1}{4}$

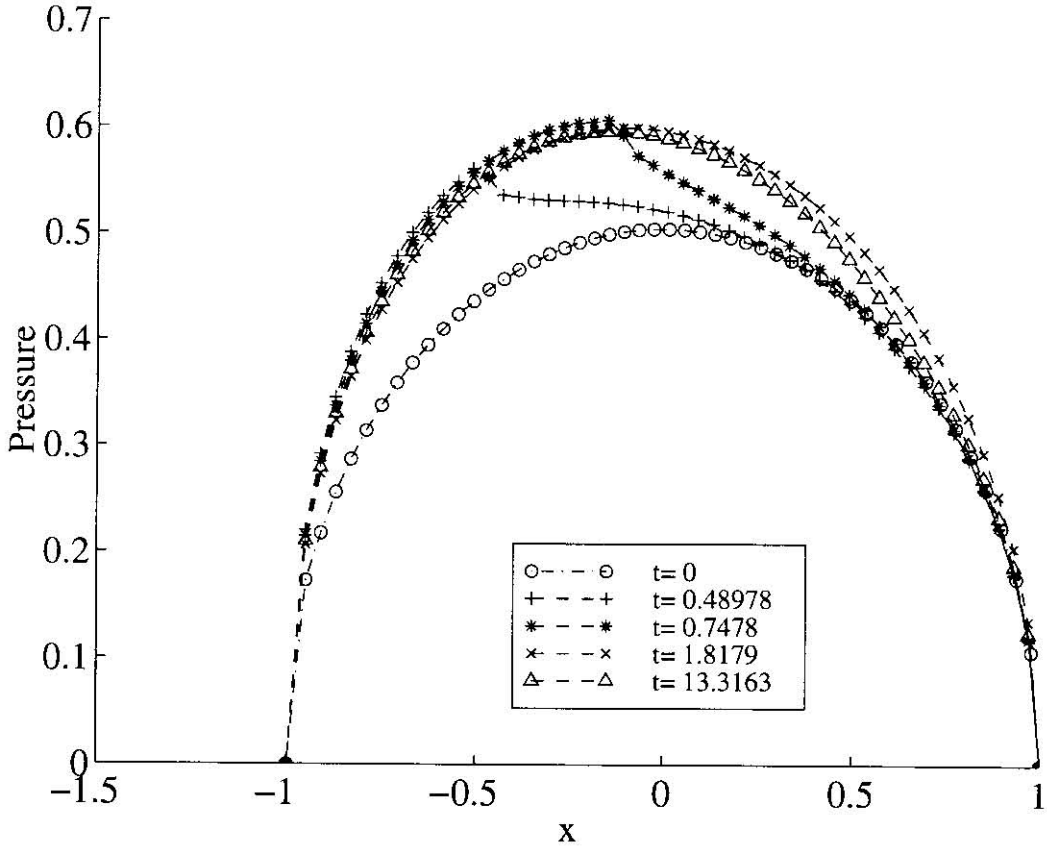

Figure 6.39: Periodically accelerating indentor: $V(t) = 1 + 0.9\sin(t)$. History of pressure distribution. $\frac{G_1}{G_0} = \frac{1}{2}$

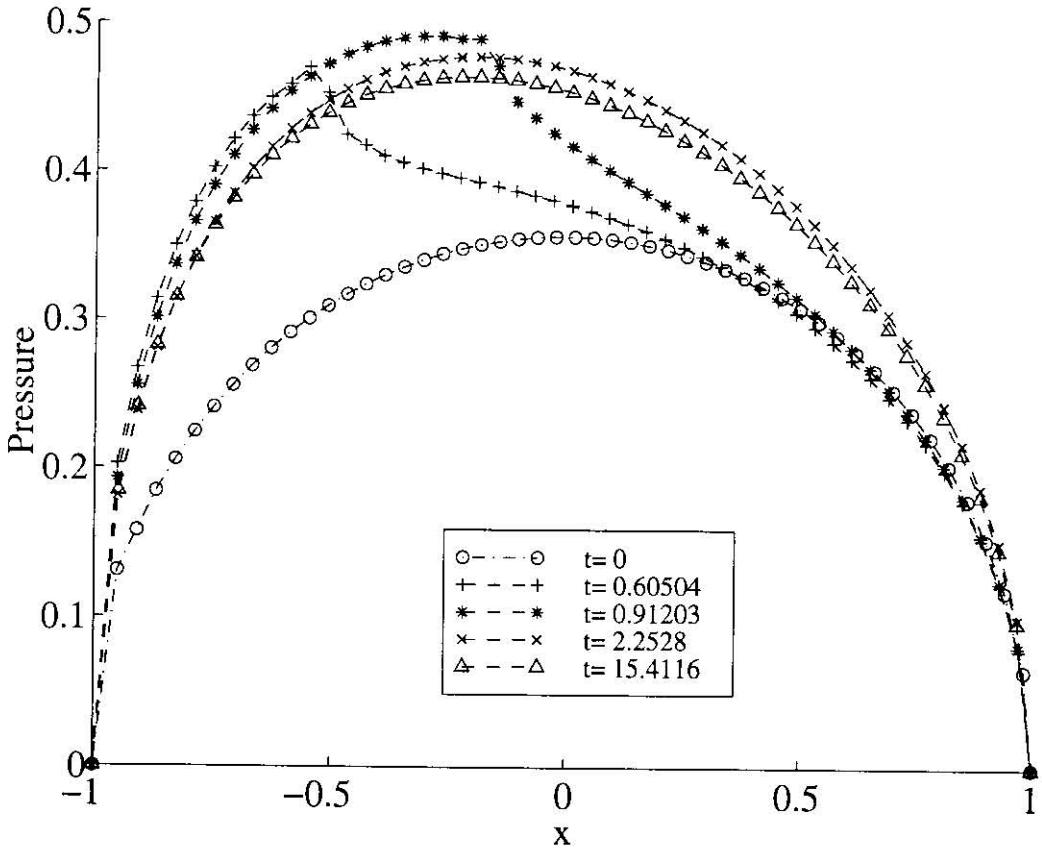

Figure 6.40: Periodically accelerating indentor: $V(t) = 1 + 0.9\sin(t)$. History of pressure distribution. $\frac{G_1}{G_0} = 1$

new acceleration period. Maximum and minimum values of hysteretic friction and the indentor tip shift are larger in the transient analysis than in the steady-state analysis. The shape of the resulting graph somewhat resembles that of the one in Figure 6.24, which, in turn, agrees with the results of Hunter [65].

Cumulative graphs of the histories of the contact interval length and hysteretic friction for viscoelastic materials with $\frac{G_1}{G_0} = \frac{1}{4}$, $\frac{G_1}{G_0} = \frac{1}{2}$ and $\frac{G_1}{G_0} = 1$ are given in Figure 6.36 and Figure 6.37 respectively. The histories of pressure distribution for the same materials are given in Figures 6.38, 6.39 and 6.40.

The distributions of stress components for the material with $\frac{G_1}{G_0} = \frac{1}{4}$ are presented in Figures 6.41 - 6.43.

6.6 Periodically Varying Speed: $V = 1 + 0.25 \sin t$

The picture for the steady-state hysteretic friction in another case, $A = 1, B = 0.25$ is qualitatively the same as before (see Figures 6.44, 6.45).

As for the transient hysteretic friction, it almost loses its characteristic hump - plateau - trough shape. The hump at the beginning of each period after the transient effects have died away, though still visible, smears out to a gradual decrease with a virtually indistinguishable point of inflection. This can be explained by observing that the relative change in the indentor speed is small compared to its absolute value, so transient effects can take place as the indentor accelerates or decelerates. Therefore, no sharp drop in the hysteretic friction occurs and the increase at the beginning of the next period appears almost right after the plateau of the previous period.

Cumulative graphs of the histories of the contact interval length and hysteretic friction for viscoelastic materials with $\frac{G_1}{G_0} = \frac{1}{4}$, $\frac{G_1}{G_0} = \frac{1}{2}$ and $\frac{G_1}{G_0} = 1$ are given in Figure 6.46 and Figure 6.47 respectively.

The histories of pressure distribution for the same materials are given in Figures 6.48, 6.49 and 6.50. The distributions of stress components for the material with $\frac{G_1}{G_0} = \frac{1}{4}$ are presented in Figures 6.51 - 6.53.

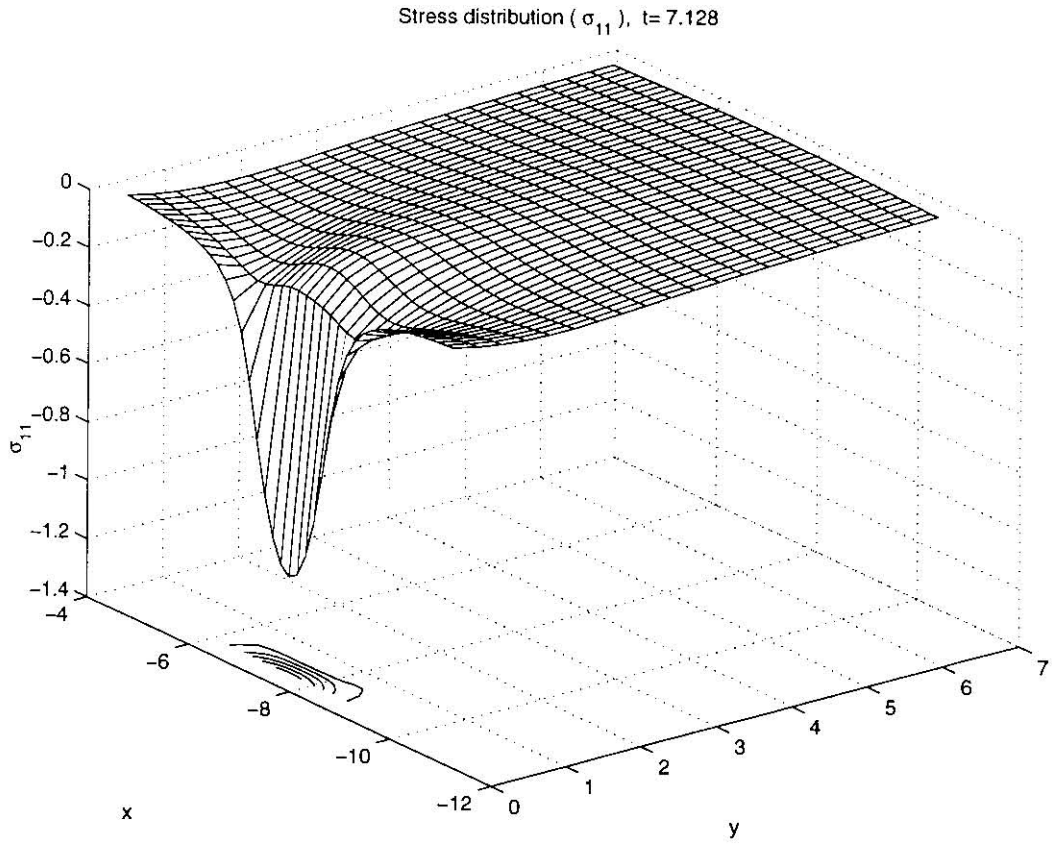

Figure 6.41: Periodically accelerating indentor: $V(t) = 1 + 0.9\sin(t)$. Stress distribution: σ_{11}. $\frac{G_1}{G_0} = \frac{1}{4}$

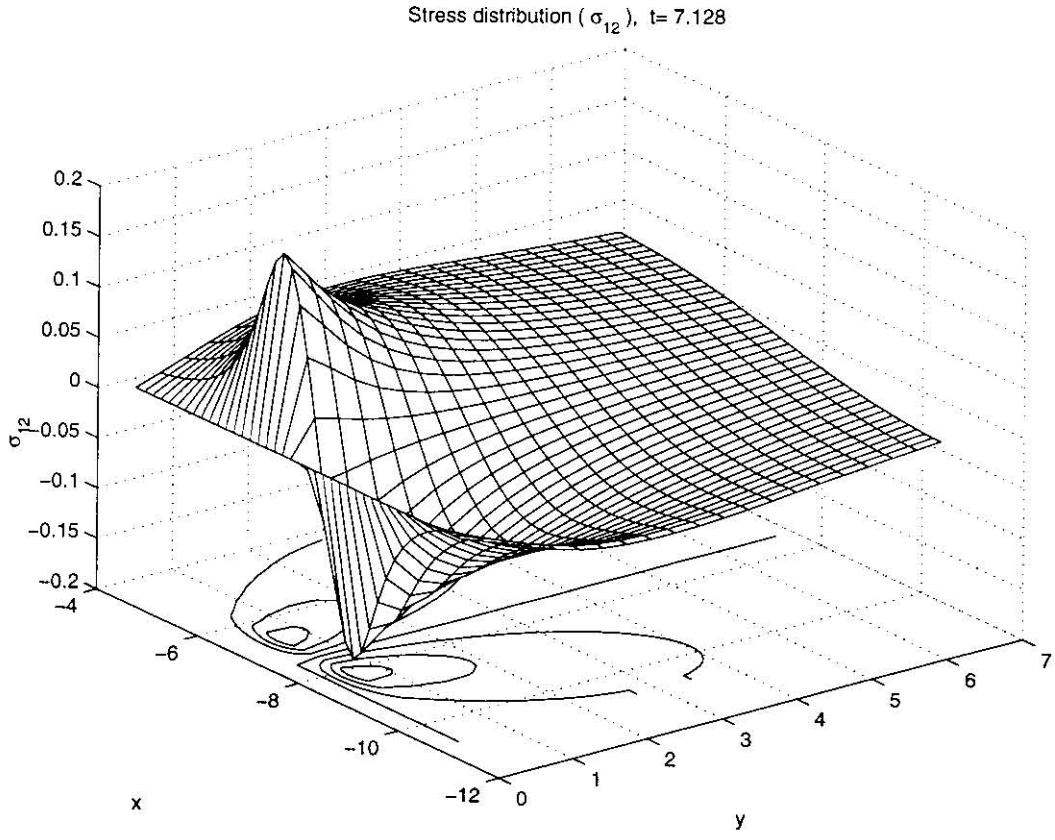

Figure 6.42: Periodically accelerating indentor: $V(t) = 1 + 0.9\sin(t)$. Stress distribution: σ_{12}. $\frac{G_1}{G_0} = \frac{1}{4}$

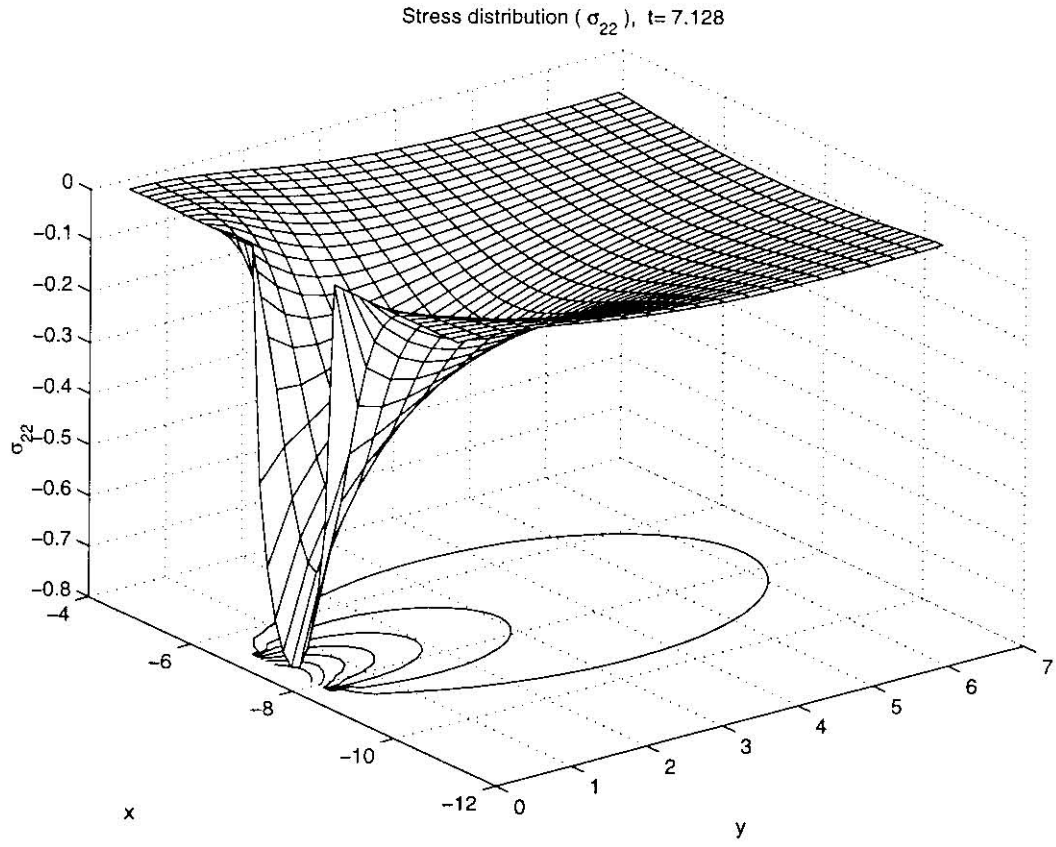

Figure 6.43: Periodically accelerating indentor: $V(t) = 1 + 0.9\sin(t)$. Stress distribution: σ_{22}. $\frac{G_1}{G_0} = \frac{1}{4}$

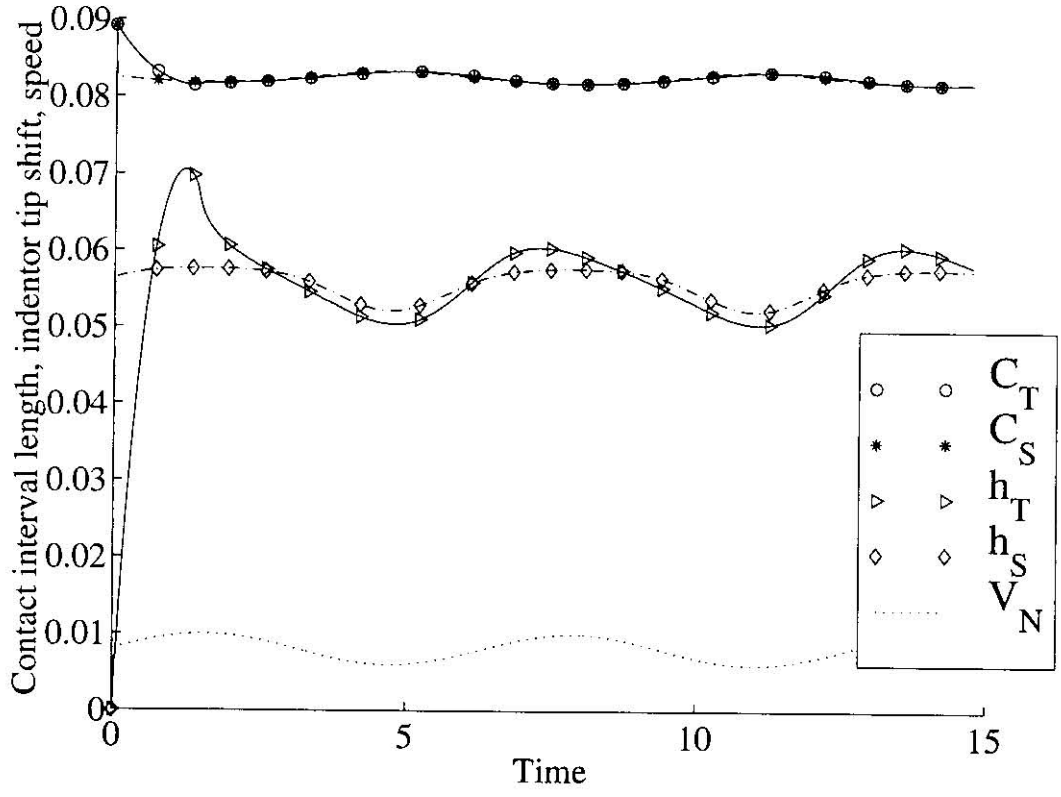

Figure 6.44: Periodically accelerating indentor: $V(t) = 1 + 0.25\sin(t)$. History of contact interval length, indentor tip shift and speed.

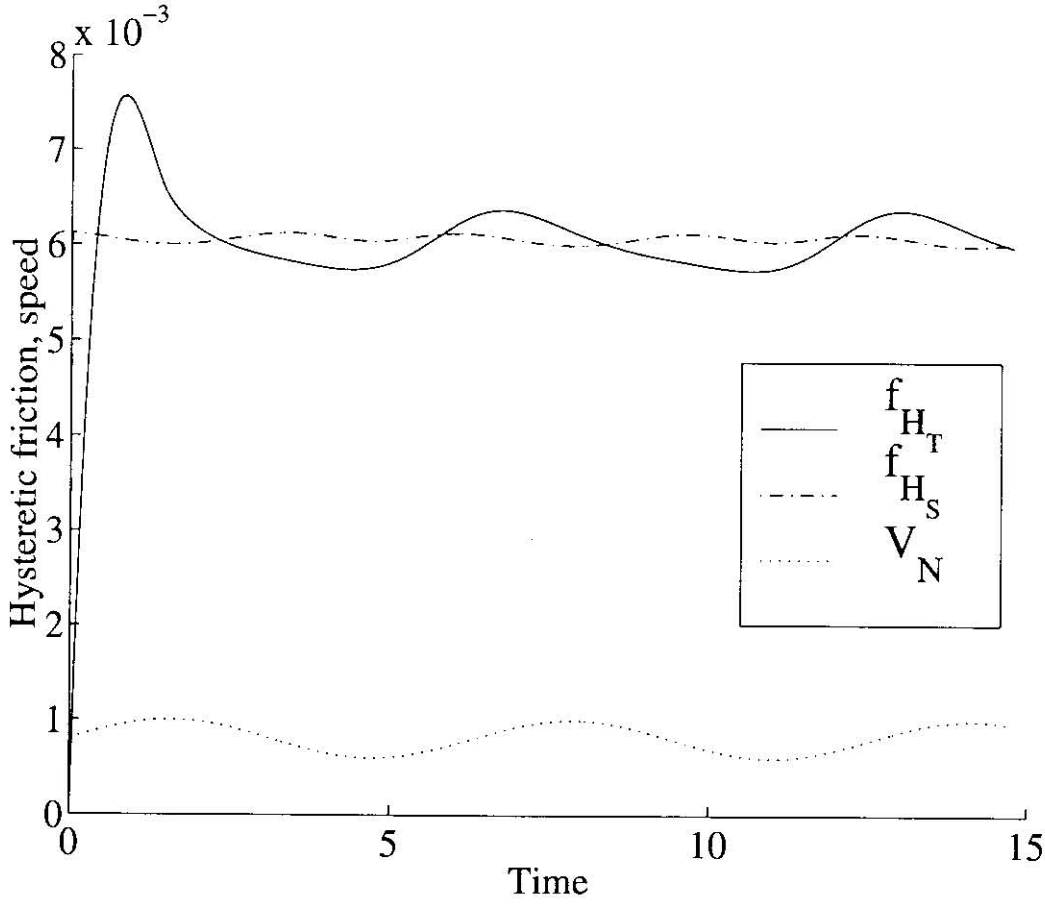

Figure 6.45: Periodically accelerating indentor: $V(t) = 1 + 0.25\sin(t)$. History of hysteretic friction and speed.

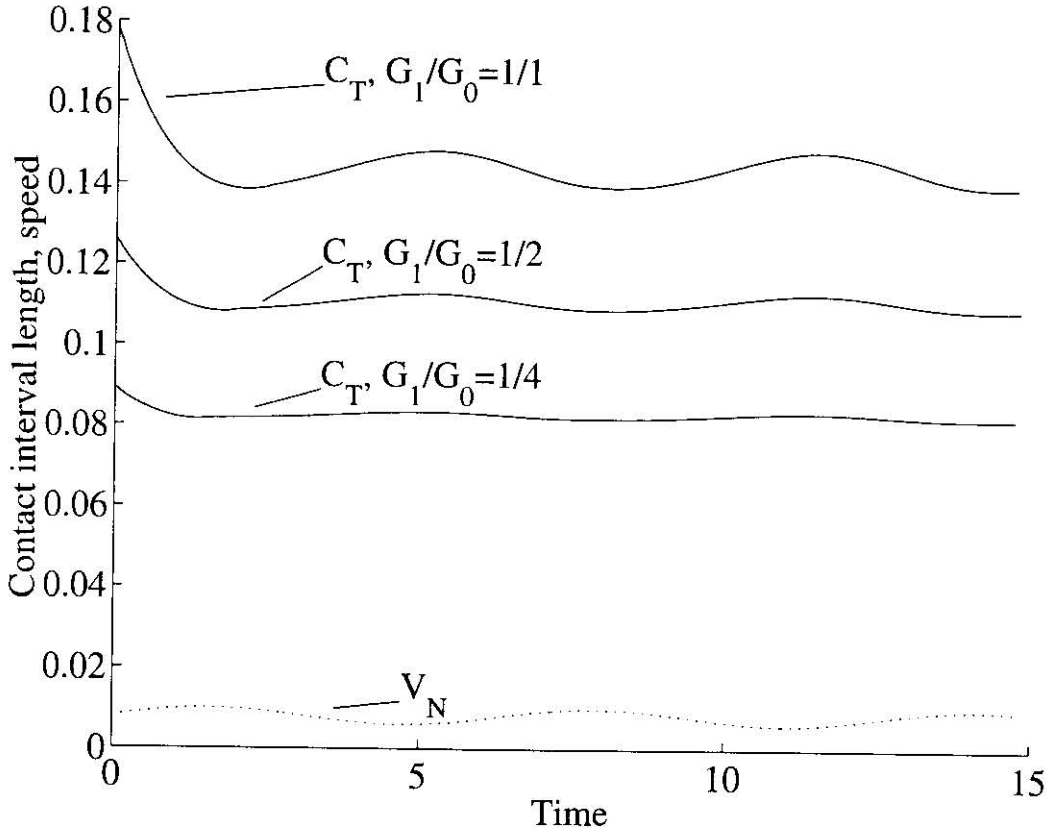

Figure 6.46: Periodically accelerating indentor: $V(t) = 1 + 0.25\sin(t)$. History of contact interval length, indentor tip shift and speed. $\frac{G_1}{G_0} = \frac{1}{4}$, $\frac{G_1}{G_0} = \frac{1}{2}$, $\frac{G_1}{G_0} = 1$

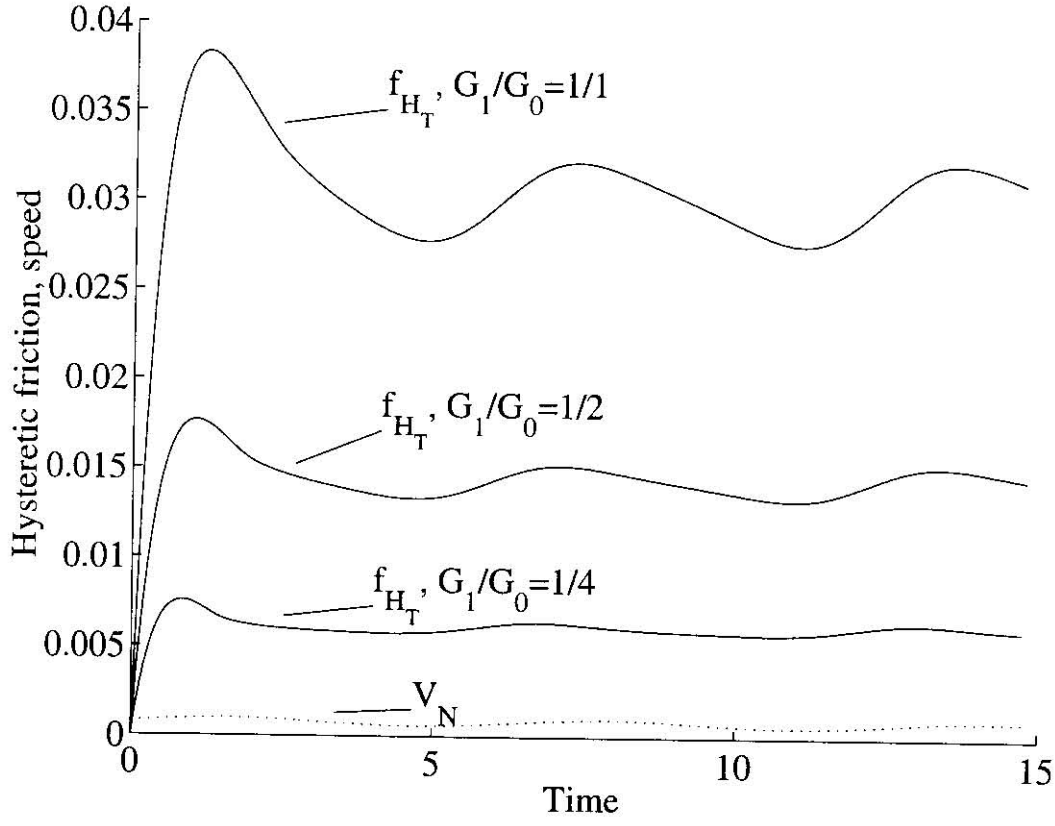

Figure 6.47: Periodically accelerating indentor: $V(t) = 1 + 0.25\sin(t)$. History of hysteretic friction and speed. $\frac{G_1}{G_0} = \frac{1}{4}$, $\frac{G_1}{G_0} = \frac{1}{2}$, $\frac{G_1}{G_0} = 1$

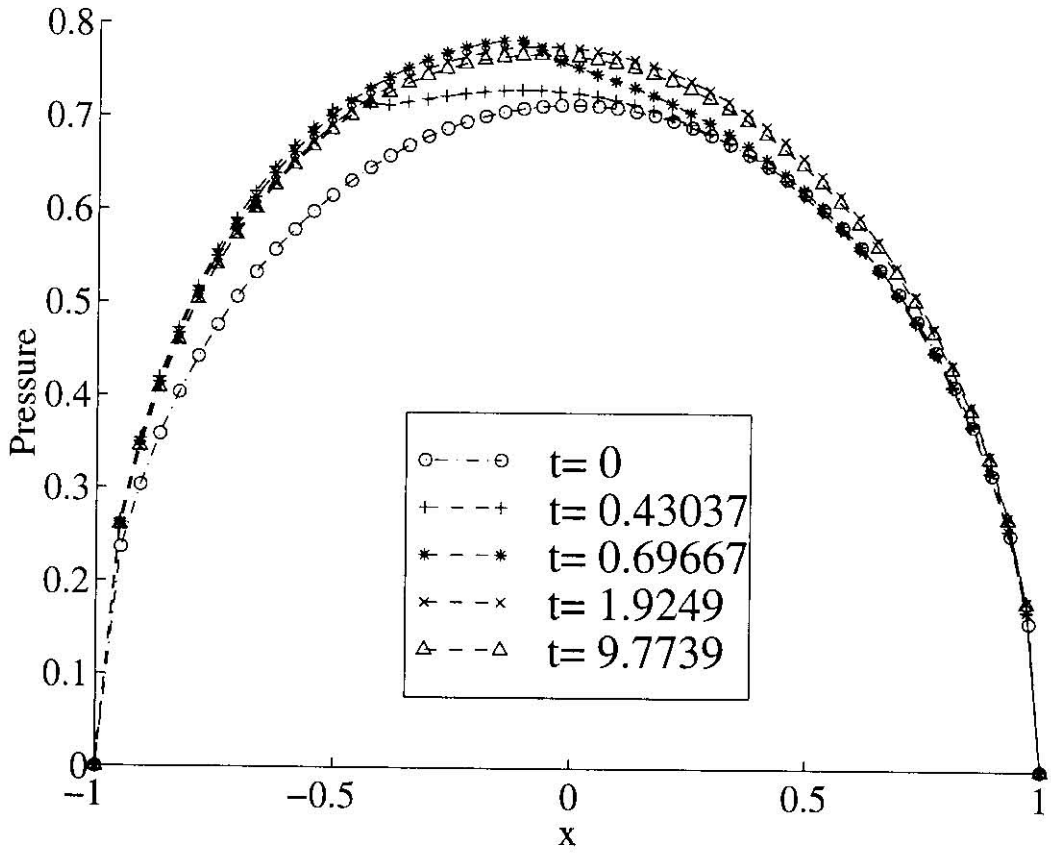

Figure 6.48: Periodically accelerating indentor: $V(t) = 1 + 0.25\sin(t)$. History of pressure distribution. $\frac{G_1}{G_0} = \frac{1}{4}$

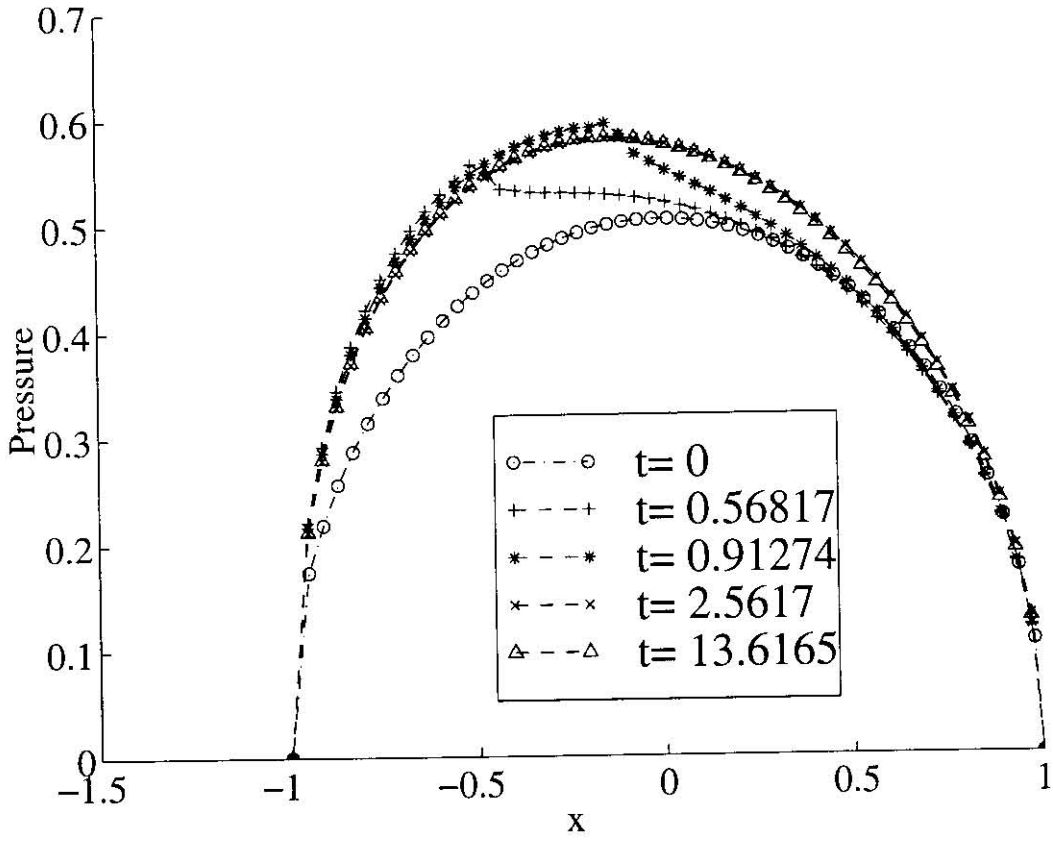

Figure 6.49: Periodically accelerating indentor: $V(t) = 1 + 0.25\sin(t)$. History of pressure distribution. $\frac{G_1}{G_0} = \frac{1}{2}$

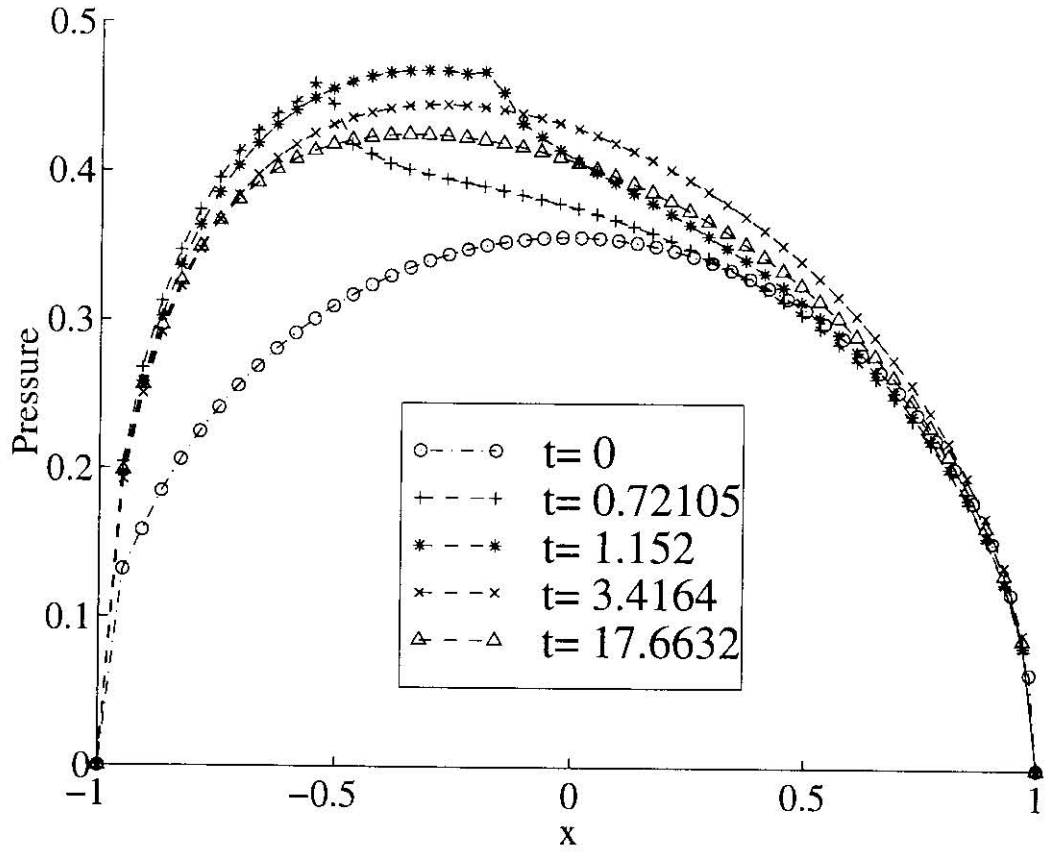

Figure 6.50: Periodically accelerating indentor: $V(t) = 1 + 0.25\sin(t)$. History of pressure distribution. $\frac{G_1}{G_0} = 1$

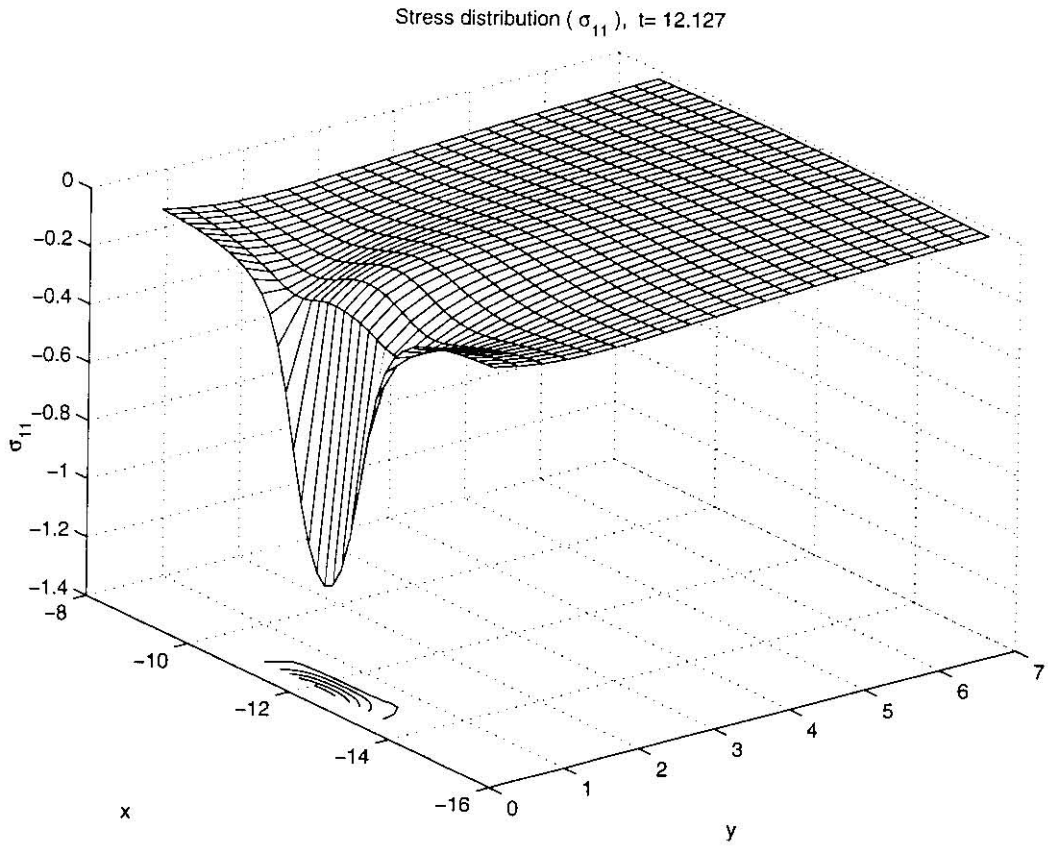

Figure 6.51: Periodically accelerating indentor: $V(t) = 1 + 0.25\sin(t)$. Stress distribution: σ_{11}. $\frac{G_1}{G_0} = \frac{1}{4}$

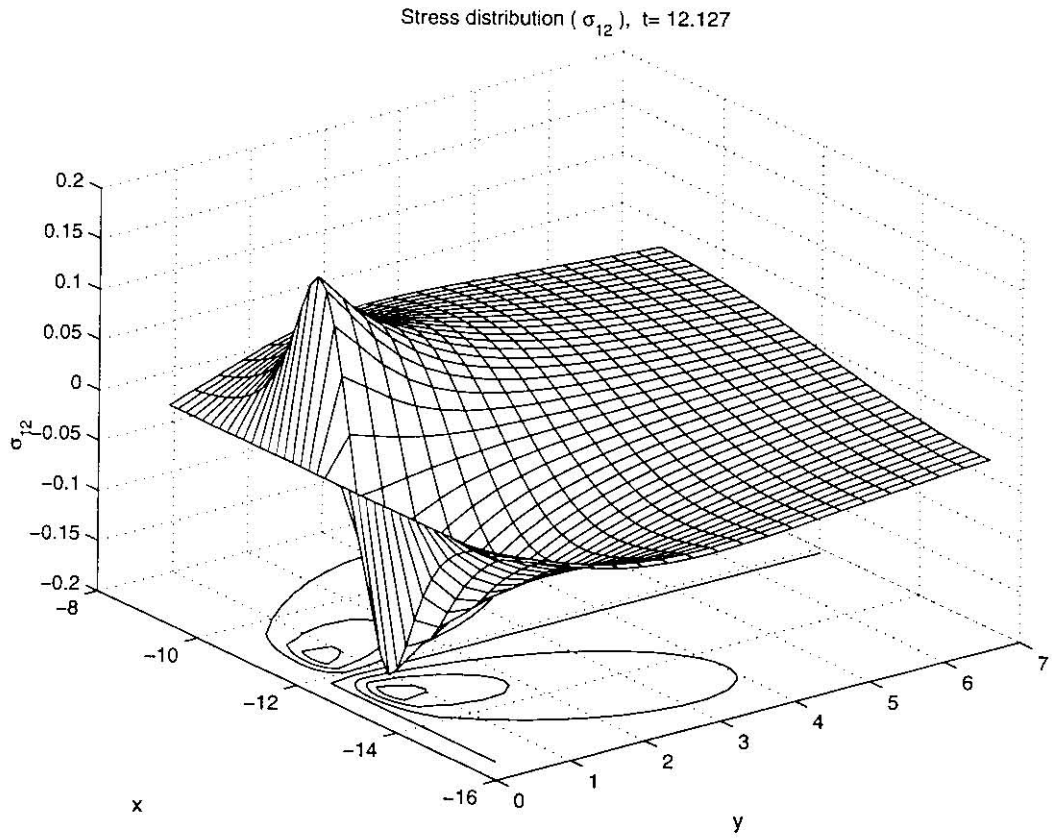

Figure 6.52: Periodically accelerating indentor: $V(t) = 1 + 0.25\sin(t)$. Stress distribution: σ_{12}. $\frac{G_1}{G_0} = \frac{1}{4}$

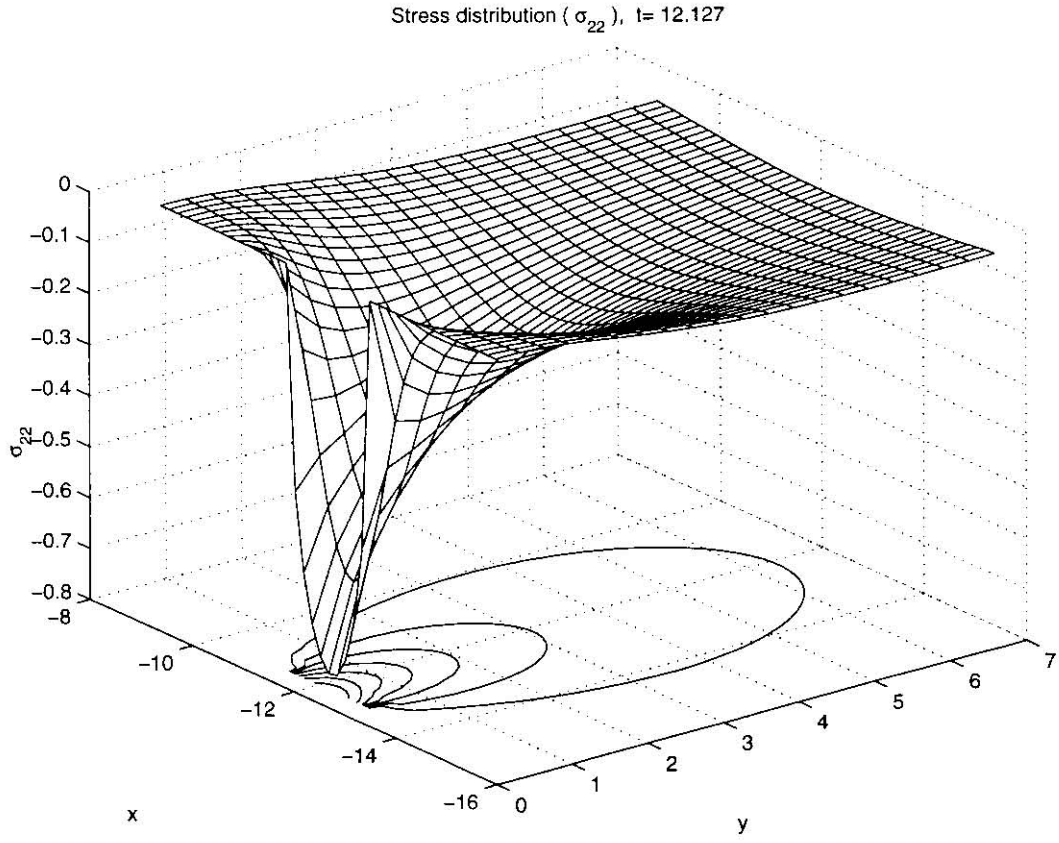

Figure 6.53: Periodically accelerating indentor: $V(t) = 1 + 0.25\sin(t)$. Stress distribution: σ_{22}. $\frac{G_1}{G_0} = \frac{1}{4}$

6.7 Periodically Varying Speed: $V = 0.5 + 0.25 \sin t$

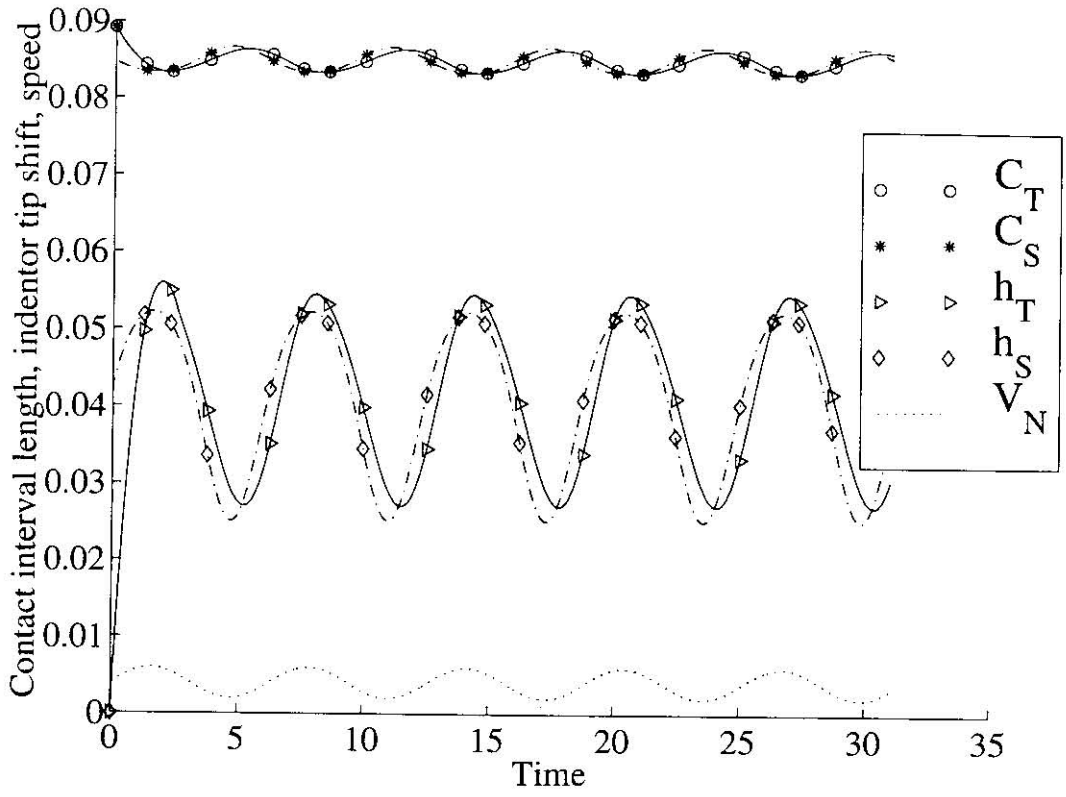

Figure 6.54: Periodically accelerating indentor: $V(t) = 0.5 + 0.25\sin(t)$. History of contact interval width, indentor tip shift and speed.

The situation changes again as we reduce the value of A to 0.5 keeping B intact at 0.25 (see Figures 6.54, 6.55). Now the transient hysteretic friction virtually mimics its steady-state counterpart which, in turn, is almost sinusoidal. The trough corresponding to the maximum speed has disappeared because the watershed value of $V_N = 1$ is now never reached. The plateau part of the graph of the transient hysteretic friction has disappeared, because the transient effects are taking place at a speed lower than the speed of the indentor. This leads us to believe that the plateau part corresponds to the transition between "high" and "low" speeds and is eliminated when the speed does not reach the "barrier" values.

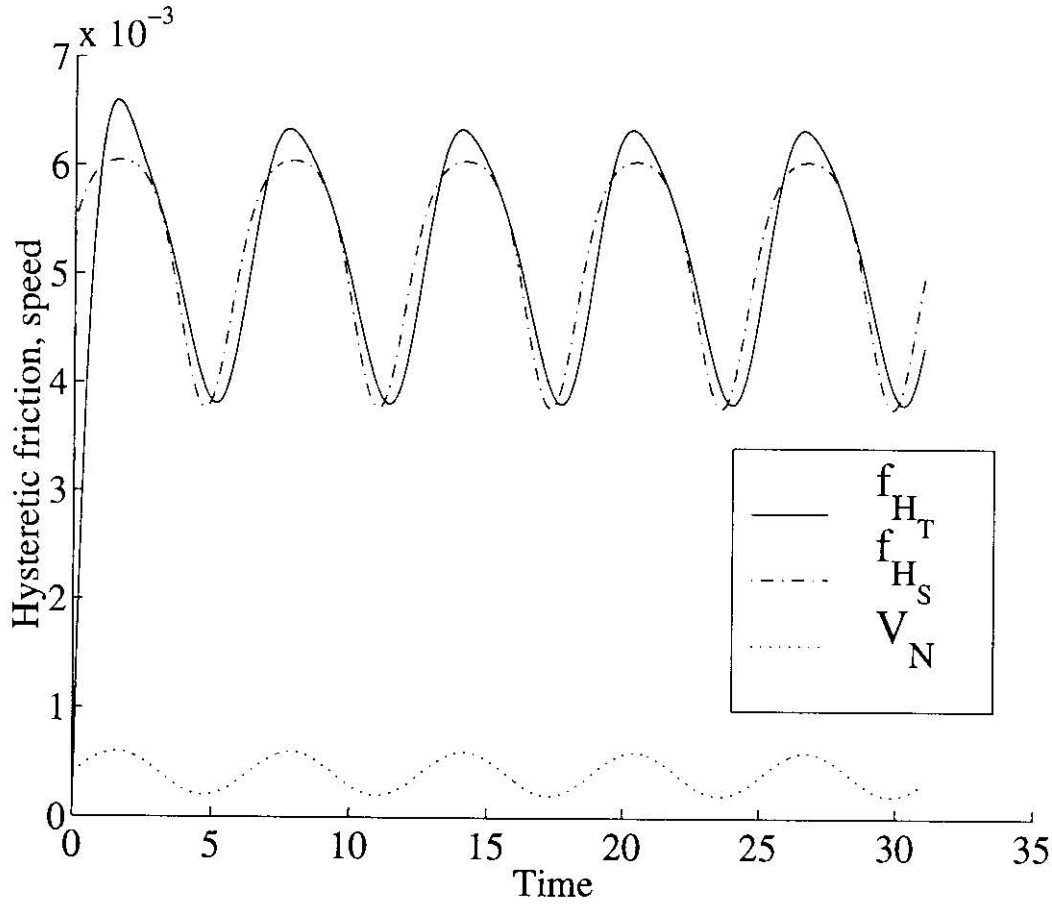

Figure 6.55: Periodically accelerating indentor: $V(t) = 0.5 + 0.25\sin(t)$. History of hysteretic friction and speed.

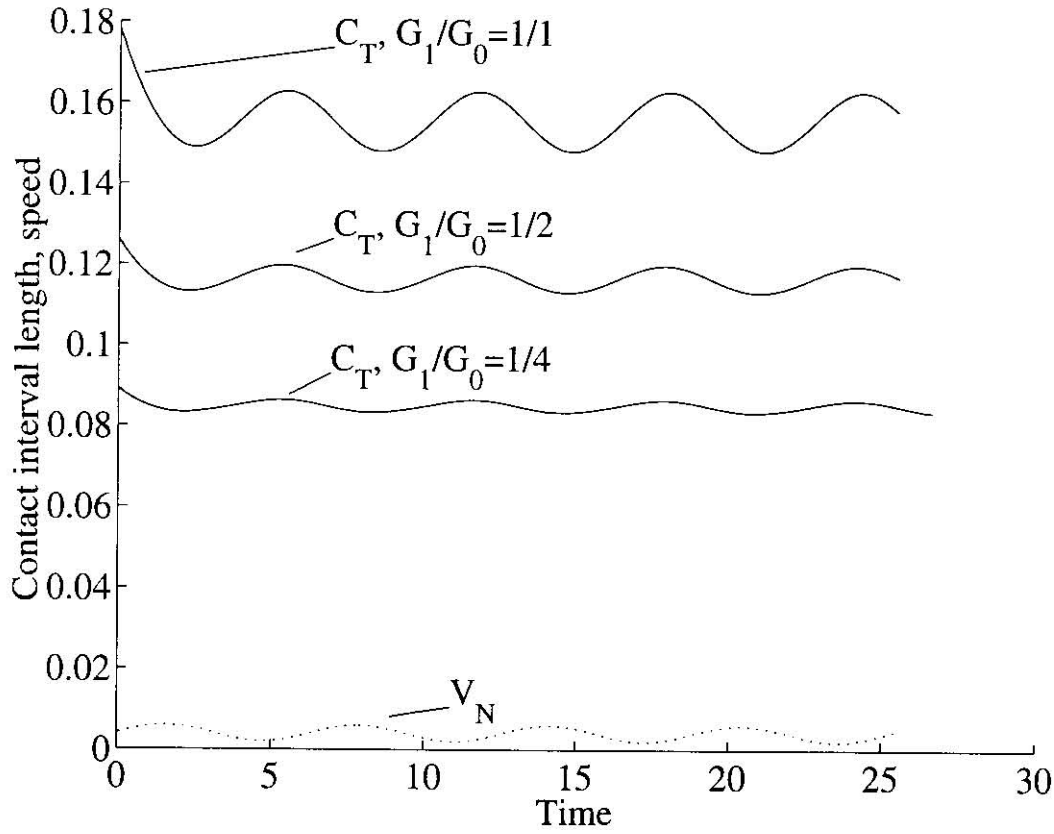

Figure 6.56: Periodically accelerating indentor: $V(t) = 0.5 + 0.25\sin(t)$. History of contact interval length, indentor tip shift and speed. $\frac{G_1}{G_0} = \frac{1}{4}$, $\frac{G_1}{G_0} = \frac{1}{2}$, $\frac{G_1}{G_0} = 1$

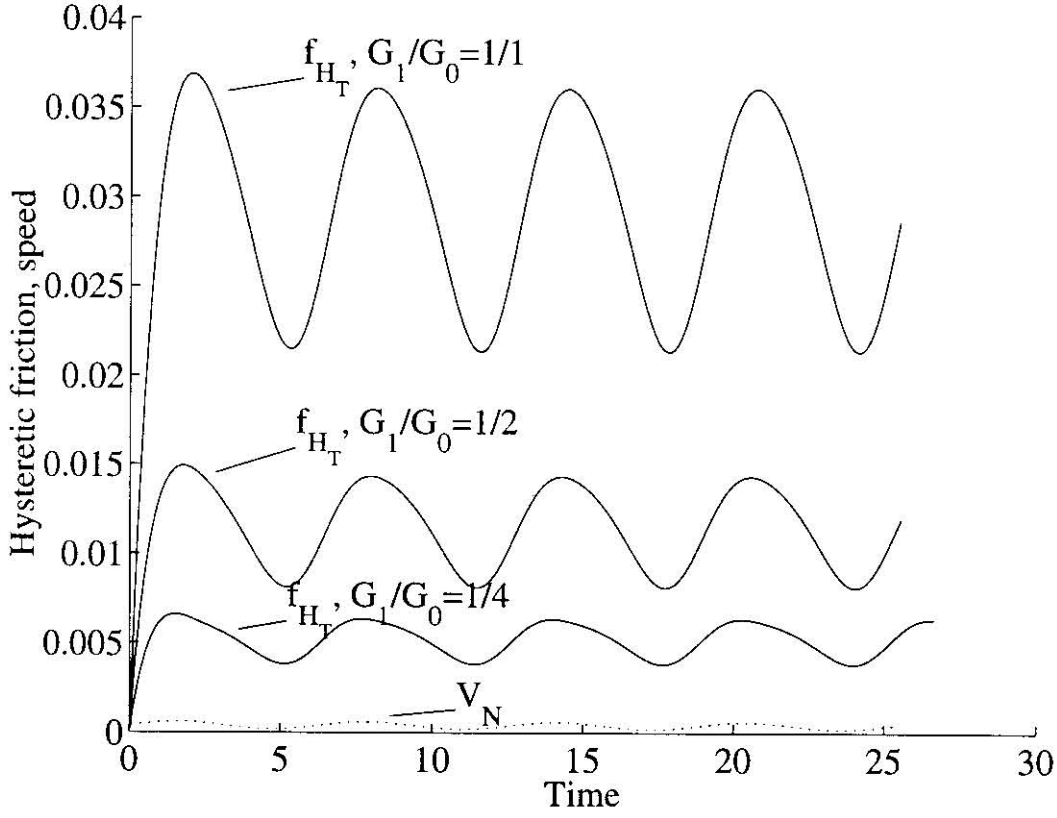

Figure 6.57: Periodically accelerating indentor: $V(t) = 0.5 + 0.25\sin(t)$. History of hysteretic friction and speed. $\frac{G_1}{G_0} = \frac{1}{4}$, $\frac{G_1}{G_0} = \frac{1}{2}$, $\frac{G_1}{G_0} = 1$

Cumulative graphs of the histories of the contact interval length and hysteretic friction for viscoelastic materials with $\frac{G_1}{G_0} = \frac{1}{4}$, $\frac{G_1}{G_0} = \frac{1}{2}$ and $\frac{G_1}{G_0} = 1$ are given in Figure 6.56 and Figure 6.57 respectively.

The histories of pressure distribution for the same materials are given in Figures 6.58, 6.59 and 6.60.

The distributions of stress components for the material with $\frac{G_1}{G_0} = \frac{1}{4}$ are presented in Figures 6.61 – 6.63.

6.8 Periodically Varying Load

For a periodically varying load moving with constant speed (Figures 6.64, 6.65), we can notice that the transient and the steady-state contact interval lengths become equal after the period of initial stabilization.

The transient indentor tip shift and hysteretic friction follow the variations in the contact interval length with a time delay. The transient hysteretic friction mimics its steady-state counterpart with a time delay as well. However, the steady-state indentor tip shift varies very slightly, in contrast with the transient indentor tip shift.

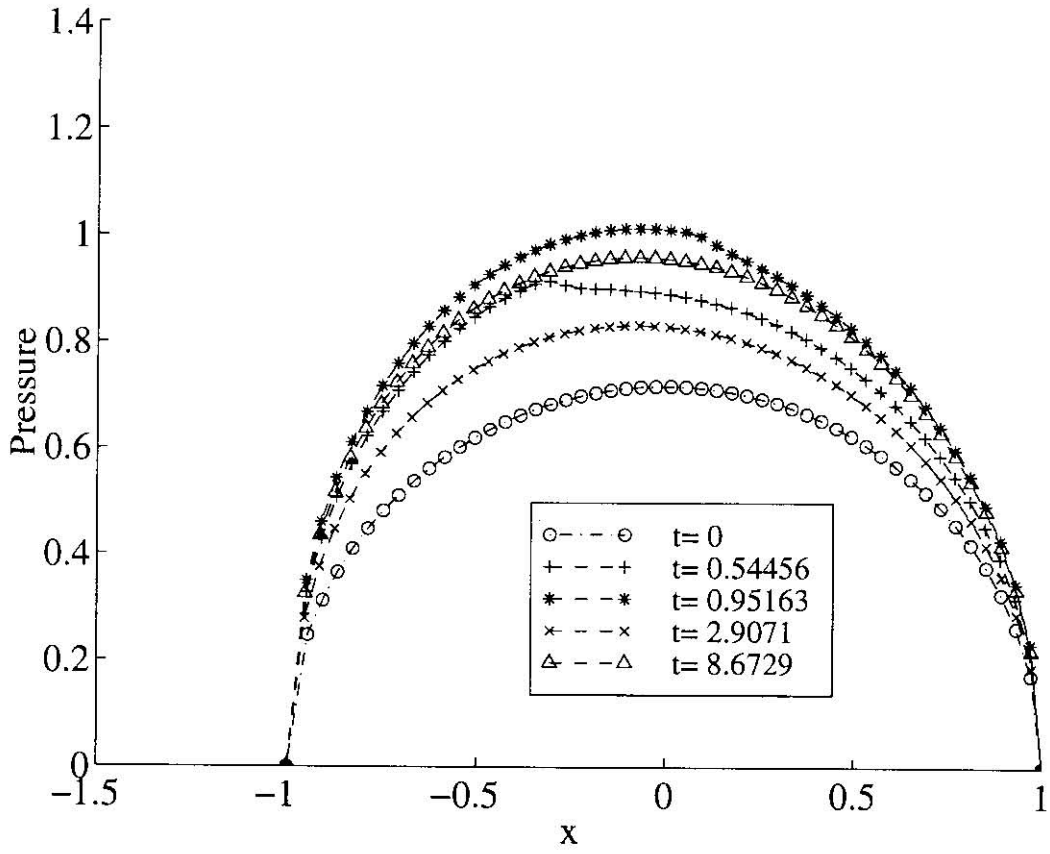

Figure 6.58: Periodically accelerating indentor: $V(t) = 0.5 + 0.25\sin(t)$. History of pressure distribution. $\frac{G_1}{G_0} = \frac{1}{4}$

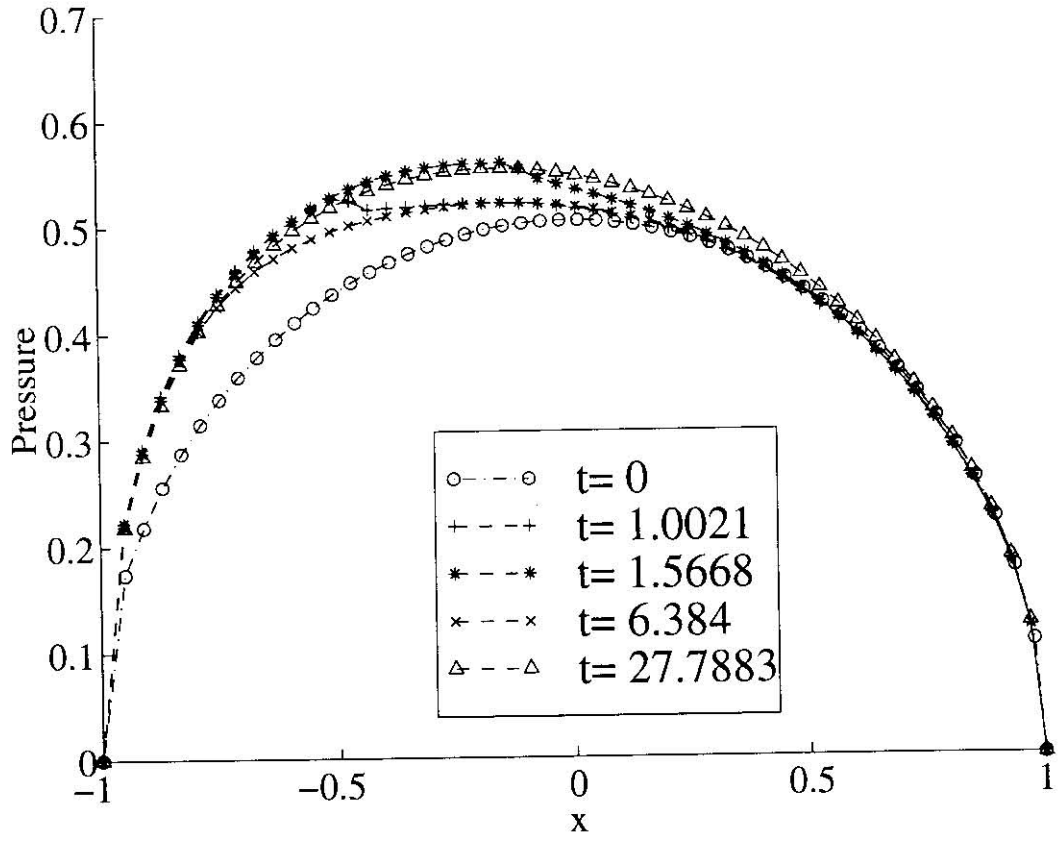

Figure 6.59: Periodically accelerating indentor: $V(t) = 0.5 + 0.25\sin(t)$. History of pressure distribution. $\frac{G_1}{G_0} = \frac{1}{2}$

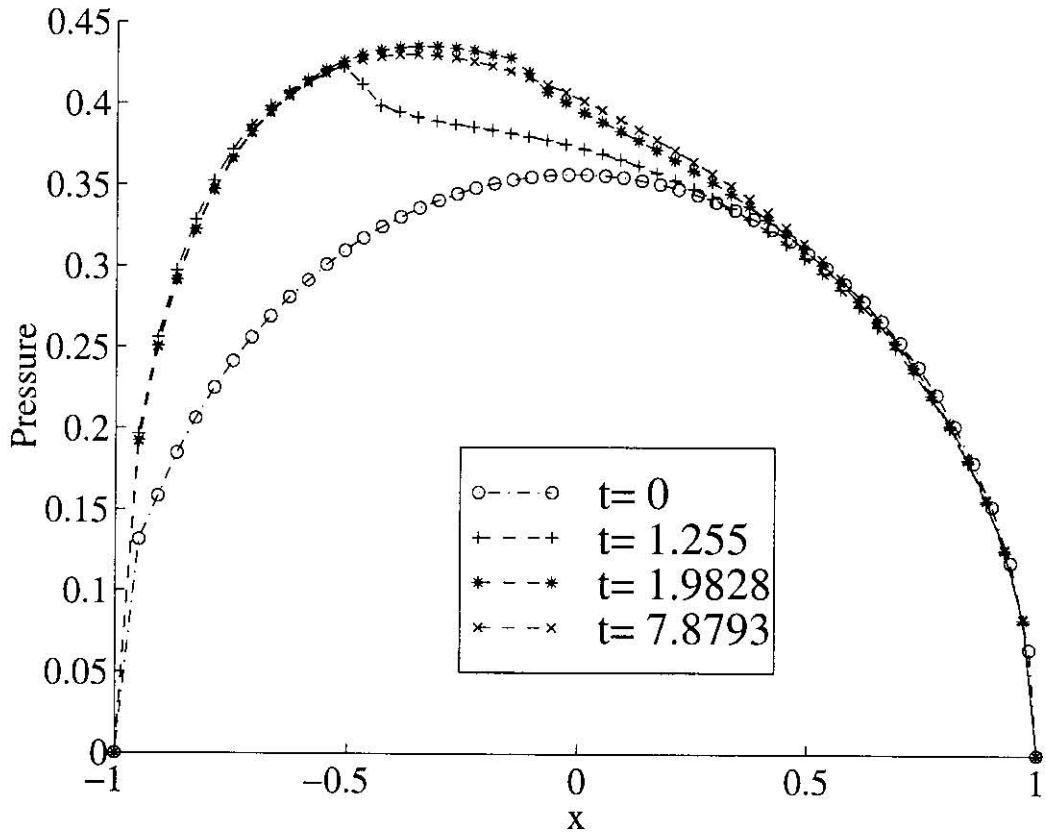

Figure 6.60: Periodically accelerating indentor: $V(t) = 0.5 + 0.25\sin(t)$. History of pressure distribution. $\frac{G_1}{G_0} = 1$

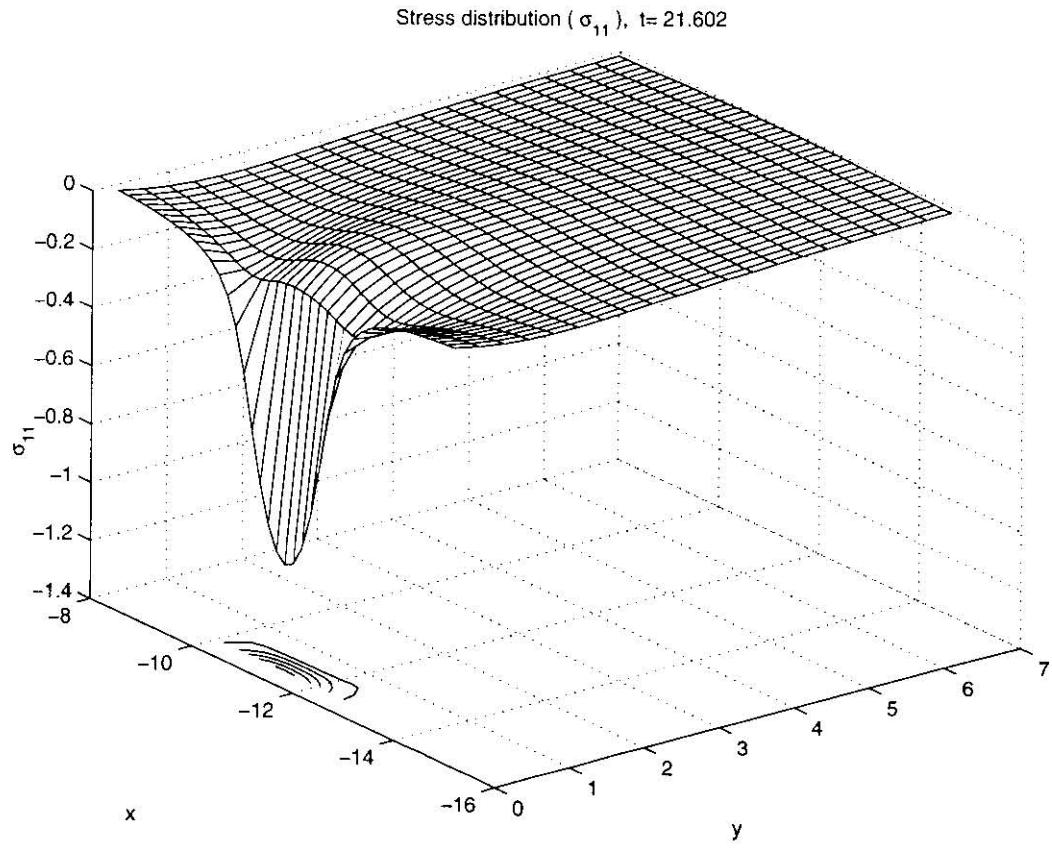

Figure 6.61: Periodically accelerating indentor: $V(t) = 0.5 + 0.25\sin(t)$. Stress distribution: σ_{11}. $\frac{G_1}{G_0} = \frac{1}{4}$

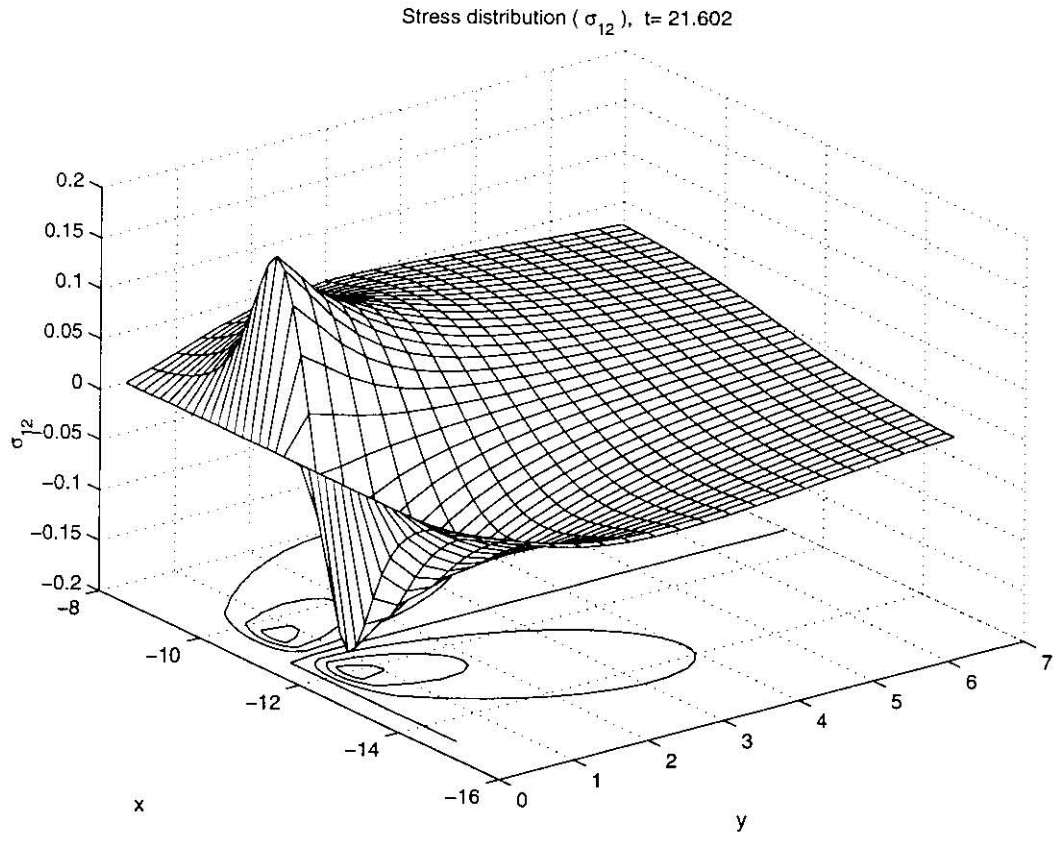

Figure 6.62: Periodically accelerating indentor: $V(t) = 0.5 + 0.25\sin(t)$. Stress distribution: σ_{12}. $\frac{G_1}{G_0} = \frac{1}{4}$

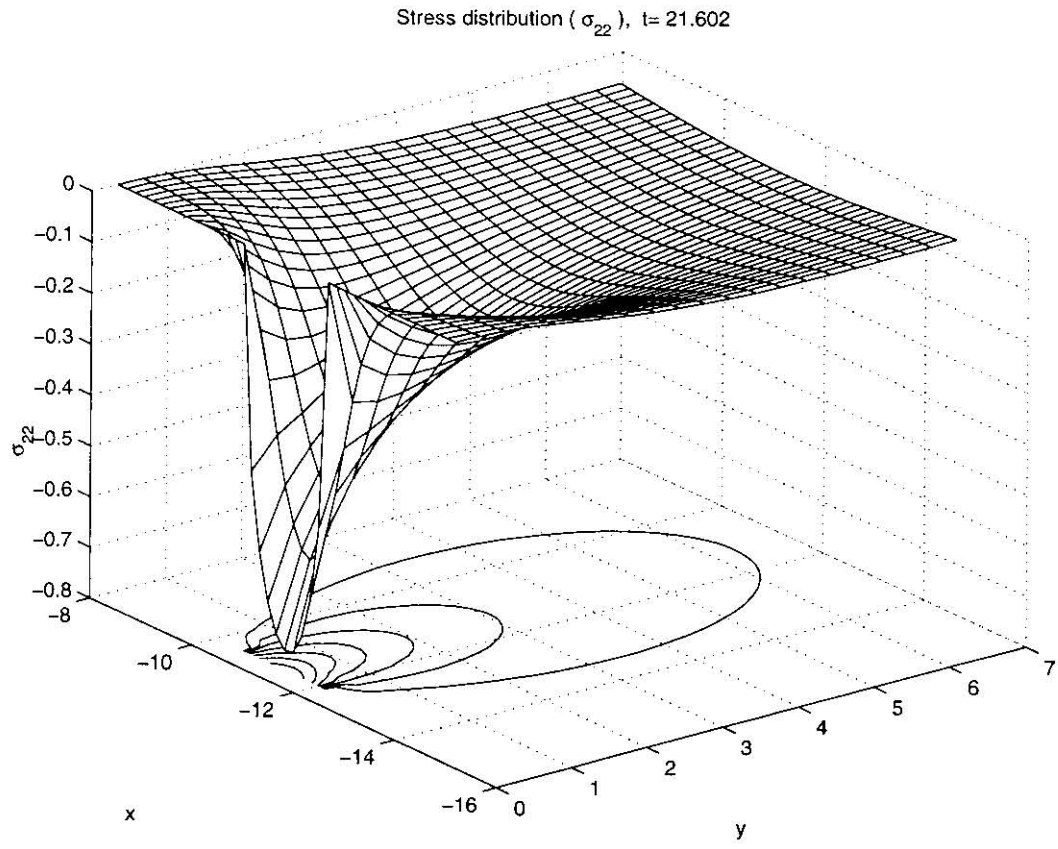

Figure 6.63: Periodically accelerating indentor: $V(t) = 0.5 + 0.25\sin(t)$. Stress distribution: σ_{22}. $\frac{G_1}{G_0} = \frac{1}{4}$

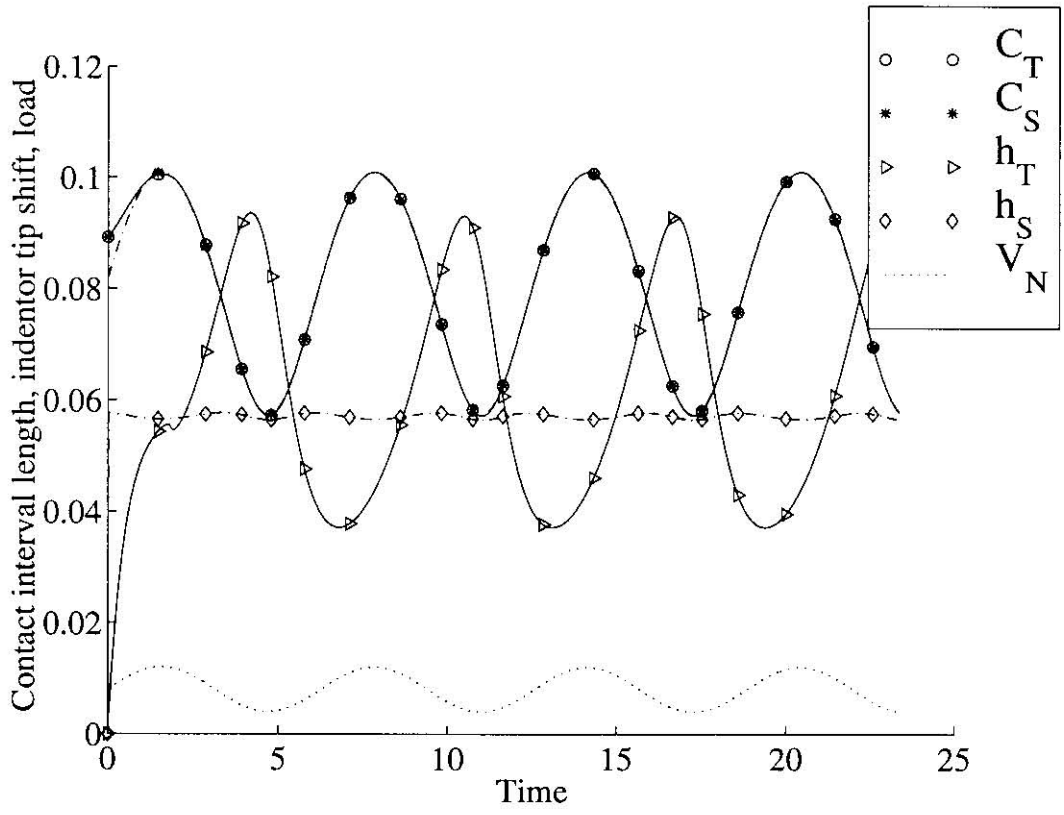

Figure 6.64: Periodically varying load: $W(t) = 1 + 0.5\sin(t)$. History of contact interval width, indentor tip shift and speed.

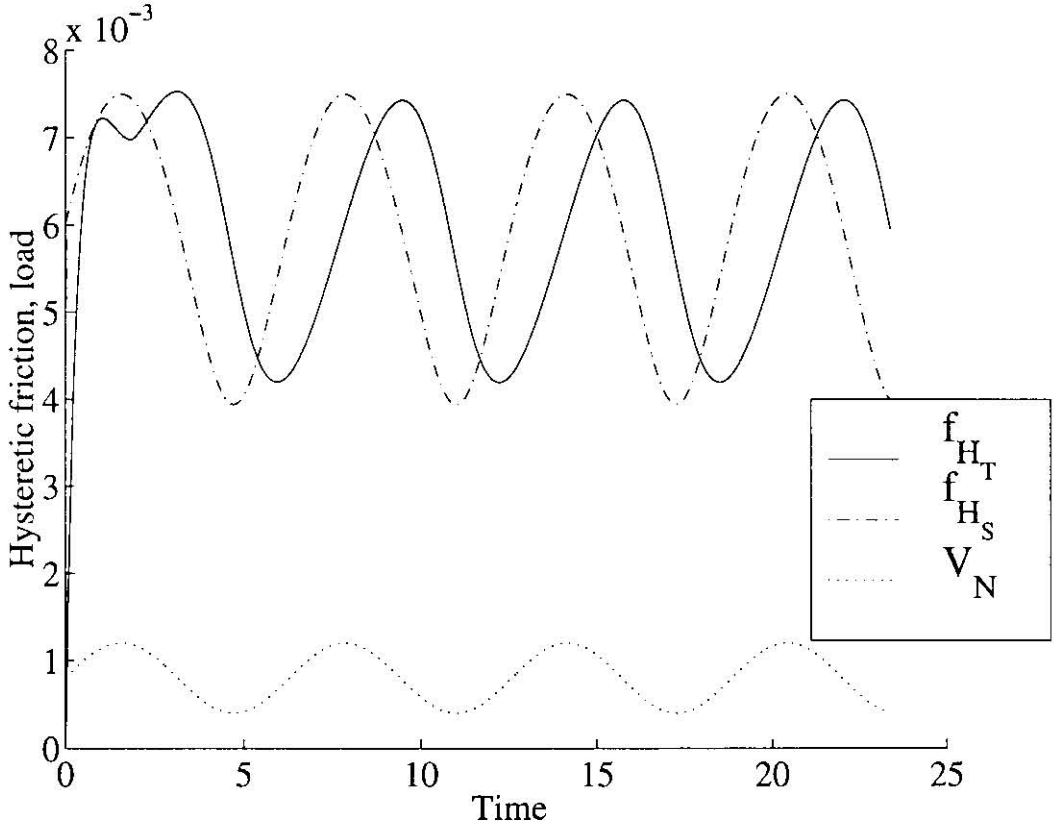

Figure 6.65: Periodically varying load: $W(t) = 1 + 0.5\sin(t)$. History of hysteretic friction and speed.

Cumulative graphs of the histories of the contact interval length and hysteretic friction for viscoelastic materials with $\frac{G_1}{G_0} = \frac{1}{4}$, $\frac{G_1}{G_0} = \frac{1}{2}$ and $\frac{G_1}{G_0} = 1$ are given in Figure 6.66 and Figure 6.67 respectively.

The histories of pressure distribution for the same materials are given in Figures 6.68, 6.69 and 6.70.

The distributions of stress components for the material with $\frac{G_1}{G_0} = \frac{1}{4}$ are presented in Figures 6.71 – 6.73.

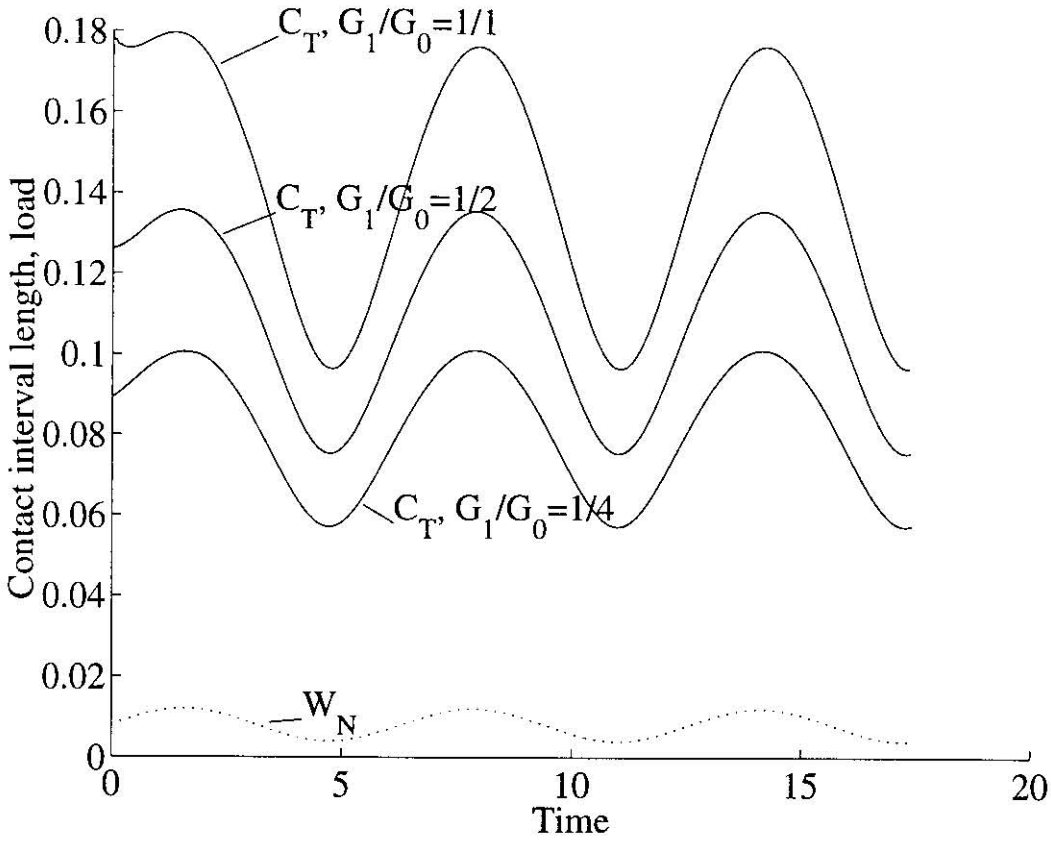

Figure 6.66: Periodically varying load: $W(t) = 1 + 0.5\sin(t)$. History of contact interval length, indentor tip shift and speed. $\frac{G_1}{G_0} = \frac{1}{4}$, $\frac{G_1}{G_0} = \frac{1}{2}$, $\frac{G_1}{G_0} = 1$

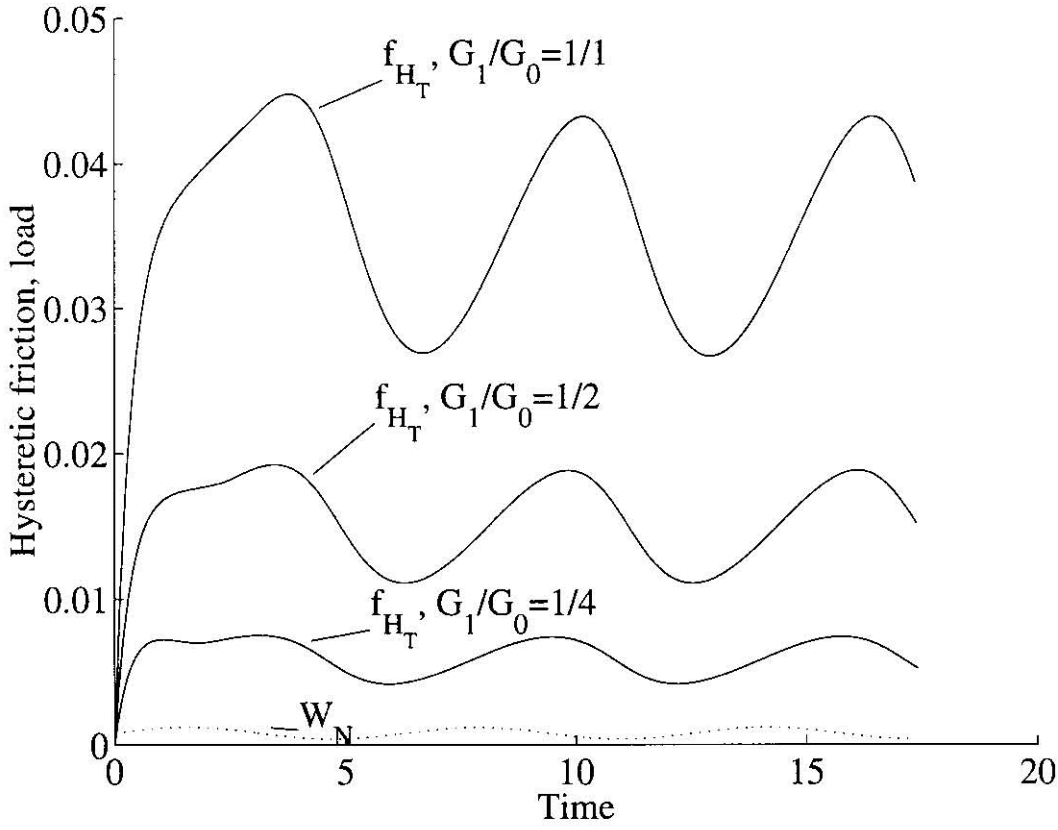

Figure 6.67: Periodically varying load: $W(t) = 1 + 0.5\sin(t)$. History of hysteretic friction and speed. $\frac{G_1}{G_0} = \frac{1}{4}$, $\frac{G_1}{G_0} = \frac{1}{2}$, $\frac{G_1}{G_0} = 1$

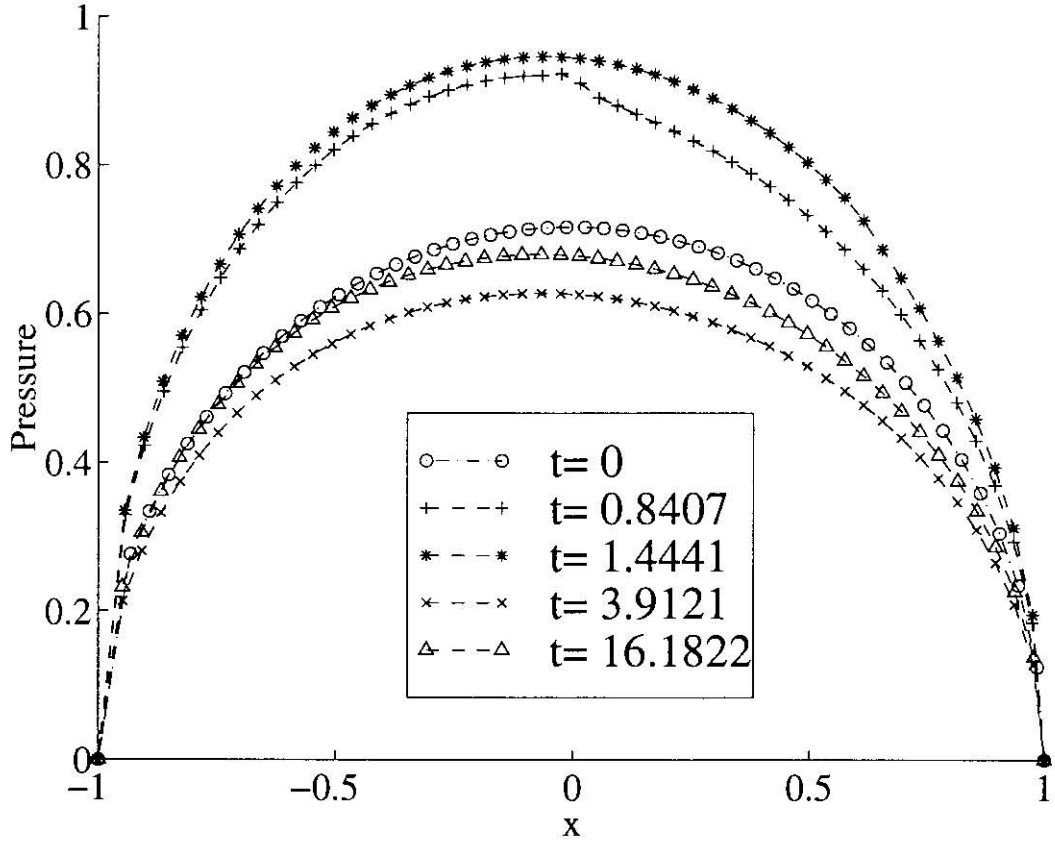

Figure 6.68: Periodically varying load: $W(t) = 1 + 0.5\sin(t)$. History of pressure distribution. $\frac{G_1}{G_0} = \frac{1}{4}$

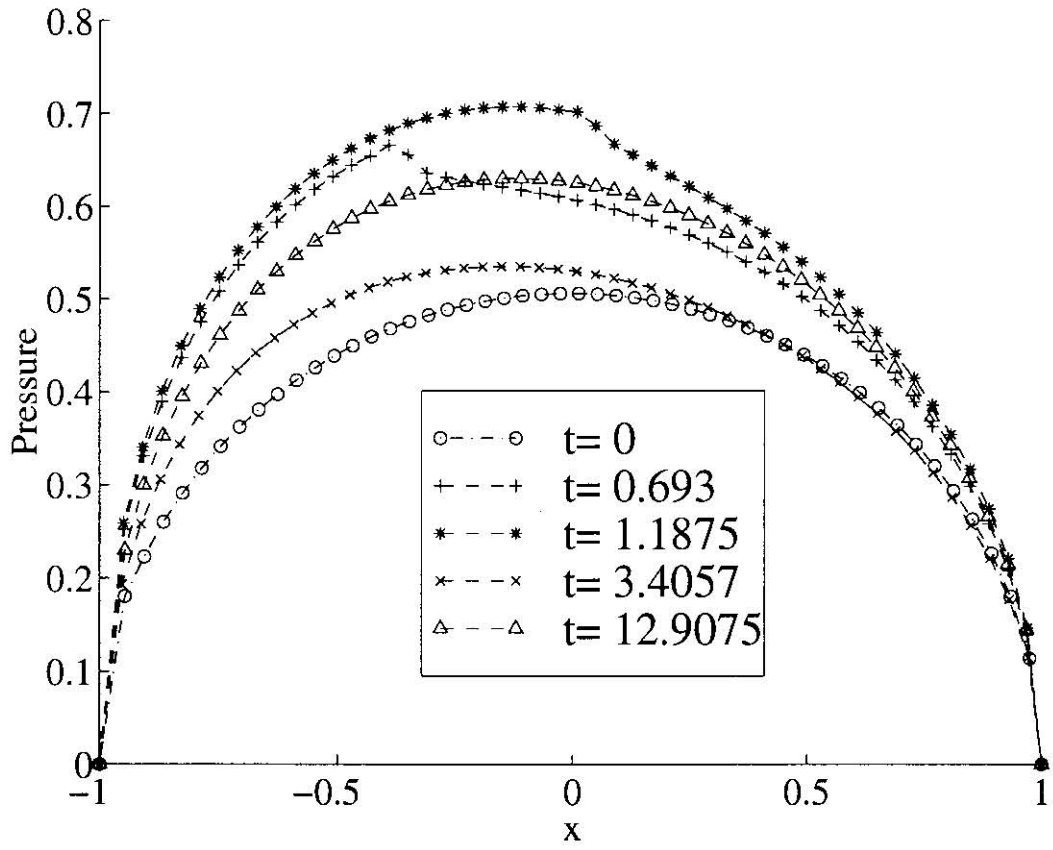

Figure 6.69: Periodically varying load: $W(t) = 1 + 0.5\sin(t)$. History of pressure distribution. $\frac{G_1}{G_0} = \frac{1}{2}$

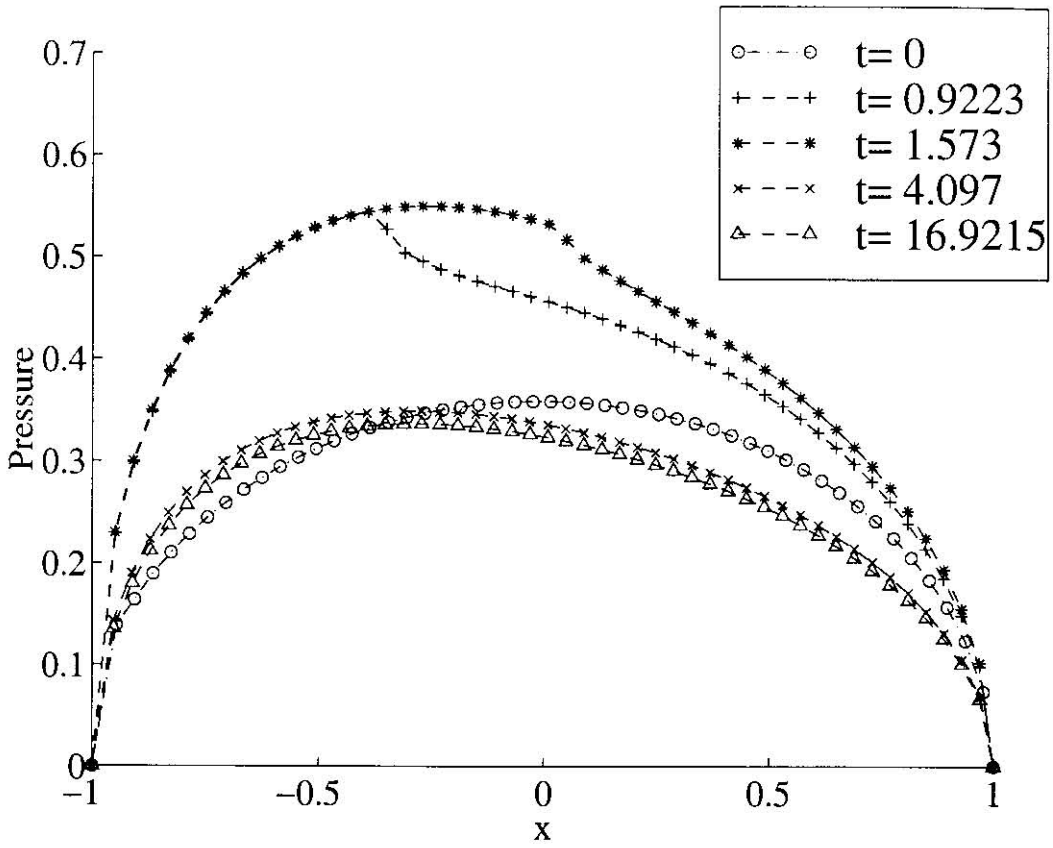

Figure 6.70: Periodically varying load: $W(t) = 1 + 0.5\sin(t)$. History of pressure distribution. $\frac{G_1}{G_0} = 1$

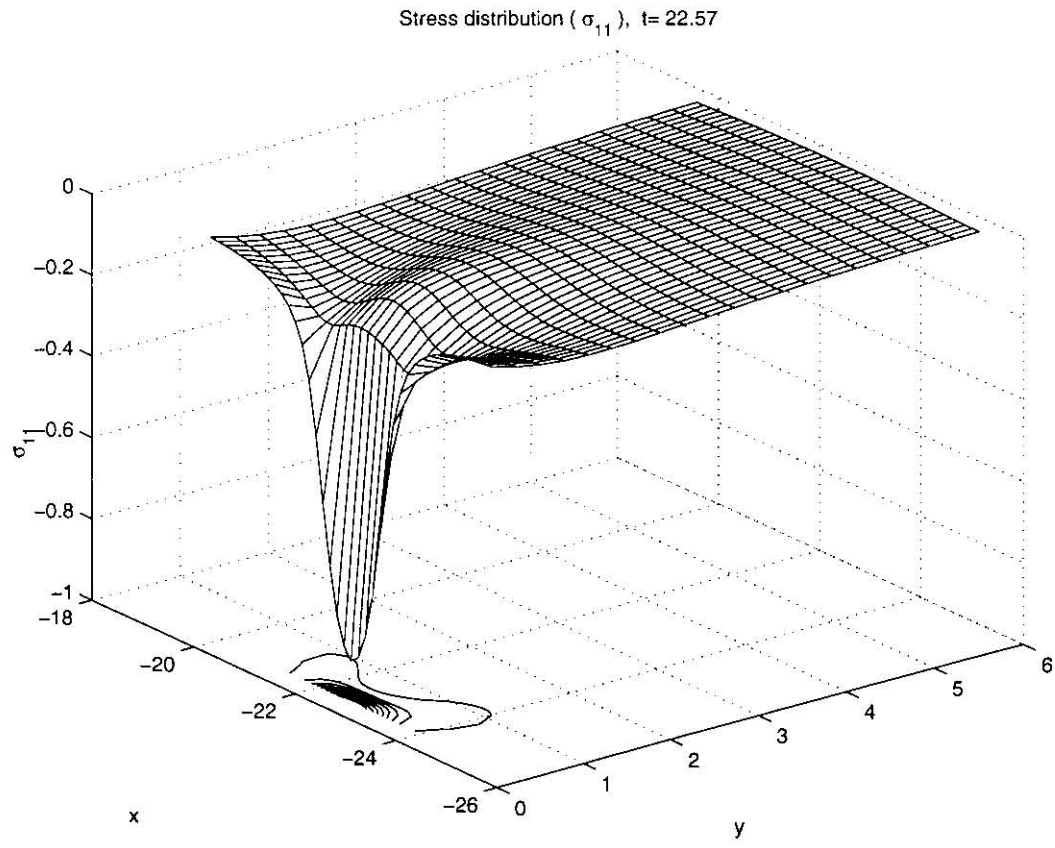

Figure 6.71: Periodically varying load: $W(t) = 1 + 0.5\sin(t)$. Stress distribution: σ_{11}. $\frac{G_1}{G_0} = \frac{1}{4}$

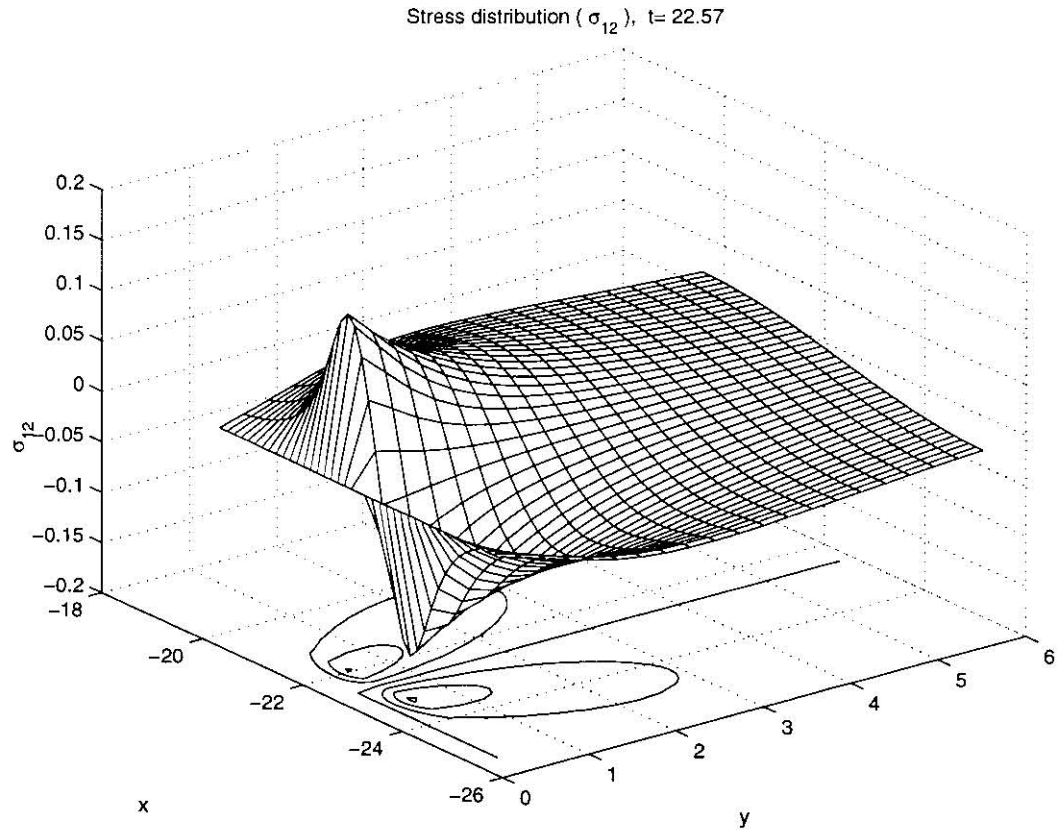

Figure 6.72: Periodically varying load: $W(t) = 1 + 0.5\sin(t)$. Stress distribution: σ_{12}. $\frac{G_1}{G_0} = \frac{1}{4}$

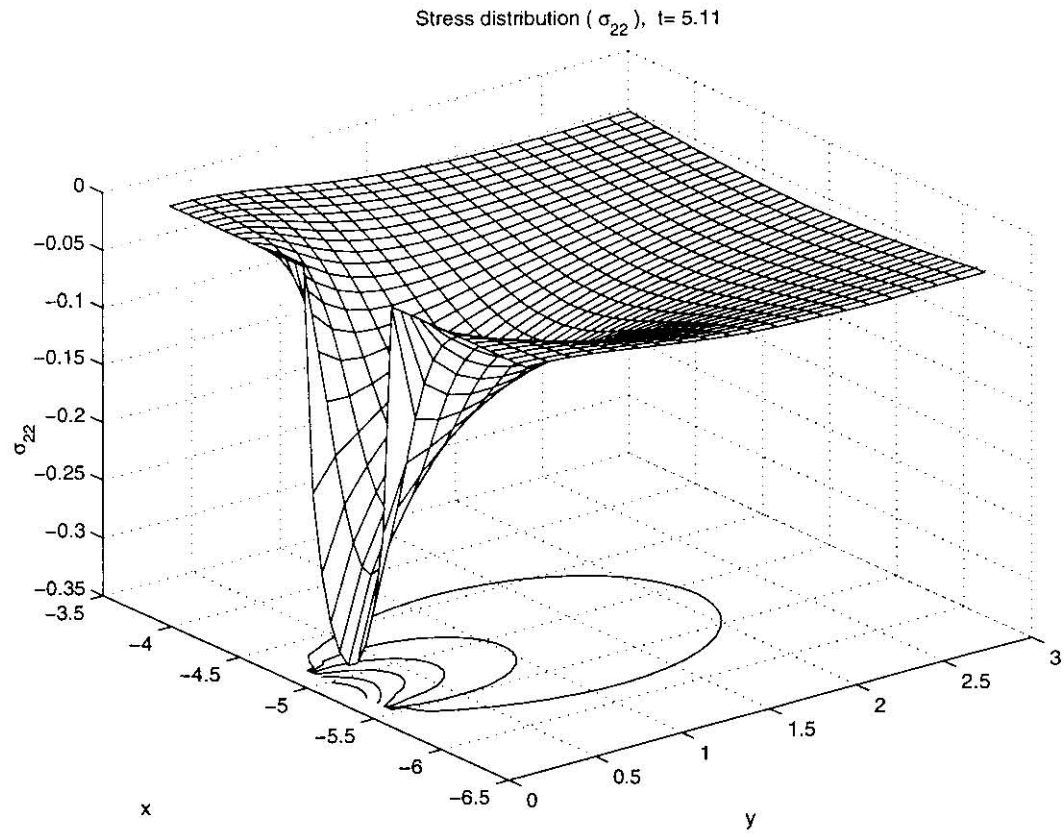

Figure 6.73: Periodically varying load: $W(t) = 1 + 0.5\sin(t)$. Stress distribution: σ_{22}. $\frac{G_1}{G_0} = \frac{1}{4}$

Chapter 7

Conclusion

In this thesis integral equation (4.3.16) subjected to subsidiary conditions (4.2.9) and (4.2.10) has been solved for the transient case for the first time. Several patterns of speed variation / loading conditions have been analyzed and histories of transient contact interval length, hysteretic friction and indentor tip shift compared with their steady-state counterparts.

It has been shown that:

1. the results obtained with the help of the transient algorithm described in Chapter 5 are consistent with the steady-state results obtained through the analytic solution;

2. in aperiodic motion the transient quantities eventually approach their steady-state counterparts as $t \to \infty$;

3. the positions of the indentor tip inside the contact intervals relative to the front and rear boundaries are substantially different in the transient and steady-state cases, even though the contact interval lengths may be the same;

4. for variable *speed* the graph shapes of transient and steady-state hysteretic friction are substantially different; the indentor tip shift mimics the behaviour of hysteretic friction;

5. after a period of acceleration, the transient value of the hysteretic friction overshoots the steady-state value;

6. higher values of the dimensionless viscoelastic ratio $\frac{G_1}{G_0}$ lead to longer contact intervals, higher hysteretic friction values and sharper peaks in the pressure distribution in the front part of the contact interval in the initial time period;

7. the pressure in the front of the contact interval is higher than in the rear. During the initial time period, there is a tangible difference between the two;

8. the distribution of stress components σ_{11}, σ_{12} and σ_{22} can be computed once $v(x,t)$ is known. The results for large times are in good agreement with known elastic stress distributions;

9. both the indentor tip shifts and the coefficients of hysteretic friction differ qualitatively for the transient and steady-state cases for a constant speed motion of the indentor under a variable load;

10. the shift of the graph of the transient compared to steady-state hysteretic friction in the case of constant speed and variable load exceeds the corresponding shift in the case of a constant load and variable speed.

Further research may include the multi-indentor case and the to-and-fro motion of a single indentor in opposite directions. However, those two cases require substantial modification of the current algorithm and its software implementation.

Bibliography

[1] Aboudi, J., The dynamic indentation and impact of a viscoelastic half-space by an axisymmetric rigid body, *Computer Methods in Applied Mechanics and Engineering*, **20** (1979), 135 – 150.

[2] Akopyan, V.N., On a periodic contact problem of the linear viscoelasticity theory, *Izvestiya Akademii Nauk Armyanskoj SSR*, **35** (1982) 3 – 15.

[3] Alblas, J.B., Kuipers, M., The contact problem of a rigid cylinder rolling on a thin viscoelastic layer, *International Journal of Engineering Sciences*, **8** (1970), 363-380.

[4] Arutyunyan, N.Kh., Manzhirov, A.V., Contact problems of mechanics of growing bodies, *Prikladnaya Matematika i Mekhanika*, **53** (1989), 145 – 158.

[5] Atkinson, K.E., *A survey of numerical methods for the solution of Fredholm integral equations of the second kind*, SIAM, Philadelphia, 1976.

[6] Badalov, F.B., Usmanov, B.I., Solvability of one non-linear equation for the quasistatic problem of the viscoelasticity theory, *Doklady Akademii Nauk UzSSR*, **5** (1984), 20 – 23.

[7] Badalov, F.B., Anzhiev B., On the existence of solution of an initial-boundary value problem for one non-linear integro-differential equation of the hereditary viscoelasticity theory, *Doklady Akademii Nauk UzSSR*, **4** (1985), 15 – 17.

[8] Badalov, F.B., Khuzhayarov, N.Yu., On the exact solution of the integro-differential equations of linear dynamical viscoelasticity, *Soviet Physics Doklady*, **33**, (1988), 229 – 231.

[9] Boltzmann, L., *Wissenschaftliche Abhandlungen*, Collected Papers, ed. F. Hasenhörl, Vol. 1, Leipzig, 1909, reprinted by Chelsea, New York, 1968.

[10] Boor, C., de, *A Practical Guide to Splines*, Springer-Verlag, New York, 1978.

[11] Bowden, F.P., Tabor, D., *The Friction and Lubrication of Solids*, Part II, Clarendon Press, Oxford, 1964.

[12] Brunner, H., Yatsenko, Y., Spline collocation methods for nonlinear Volterra integral equations with unknown delay, *Journal of Computational and Applied Mathematics*, **71** (1996), 67 – 81.

[13] Brunner, H., Iterated collocation methods for Volterra integral equations with delay agruments, *Mathematics of Computation*, **62** (206) (1994), 581 – 599.

[14] Carini, A., de Donato, O., Fundamental solutions for linear viscoelastic continua, *International Journal of Solids and Structures*, **29** (23), (1992), 2989 – 3009.

[15] Chertok, D.L., Lardner, R.W., Variational data assimilation for a nonlinear hydraulic model, *Applied Mathematical Modelling*, **20** (1996), 675 – 682.

[16] Chertok, D.L., Golden, J.M. and Graham, G.A.C., Hysteretic friction in the transient viscoelastic rolling contact problem, *CAMS 1997 Annual Meeting* Toronto, Ontario, May 30 - June 1, 1997.

[17] Chertok, D.L., Golden, J.M. and Graham, G.A.C., The transient motion of a parabolic indentor across a viscoelastic half-space, *Ninth Meeting of the Working Group of the Scientific Council on the World Ocean Problems of the Russian Academy of Science*, Moscow, June 7 -9, 1997.

[18] Chertok, D.L., Golden, J.M. and Graham, G.A.C., Hysteretic friction for the transient rolling contact problem of linear viscoelasticity, 1997, submitted for publication.

[19] Christensen, R.M., *Theory of Viscoelasticity: An Introduction* (2nd ed.) Academic Press, New York, 1982.

[20] Ciobanu, Gh. Gr., On stability of solution in linear viscoelasticity, *Andaele stiintifice ale Universitătii "Al.I. Cuza" din Iaşi*, **30**, s. Ia., Matematică, 1984.

[21] Coulomb, C.A., de: Thĕorie des machines simples, en ayant égard au frottement de leur parties st à la roideur des cordages, *Mémorie de Mathématique et de Physique de l'Académie Royale*, **10** (1785), 161 – 332.

[22] Davis P.J., Rabinowitz P., *Methods of numerical integration*, 2nd ed., Academic Press, Orlando, 1984.

[23] Delves, L.M. and Mohamed, J.L., *Computational Methods for Integral Equations*, Cambridge University Press, 1985.

[24] Dobordzhginidze, L.G., A plane contact problem in elasticity theory for viscoelastic bodies, *Trudy Tbilisskogo Matematicheskogo Instituta im. M.A. Razmadze*, **87** (1987), 54 – 61.

[25] Drozdov, A.D., Kolmanovskii, V.B., *Stability in Viscoelasticity*, Elsevier Science, Amsterdam, 1994.

[26] Drozdov, A.D.: *Finite Elasticity and Viscoelasticity: A Course in the Nonlinear Mechanics of Solids*, World Scientific, Singapore, 1996.

[27] Dupuit, A.J.E.J., Mémoire sur le triage des voitures et sur le frottement du roulement, *Annales des ponts et chausées*, **3** (1842), 261 – 335.

[28] Duvaut, G., Lions, J.-L., *Les Inéquations en Méchanique et en Physique*, Dunod, Paris, 1972.

[29] Evans, G., *Practical Numerical Integration*, John Wiley & Sons, Chichester, 1993.

[30] Fabiano, R.H., Ito, K.: An approximation framework for equations in linear viscoelasticity with strongly singular kernels, *Quarterly of Applied Mathematics*, **52** (1) (1994), 65 - 81.

[31] Fan, H.Z., Golden, J.M., Graham, G.A.C.: The problem of several indentors moving on a viscoelastic half-plane. *Journal of Applied Mechanics*, **62** (1995), 380-389.

[32] Fichera, G., Problemi elastostatici con vincoli unilaterale: il probleme di signorini con anbigue condizioni al contorno, *Memorie Accademie Nazionale Dei Lincei*, Ser. 8,7, 1964, pp. 91 - 140.

[33] Figueiredo, I., Trabucho, L., A class of contact and friction dynamic problems in thermoelasticity and in thermoviscoelasticity, *International Journal of Engineering Sciences*, **33** (1995), 45 - 66.

[34] Figueiredo, I., Trabucho, L.: Some existence results for contact and friction problems in thermoelasticity and in thermoviscoelasticity, in: *Asymptotic Methods for Elastic Structures* (ed. by P. Ciarlet et al.), Walter de Gruyter, Berlin, 1995, pp. 223 — 235.

[35] Flom, D.G. and Bueche, A.M. Theory of Rolling Friction for Spheres, *Journal of Applied Physics*, **30** (11) (1959), 1725 - 1730.

[36] Flom, D.G., Dynamic mechanical losses in rolling contacts, in: *Rolling Contact Phenomena* (ed. by J.B. Bidwell), Elsevier, Amsterdam, 1962, pp. 97 - 109.

[37] Flügge, W., *Viscoelasticity* (2nd ed.), Springer-Verlag, New York, 1975.

[38] Galin, L.A., *Contact Problem in the Classical Theory of Elasticity and Viscoelasticity*, (In Russian). Nauka, Moscow, 1980.

[39] Godunov, S.K., Zabrodin, A.V., Ivanov, M.Ya, Kraiko, A.N., Prokopov, G.P., *Numerical Solution of Multi-dimensional Gas Dynamics Problems*, Nauka, Moscow, 1976.

[40] Golden, J.M., Hysteretic friction of a plane punch on a half-plane with arbitrary viscoelastic behaviour, *Quarterly Journal of Mechanics and Applied Mathematics*, **30** (1977), 23 – 49.

[41] Golden, J.M., The problem of a moving rigid punch on an unlubricated viscoelastic half-plane, *Quarterly Journal of Mechanics and Applied Mathematics*, **32** (1979), 25 – 52.

[42] Golden, J.M., Frictional viscoelastic contact problems, *Quarterly Journal of Mechanics and Applied Mathematics*, **39** (1986), 125 – 137.

[43] Golden, J.M., Graham, G.A.C., The transient quasi-static plane viscoelastic moving load problem, *International Journal of Engineering Science*, **25** (1987), 65 – 84.

[44] Golden, J.M., Graham, G.A.C., The steady-state plane normal viscoelastic contact problem, *International Journal of Engineering Science*, **25** (1987), 277 – 291.

[45] Golden, J.M., Graham, G.A.C., *Boundary Value Problems in Linear Viscoelasticity*, Springer-Verlag, Berlin, 1988.

[46] Golden, J.M., Graham, G.A.C., Lan, Q., Three-dimensional steady-state indentation problem for a general viscoelastic material, *Quarterly Journal of Mechanics and Applied Mathematics*, **52** (2) (1994), 449 – 468.

[47] Golden, J.M., Graham, G.A.C., General methods in non-inertial viscoelastic boundary value problems, in: *Crack and Contact Problems for Viscoelastic Bodies* (ed. by G.A.C. Graham and J.R. Walton), Springer-Verlag, Vienna, 1995, pp. 102 – 225.

[48] Golden, J.M., Graham, G.A.C., The viscoelastic moving contact problem with inertial effects included, *Quarterly Journal of Mechanics and Applied Mathematics*, **49** (1996), 107 - 135.

[49] Goldshtein, R.V., Zazorskii, A.F., Spektor, A.A., Fedorenko, R.P., Solution by variational methods of three-dimensional rolling contact problems with slipping and adhesion, *Uspekhi Mekhaniki*, **5** (3 - 4) (1982), 61 - 102.

[50] Graham, G.A.C., The contact problem in the linear theory of viscoelastcity, *International Journal of Engineering Science*, **3** (1965), 27 - 46.

[51] Graham, G.A.C., The contact problem in the linear theory of viscoelastcity where the time dependent contact area has any number of maxima and minima, *International Journal of Engineering Science*, **5** (1967), 495 - 514.

[52] Graham, G.A.C., The correspondence principle of linear viscoelasticity theory for mixed boundary value problems involving time-dependent boundary regions, *Quarterly of Applied Mathematics*, **26** (1968), 167 - 174.

[53] Graham, G.A.C., Sabin, G.C.W., The correspondence principle of linear viscoelasticity for problems that involve time-dependent regions, *International Journal of Engineering Science*, **11** (1973), 123 - 140.

[54] Graham, G.A.C., Viscoelastic contact problems with friction, *International Journal of Engineering Science*, **18** (1980), 191 - 196.

[55] Graham, G.A.C., Golden, J.M., The generalized partial correspondence principle in linear viscoelasticity, *Quarterly of Applied Mathematics*, **46** (3) (1988), 527 - 538; **49** (2) (1991), 379 - 397.

[56] Graham, G.A.C., Golden, J.M., The three-dimensional steady-state viscoelastic indentation problem, *International Journal of Engineering Sciences*, **26** (1988), 121 - 126.

[57] Green, A.E., Zerna, W., *Theoretical Elasticity*, Oxford University Press, 1968.

[58] Greenwood, J.A., Tabor, D., Hysteresis losses in rolling and sliding friction, *Proceedings of the Royal Society (London)*, **259(A)**, (1961), 180 - 507.

[59] Gurtin, M.E., Sternberg, E., On the linear theory of viscoelasticity, *Archive for Rational Mechanics and Analysis* **2** (1962), 291 - 356.

[60] Han Guoqiang, Zhang Liqing, Asymptotic expansion for the trapezoidal Nyström method of linear Volterra-Fredholm equations, *Journal of Computational and Applied Mathematics*, **51** (1994), 339 - 348.

[61] Harrison, D., Whiteman, J.R., Yettram, A.L., Finite element modelling of viscoelastic material response of polymeric structures, in: *The Mathematics of Finite Elements and Applications, V*, Academic Press, London, 1985, pp. 137 - 147.

[62] Hertz, H., Über die Berürung fester elastischer Körper, *Journal für reine und angewandte Mathematik (Crelle)*, **92** (1882), 156 - 171.

[63] Hills, D.A., Nowell, D., Sackfield, A., *Mechanics of Elastic Contacts*, Butterworth-Heinemann, Oxford, 1993.

[64] Hunter, S.C., The Hertz problem for a rigid spherical indentor and a viscoelastic half-space, *Journal of the Mechanics and Physics of Solids*, **8** (1960), 219 - 234.

[65] Hunter, S.C., The rolling contact of a rigid cylinder with a viscoelastic half-space, *Journal of Applied Mechanics*, **28** (1961), 611 - 617.

[66] Janovsky, V., Shaw, S., Warby, M.K., Whiteman, J.R., Numerical methods for solving problems of viscoelastic isotropic solid deformation, *Journal of Computational and Applied Mathematics*, **63** (1995), 91 - 107.

[67] Jarušek, J., Contact problems with given time-dependent friction force in linear viscoelasticity, *Commentationes Mathematicae Universitatis Carolinae*, **31** (1990), 257 - 262.

[68] Jarušek, J., Eck, C., Dynamic contact problems with friction in linear viscoelasticity, *Comptes Rendus des Sances de l'Acadmie des Sciences. Srie I*, **t. 322** (1996), 497 – 502.

[69] Jarušek, J., Dynamic contact problems with given friction for viscoelastic bodies, *Czechoslovak Mathematical Journal*, **46** (121) (1996), 475 – 487.

[70] Johnson, K.L., *Contact Mechanics*, Cambridge University Press, 1985.

[71] Kalker, J.J.: *Three-Dimensional Elastic Bodies in Rolling Contact*, Kluwer, Dodrecht, 1990.

[72] Kaminskii, A.A., Kekukh, S.A., Method of solving problems of the linear theory of viscoelasticity for anisotropic materials (in the presence of cracks), *International Applied Mechanics*, **30** (4) (1994) 320 – 327.

[73] Khludnev, A.M., Contact viscoelastoplastic problem for a beam, in: *Free Boundary Problems in Continuum Mechanics*, Birkhaúser Verlag, Basel, 1992, pp. 159 – 166.

[74] Khludneva, E. Yu., Numerical solution of a contact problem for a viscoelastic plate, in: *Free Boundary Value Problems of Continuum Mechanics*, Sibirskoye otdeleniye Akademii Nauk SSSR, Institut Gidrodinamiki, **v. 101**, 1991, pp. 132 – 139.

[75] Kikuchi, N., Oden, J.T., *Contact Problems in Elasticity: A Study of Variational Inequalities and Finite Element Methods*, SIAM, Philadelphia, 1988.

[76] Kim, Jong Uhm, A one-dimensional dynamic contact problem in linear viscoelasticity, *Mathematical Methods in Applied Sciences*, **13** (1990), 55 – 79.

[77] Kolosov, G.V.: *On an Application of Complex Function Theory to a Plane Problem of the Mathematical Theory of Elasticity*, Yuriev, 1909.

[78] Korobeinikov, S.N., Alyokhin, V.V., Application of a finite-element method to two-dimensional contact problems, in: *Free Boundary Problems in Continuum*

Mechanics, International Series of Numerical Mathematics, **v. 106**, Birkhäuser Verlag, Basel, 1992, pp. 167 – 177.

[79] Kresin, G.T., Mazya, V.G., On the maximum of displacements in a viscoelastic half-space (a three-dimensional model), *Vestnik Leningradskogo Universiteta*, **22** (1985), 47 – 51.

[80] Kuczma, M.S., Demkowics, L., An adaptive algorithm for unilateral viscoelastic contact problems for beams and plates, *Computer Methods in Applied Mechanics and Engineering*, **101** (1992), 183 – 196.

[81] Ladopoulos, E.G., On the numerical solution of the multidimensional singular integrals and integral equations, used in the theory of linear viscoelasticity, *International Journal of Mathematics and Mathematical Sciences*, **11** (3), (1988), 561 – 574.

[82] Lavrent'ev, M.A., Shabat, B.V., *Methods of the Theory of Functions of a Complex Variable*, Moscow, Nauka, 1973.

[83] Lee, E.H., Stress analysis in viscoelastic bodies, *Quarterly of Applied Mathematics*, **13** (1955), 183 – 190.

[84] Lee, E.H., Viscoelastic stress analysis, in *Structural Mechanics*,Proceedings of the First Symposium on Naval Structure Mechanics (ed. by J.N. Goodier, N.J. Hoff), Pergamon, Oxford, 1960, pp. 456 – 482.

[85] Lee, E.H., Radok, J.R.M., The contact problem for viscoelastic bodies, *Journal of Applied Mechanics*, **27** (1960), 438 – 444.

[86] Lewis, P.E., Ward, J.P., *The Finite Element Method: Principles and Applications*, Addison-Wesley, Wokingham, 1991.

[87] Love, A.E.H., *A Treatise on the Mathematical Theory of Elasticity*, Cambridge University Press, 1934.

[88] Mark, J. and Meister, E.: Initial-boundary value problems in linear viscoelasticity on the half-space, *Mathematical Methods in the Applied Sciences*, **18** (1995), 1181 - 1214.

[89] Maxwell, J.C., On the dynamical theory of gases, *Philosophical transactions of the Royal Society of London. Series A. Mathematical, Physical Sciences and Engineering*, **157** (1867), 49 - 88.

[90] May, M.D., Morris, E.L., and Attack, D., Rolling friction of a hard cylinder over a viscoelastic material, Journal of Applied Physics, **30** (1959), 1713 - 1724.

[91] Merzhievsky, L.G., Reznyansky, A.D., Numerical calculation of movable free and contact boundaries in problems of dynamic deformation of viscoelastic bodies, in *Free Boundary Problems in Continuum Mechanics*, International Series of Numerical Mathematics, **v. 106**, Birkhäuser Verlag, Basel, 1992, pp. 205 - 213.

[92] Moore, D.F., *Viscoelastic Machine Elements: Elastomers and Lubricants in Machine Systems*, Butterworth-Heinemann, Oxford, 1993.

[93] Morland, L.W., A plane problem of rolling contact in linear viscoelasticity theory, *Journal of Applied Mechanics*, **29** (1962), 345 - 352.

[94] Morland, L.W., Exact solutions for rolling contact between viscoelastic cylinders, *Quaterly Journal of Mechanics and Applied Mathematics*, **20** (1967), 73 - 106.

[95] Morland, L.W., Rolling contact between dissimilar viscoelastic cylinders, *Quarterly of Applied Mathematics*, **25** (1968), 363 - 376.

[96] Movlyankulov, Kh., Filatov, A.N., Method of freezing of non-linear integro-differential equations, *Doklady Akademii Nauk SSSR, Fizika*, **287** (2) (1986), 317 - 320.

[97] Movlyankulov, Kh.: Generalization of the freezing method to nonlinear equations of viscoelasticity, in: *Qualitative theory of complex systems*, Leningradskij Gosudarstvennyj Pedagogicheskij Institut, Leningrad, 1986.

[98] Muskhelishvili, N.I., *Some Basic Problems of the Mathematical Theory of Elasticity*, 4th ed. [English translation by J.R.M. Radok], Noordhoff, Groningen, 1963.

[99] Nachman, A., Walton, J.R., The sliding of a rigid indentor over a power law viscoelastic layer, *Journal of Applied Mechanics*, **45** (1978), 111 - 113.

[100] Norman, R.H., The rolling friction of cylinders on planes, *British Journal of Applied Physics*, **13** (1962), 358 - 361.

[101] Oden, J.T., Becker, E.B., Lin, T.L., Demkowicz, L., Formulation and finite element analysis of a general class of rolling contact problems with finite elastic deformations, in: *The Mathematics of Finite Elements and Applications, V*, Academic Press, London, 1985, pp. 505 - 532.

[102] Oden, J. T., Lin, T.L., On the general rolling contact problem for finite deformations of a viscoelastic cylinder, *Computer Methods in Applied Mechanics and Engineering* **57** (1986), 297 - 367.

[103] Panek, C., Kalker, J.J., Three-dimensional contact of a rigid roller traversing a viscoelastic half-space, *Journal of the Institute Mathematics and Its Applications* **26** (1980), 299 - 313.

[104] Pavlov, S.M., Svetashkov, A.A., Iteration method for solving linear viscoelasticity problems, *Izvestiya Vysshikh Uchebnykh Zavedenii, Fizika*, **4**, April 1993, 129 - 136.

[105] Pipkin, A.C., *Lectures on Viscoelasticity Theory*, Springer-Verlag, New York, 1972.

[106] Rabotnov, Yu.N., *Elements of hereditary mechanics of solid bodies*, Nauka, Moscow, 1977.

[107] Reynolds, O., On rolling-friction, *Philosophical Transactions of the Royal Society of London. Series A. Mathematical, Physical Sciences and Engineering*, **166** (1876), 155 - 174.

[108] Rossikhin, Yu. A., Shitikova, M.V., Ray expansions for the solution of dynamic problems of linear viscoelasticity, *Soviet Applied Mechanics*, **27** (1) (1991), 77 - 82.

[109] Shames, I.H., Cozzarelli, F.A., *Elastic and Inelastic Stress Analysis*, Prentice-Hall, Englewood Cliffs, New Jersey, 1992.

[110] Shen, Y., Pen Y., Stress and fracture analysis of viscoelastic large strain problem by finite element method, in: *Proceedings of the International conference on nonlinear mechanics, Oct. 28 - 31, 1985, Shanghai, China (editor-in-chief Chien Wei-Zang)*, Science Press, Beijing, 1985, pp. 1303 - 1306.

[111] Singh, M., Influence of couple stresses on singular stress concentration in microelastic solids, *Indian Journal of Pure and Applied Mathematics*, **14(8)** (1983), 1056 - 1074.

[112] Smith, H.V., *Numerical Methods of Integration*, Chartwell-Bratt-Studentliteratur, Lund, 1993.

[113] Sokolnikoff, I.S., *Mathematical Theory of Elasticity*, McGraw-Hill, New York, 1956.

[114] Squire, W., *Integration for engineers and scientists*, American Elsevier, N.Y., 1970

[115] Tabor, D., Mechanism of rolling friction, *Journal of Theoretical, Experimental and Applied Physics*, **43(7)** (1952), 1055 - 1059.

[116] Telega, J., Quasi-static Signorini's contact problem with friction and duality, in: *International Series on Numerical Mathematics*, **101**, Birkhaüser Verlag, Basel, 1991, pp. 199 - 214.

[117] *The numerical solution of nonlinear problems* (ed. by Christopher T.H. Baker and Chris Philips), Clarendon Press, Oxford, 1981.

[118] Timoshenko, S., Goodier, J.N. *Theory of Elasticity*, McGraw-Hill, 1951.

[119] Ting, T.C.T., The contact stresses between a rigid indentor and a viscoelastic half-space, *Journal of Applied Mechanics*, **33** (1966), 845 - 854.

[120] Ting, T.C.T., Contact Problems in the Linear Theory of Viscoelasticity, *Journal of Applied Mechanics*, **35** (1968), 248 - 254.

[121] Tschoegl, Nicholas W., *The Phenomenological Theory of Linear Viscoelastic Behavior: an Introduction*, Springer-Verlag, Berlin, 1989.

[122] *User's manual: IMSL MATH/LIBTRARY* IMSL, Inc., 1990

[123] Volkov, L.G., Realization and convergence of difference schemes for nonlinear viscoelasticity equations, *Differential Equations*, **27** (7) (1991), 781 - 788.

[124] Volterra, V., Sulla equazioni integrodifferenziali della teoria dell'elasticitá, *Atti della Reale Accademia dei Lincei*, **18(2)**, (1909), 295.

[125] Walton, J.R., The sliding with Coulomb friction of a rigid indentor over a power-law inhomogeneous linearly viscoelastic half-plane, *Journal of Applied Mechanics*, **51** (1984), 289 - 293.

[126] Walton, J.R., Nachman, A., Schapery, R.A., The sliding of a rigid indentor over a power-law viscoelastic half-space, *Quarterly Journal of Mechanics and Applied Mathematics*, **31** (1978), 296 - 321.